R·I·T | KATE GLEASON *College of* ENGINEERING

# INTERACTION OF DROPLET AND SIDEWALLS WITH MODIFIED SURFACES IN A PEMFC GAS FLOW CHANNEL

by

**Mihir M. Shah**

A Thesis Submitted in Partial Fulfillment of the Requirements for the Degree of

**MASTER OF SCIENCE**

in

**MECHANICAL ENGINEERING**

DEPARTMENT OF MECHANICAL ENGINEERING

KATE GLEASON COLLEGE OF ENGINEERING

ROCHESTER INSTITUTE OF TECHNOLOGY

ROCHESTER, NY 14623

JULY 2014




**Approved by:**

_____ _____

**Dr. Satish G. Kandlikar** Date

*Thesis Advisor*

Professor, Department of Mechanical Engineering

_____ _____

**Dr. Robert Stevens** Date

*Committee Member*

Professor, Department of Mechanical Engineering

_____ _____

**Dr. Jason R. Kolodziej** Date

*Committee Member*

Professor, Department of Mechanical Engineering

_____ _____

**Dr. Agamemnon Crassidis** Date

*Department Representative*

Professor, Department of Mechanical Engineering

## Abstract

A Proton Exchange Membrane Fuel Cell (PEMFC) is a clean and highly efficient way of power generation used primarily for transportation applications. Hydrogen and air are supplied to the fuel cell through gas channels, which also remove liquid water generated in the fuel cell. The clogged channels prevent reactant transport to the electrochemically active sites which comprise one of the channel walls and thus, degrading the performance of the cell. Proper management of the product water is a current topic of research interest in commercialization of fuel cell vehicles. Liquid water, produced as by-product of the fuel cell reaction, can clog the gas channels easily since surface tension of water is significant at this length scale. In a PEMFC channel cross-section, water is assumed to be produced in the channel at the center along the flow axis. This assumption is primarily valid and extensively used for experimental purposes. However in a real PEMFC, the water entry is not constrained at the channel center. Hence, more investigations are made using water entry at channel corner (land region) which resulted in contradicting prior results for the water feature behavior for all relevant PEMFC operating conditions, leading to adverse two-phase flow behavior- including slug blockage and fluctuations at channel end. Very limited research is available to study the effect of gas channel surface modifications on the two–phase flow behavior and local PEMFC performance. In this study, the droplet–sidewall dynamic interactions and two–phase local pressure drop across the water droplet present in a PEMFC channel with trapezoidal geometries with surface modifications are studied. These surface modifications include micro-grooves that possess a hybrid wetting regime that will initiate and guide the water feature at channel ends to eject with general ease. Slugs are reduced to films after ejection and thus channel blockage is avoided overcoming the problems caused by water influx at channel corner or under the land.

## Acknowledgements

It is with immense pleasure and satisfaction that I am presenting this thesis to you. It has always been my passion to pursue science in its purest form. This opportunity of working on my graduate thesis has instilled scientific exactness, better engineering aptitude and a multitude of other skills in me for which I could not be more thankful of. There were many times when I ran out of patience but did not give up. This pursuit of knowledge and the constant inspiration to do better and more has brought me to this milestone and I have more faith in myself than ever before.

I would like to express deep gratitude for the guidance provided by my advisor, Dr. Kandlikar, throughout my research and studies. His enthusiasm, vision and inspiration was something that kept me going throughout and I am sure that I will remember his words and attitude towards work for the rest of my career. I hope to continue this wonderful association in the time to come. I can't thank him enough for his continuous support.

I would like to thank the members of the Fuel Cell Group at TAMFL including Rupak, Mustafa, Preethi and Evan for their constant guidance, help and providing an environment that I looked forward to work in every day. They set new levels of excellence that I have tried to reach at my level best. I cannot thank Valentina, Andrew and Alyssa enough for the hands-on support they have provided during my work. I would also like to thank all the fellow members of the Thermal Analysis, Microfluidics, and Fuel Cell Lab. I would like to acknowledge the support of the entire Mechanical Engineering Department staff and the Machine Shop staff including Dave Hathaway, Rob Kraynik and Jan Maneti. The entire RIT family including faculty and staff made my stay safe and enjoyable.

I would like to thank my parents Milind and Medha along with my extended family for their unending support. Without their motivation and support, I would not have reached where I am today. They are constant reminders to me that there is always more that can be achieved and not be satisfied with mediocre. I have and will give my best to fulfill that. I would like to thank my little sister Mitisha, who by her own ways has always taught me new lessons, loved and supported me unconditionally.

Finally, I want to appreciate the support of my friends back home and here in Rochester. I would like to thank Abhishek, Shardul, Mayuresh, Tushar, Ashwini, Shriya, Mitali, Wanda, Joe and many others who made my stay in Rochester a cherished one. I would also like to thank my best friend Kaushik for always being there for me. All the other special friends who met me and stood by me before, during and after I started this journey, made it all worthwhile.

I have always believed that my grandparents were the ones who made me what I am today. This work is dedicated to their memory and the values they taught me as the best- love, kindness and friendship.

# TABLE OF CONTENTS

LIST OF FIGURES .....viii

LIST OF TABLES .....xiii

NOMENCLATURE .....xiv

1. Introduction .....1

1.1. Alternative Powertrains and Environmental Concerns…….....1

1.2. Proton Exchange Membrane Fuel Cells .....3

1.3. Bipolar Plate And Fuel Cell Channel Design Constraints .....5

1.4. Water Management in PEMFC and Effect of Channel Geometry .....7

2. Literature Review and Motivation .....9

2.1. Effect of Channel Geometry and Flow Field Dimensions and Geometry on Fuel Cell Performance .....9

2.2. Microchannel Modifications for Better Water Removal Characteristics.....14

2.3. Assumptions Made in Past PEMFC Channel Studies .....18

3. Objectives .....21

4. Approach .....22

4.1. Design of Setup .....24

4.2. Grooved Channel Walls- Proof of Concept .....26

4.3. Grooved Channel Design- Characterization .....29

4.4. Data Acquisition and Reduction .....33

4.5. Experimental Procedure .....35

5. Results and Discussions .....39

5.1. Pressure Drop Validations and Visual Results Correlations for Plain Sidewall Channels (Water injection near channel exit (12.7 mm away from channel exit)) .....40

5.2. Contact Angles for All Channel Surfaces Tested .....48

5.3. Droplet Sidewall Interaction (Grooved Sidewall-GDL) .....50

5.4. Effect of Grooved Channel Designs on Water Accumulation .....55

5.5. Manufacturing Considerations and Grooved Channels .....60

5.6. Pressure Drop Validations and Visual Results Correlations for All Channel Designs (Water Injection Upstream (~ 76 mm away from channel exit, inside the channel)) .....64

6. Conclusions .....84

7. Future Work .....87

APPENDICES .....88

Appendix I .....88

a. Superficial Airflow Rate Calculation

Appendix II .....90

a. Engineering Drawings

## LIST OF FIGURES


Figure 1. PEMFC Construction and Mass Transport .....4

Figure 2. Fuel Cell Graphite Bipolar Plate .....6

Figure 3. Stamping Process for Bipolar Plates .....6

Figure 4. V-I Curve of a PEMFC showing the different losses that occur during the working cycle, Adapted from [1] .....7

Figure 5. Cases of Water Droplet Injection in a PEMFC Channel [2] .....11

Figure 6. Concuss-Finn Condition (a) Image of Concuss–Finn wedge container modeled and (b) plot of Concuss–Finn condition for wedge container reproduced from [5] .....12

Figure 7. Schematic of Channel Design and Integration in Fuel Cell Flow Field [11].....13

Figure 8. Grooved Substrate- Parameters Studied in [15].....15

Figure 9. Wetting Regimes on Grooved Substrates- Wenzel ad Cassie-Baxter adopted from [19] .....16

Figure 10. GDL Mass Transport .....18

Figure 11. Channel Geometry and Entry Locations .....19

Figure 12. Concuss-Finn Plot, Water Injection at Channel Corner .....22

Figure 13. Droplet Filling for Corner Entry .....23

Figure 14. Ex-Situ Experimental Section Assembly Parts .....24

Figure 15. Experimental Setups for a) Configuration 1 and b) Configuration C2.....25

Figure 16. Droplet-Grooved Sidewall Interaction-Stage 1 .....27

Figure 17. Droplet-Grooved Sidewall Interaction - Stage 2 .....27

Figure 18. Droplet-Grooved Sidewall Interaction - Stage 3 .....28

Figure 19. Droplet-Plain Sidewall Interaction .....28

Figure 20. Experimental Setup Arrangement- Grooves Visualization .....29

Figure 21. a) 0 min: Droplet #1 appears, enters the grooves, b) 10 min: Droplet #2 appears, enters groove, c) 26 min: Droplets coalesce and enter 7 grooves in total .....30

Figure 22. a) 52 min: Slow rise in droplet level over the grooves and after 26 minutes after coalescing of the two droplets, significant rise in capillary effect for some time. b) 81 min: The rise in the grooves due to capillary effect is seen to reach the top face and the end of the groove .....31

Figure 23. The droplet reaches top wall and there is no more increase in its overall rise at the end of 99 minutes, where the test was ended .....31

Figure 24. Channel Sidewall with Grooved Surface- Groove Details .....32

Figure 25. Experimental Test Setup with Auxiliary Control Systems .....33

Figure 26. LabView Interface and Block Diagram of the VI used for Data Acquisition .....34

Figure 27. Experimental Setup for Visualizing Droplet-Sidewall Interaction (Configuration C1) .....35

Figure 28. Experimental Setup for Visualizing Droplet-Sidewall Interaction (Configuration C2) .....37

Figure 29. Droplet-sidewall Interaction, Plain Trapezoidal Channel, 0.5 m/s .....41

Figure 30. Non-Grooved (Plain) Channel Sidewalls- Pressure Drop for Low Air Velocities (C1.1 a).....42

Figure 31. Non-Grooved (Plain) Channel Sidewalls- Pressure Drop for High Air Velocities (C1.1 a) .....42

Figure 32. First Slug Formation and Removal for Higher Air Velocities (≥ 0.5 m/s), 0 to 8 min .....43

Figure 33. Droplet Sticking Phenomenon for High Air Velocities (≥ 0.5 m/s), 8-10 min .....44

Figure 34. Effect of Orientation on Static Advancing and Receding Contact Angles ($\theta_A$, $\theta_{R)}$ .....49

Figure 35. Grooved Surface- Contact Angles Around the Droplet Periphery.....50

Figure 36. Exploded View of the Experimental Setup Assembly .....52

Figure 37. First 7 minutes after droplet emergence in the channel .....52

Figure 38. Minutes 7-17 after droplet emergence in the channel .....53

Figure 39. Image sequences before and just after slug ejection- a) Plain Channel (C1.1 a) b) One Grooved sidewall (C1.2 a) c) Both grooved sidewall (C1.3 a) .....55,56

Figure 40. Pressure Drop Signatures for: a) Plain Channels (C1.1 a), b) One Grooved Sidewall Channels(C1.2 a) .....57

Figure 41. Droplet Accumulation and Blockage after Slug 1 exits the channel- One Grooved Sidewall (C1.2 a) .....58

Figure 42. Droplet Accumulation and Blockage after Slug 1 exits the channel- One Grooved Sidewall (C1.2 a) .....59

Figure 43. Pressure Drop Signature- One Grooved Sidewall- Teflon Coating on Groove Tops (C1.2 b) .....60

Figure 44. Droplet-Sidewall Interaction (Both grooved sidewalls, C1.3, 0.5 m/s) ....61

Figure 45. Pressure Drop Signature- Both Grooved Sidewall, C1.3 .....62

Figure 46. Pressure Drop Signatures- Water Entry Upstream C2- Plain Sidewall Channel (C2.1 a) .....63

Figure 47. Pressure Drop Signatures- Water Entry Upstream C2- Both Grooved Sidewall (C2.2 a) .....64

Figure 48. Water Feature Size and Shape Transition- Upstream to Ejection (C2.1 a).....66

Figure 49. Both Grooved Sidewalls (C2.3a) - Top View Image Sequence (L-R).....66

Figure 50. Water Feature Size and Shape Transition- Upstream to Ejection (Both Grooved Sidewalls, C2.3) .....67

Figure 51. Peak Pressure Drop- All Channel Designs and Air flow velocities (Water Injection Near Channel Exit, C1) .....72

Figure 52. Pressure Drop Variation for Channels with One Grooved Sidewall (Effect of Teflon Coat on Groove Tops)- C1.3 .....73

Figure 53. Peak Pressure Drop- All Channel Designs and Air flow velocities (Water Injection Upstream, C2) .....74

Figure 54. Comparison of Theoretical Predictions with the Experimental Data Showing the Variation of Grooved Surface Contact Angle with Plain Surface Contact AngComparison of Theoretical Predictions with the

Experimental Data Showing the Variation of Grooved Surface Contact Angle with Plain Surface Contact Anglee .....81

Figure 55. Slug Motion Speeds- C2.1 (a), C2.2 (a) and C2.3 (a) .....83

## LIST OF TABLES

Table 1. Experiments for the Proof of Concept .....26

Table 2. Operating Flow Conditions used for Testing .....35

Table 3. Summary of Droplet-Sidewall Interaction Results- Plain Sidewall (C1.1 a) .....47

Table 4. Contact Angles of All Channel Surfaces Tested .....48

Table 5. Summary of Droplet-Sidewall Interaction Results- One Grooved Sidewall (C1.2 a) .....54

Table 6. Summary of Droplet-Sidewall Interaction Results- Water Injection Upstream (C2.1, C2.2, C2.3 a) .....68

## NOMENCLATURE

1. PEMFC- Proton Exchange Membrane Fuel Cell
2. $W_P$ – Groove Pillar Width
3. $D_G$ – Groove Depth
4. W- Groove width
5. CA- Contact Angle
6. $\theta_A$ - Static Advancing Contact Angle
7. $\theta_R$ - Static Receding Contact Angle
8. $\frac{\partial P}{\partial y}$ - Pressure difference along the liquid filament.
9. G(A) - Geometry-dependent factor along the flow-field (grooves)
10. ΔP - Pressure Drop across the channel feature
11. s- Seconds
12. min- Minutes
13. Stoich- Stoichiometric Ratio
14. GDL- Gas Diffusion Layer
15. $\gamma_{SV}$ – Surface Tension at the Solid- Vapor Interface
16. $\gamma_{SL}$ – Surface Tension at the Solid- Liquid Interface
17. $\gamma_{LV}$ – Surface Tension at the Liquid-Vapor Interface
18. ΔE – Energy Gradient

# 1. Introduction

## 1.1. Alternative Powertrains and Environmental Concerns

The last few decades have been significant in terms of bringing attention to the drawbacks of non-renewable sources of energy. Multiple options to derive energy apart from the non-renewable ones such as coal, oil, gas and wood have been on the horizon for quite some time. Many nations across the world focused their energy policies based on the rise of these alternative sources of energy including solar, wind, tidal, geo-thermal, biomass and algae. The need of these sources concerned many as the proofs of global warming and climate change started taking its toll and was addressed at global summits of nations. This accelerated a growth of renewable energy sources led to economic investments and thus good research. Applications of energy involve important needs of day-today human lives. Power for businesses, homes and transportation were the very firsts that needed to be addressed. Automobiles were discovered at the dawn of the 19$^{th}$ century and brought a great revolution. Gasoline and diesel powered engines currently run most of the vehicles – roads and highway (commercial and consumer), railway locomotives, aviation, shipping and industrial vehicles.

However the source of gasoline and diesel is oil which has limited reserves world over and mainly concentrated in certain regions of the world. This leads to tremendous foreign investment and dependence on other economies for energy. Therefore, the research and development of power sources to run engines and vehicles was triggered and has been nurtured over the years by almost all automotive manufacturers and United States federal agencies, organizations and national laboratories. Simultaneous research efforts in the field of fuel economics, environment and effects of carbon and green-house gas emissions have directed

research in the field of alternative Powertrains. Lithium-ion batteries, hydrogen fuel cells, CNG and hybrids of one of these technologies with gasoline have been the prominent options that have proved successful technologically and commercially. There are however, certain limitations to their full-scale commercialization as phasing out of gasoline powered vehicles will take time and will be happening step-by-step. The US Department of Energy directives suggest the process to be completed by the end of year 2035. The phases however, are defined every five years in terms of well –to-wheel efficiencies and a few other parameters (emission standards) to monitor the powertrain performance. Regulations are also laid by the US Environmental Protection Agency (EPA) which defines carbon emission standards.

Hydrogen can be derived from any hydrocarbon and the process is relatively clean and economical. There are many types of fuel cells such as Solid Oxide, Alkaline and Polymer Electrolyte or Proton Exchange Membrane Fuel Cells (PEMFC). The PEMFCs are ideally suitable in the transportation sector. They are lightweight, low temperature fuel cells with no moving parts. This reduces complex systems involved with other fuel cells and makes a good combination for use in automotive vehicles. Fuel cells have multiple other advantages such as least $NO_x$ emissions compared to US national power grid average, reciprocating and internal combustion engines and turbines. The IC engines have an overall efficiency as poor as 18-20%, while PEMFCs on the other hand can have an overall efficiency of up to 65-80% depending on the combination of systems it has been coupled with to make the powertrain or stationary power system.

## 1.2. Proton Exchange Membrane Fuel Cells (PEMFCs)

A PEMFC is an electrochemical system that utilizes Hydrogen gas and Oxygen from air to react in a chemical reaction to produce electric current and liquid water as the reaction product. The reaction takes place in an electrochemical system that consists of two electrodes, a polymer electrode membrane assembly with a catalyst layer where the chemical reaction takes place. The Cathode and Anode are separated from the catalyst layer by a porous diffusion medium known as a Gas Diffusion Layer (GDL) which is made of carbon fibers. This layer is responsible for the diffusion of reactant gases into the cell-catalyst layer and membrane-electrode assembly. The polymer electrode conducts only protons due to its chemical and physical properties enhanced by the Platinum catalyst layer. Due to this property, Hydrogen gas from the Anode is separated to $H_2$ ions and electrons as it moves through the cell assembly. Oxygen from the Cathode combines with these $H^+$ ions in the form of $O_2$ ions to form water and heat. The Hydrogen gas is separated into its ions and electrons which are conducted by the circuit connected across the two electrodes. Electric load can be connected here to utilize the current thus produced. These cells are connected in stacks to form power units that can supply energy for the motion of the electric motors that run the drivetrain or wheels in an automotive application. These cells are low temperature units that work at 50-100$^o$ C. This is an advantage as high temperature hazards are avoided and hence make it ideal for even space applications, which utilized the Alkaline fuel cells developed earlier which have multiple technical difficulties. A PEMFC thus has a constant output in the form of water. This water generation process can be correlated to the rate of chemical reaction and the amount of reactants consumed. Figure 1 below shows the PEMFC structure with all important components.

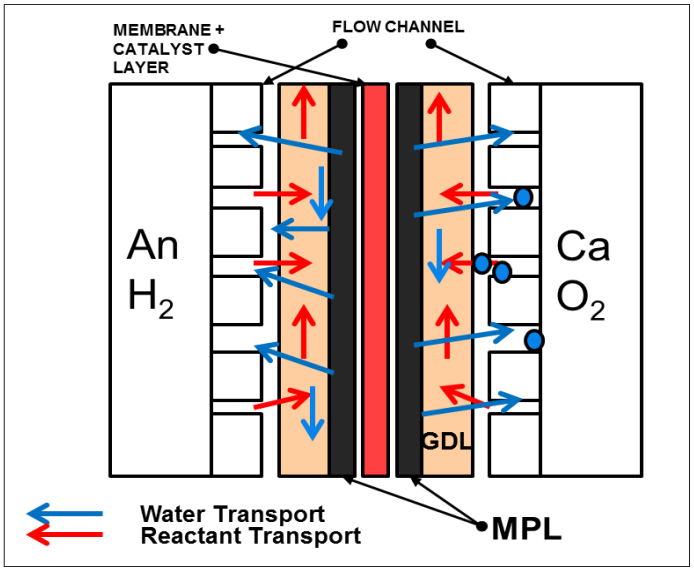


**Fig. 1.** PEMFC Construction and Mass Transport

As shown in Figure 1, gases travel from the electrodes to the gas diffusion medium which transport it to the reaction surface. Thus water is produced as a result of the on the GDL-channel interface at the Anode side as shown due to the chemical reaction taking place on the catalyst layer inside the cell. Apart from this reactant by-product water, the humidified reactant gases are supplied to the cell to improve cell chemical reaction kinetics and also avoid dryout of the membrane. Membrane dryout can cause severe issues in the PEMFC including permanent breakdown. These humidified gases condense in the flow field as they travel, due to the lower temperatures of the air flow in the channels. This causes more water droplets to be formed and accumulated in the channels. This complicates the water management issue further. However, it is essential that reactant gases are humidified to a certain extent as membrane and cell dryout has adverse effects that could even lead to cell breakdown and hence needs to be avoided.

## 1.3. Bipolar Plate and Fuel Cell Channel Design Constraints

Fuel cell assembly usually consists of different components that include compression plates, bipolar plates, insulation gaskets, Silicon gasket, diffusion media (GDL), current collector plates and MEA (Membrane Electrode Assembly) which are assembled in order. A bipolar plate consists of microchannels that carry the reactant gases to the diffusion media and effectively to the gas diffusion layer. Bipolar plates usually go between the diffusion media and the MEA. There is a border gasket around the plate. The bipolar plate is usually made from sheet metal in the required size by blanking. It further is either cold forged or drawn to form the channels. Channel cross-sections can be of different shapes such as rectangular, circular, trapezoidal and triangular. This shape has an effect on the water accumulation in the cell, essentially on fuel and oxidant flow rates. The wetting behavior or hydrophobicity and hydrophilicity of channel walls and the GDL also have an effect on the water behavior. Thus the channel and stack design are not only crucial for the fuel cell as essential component design, but it affects the total size of the fuel cell, the flow rates, pressure drop, extent of structural support, heat and water generation. Thus it has a significant impact on fuel cell performance overall. For designing and manufacturing the fuel cell stack factors such as channel dimensions, shape and orientation, material selected and methods for assembling the cell components together are important as the ultimate challenge is not only have a highly efficient stack but a stack design that can be mass produced. Figure 2 shows a bipolar plate having microchannels fabricated on a graphite plate. The studies in this work are carried out at a larger scale, considering the challenges in the optical visualization of the small channels as in Figure 2. Figure 3 shows the steps in manufacturing a commonly used bipolar plate using stamping.

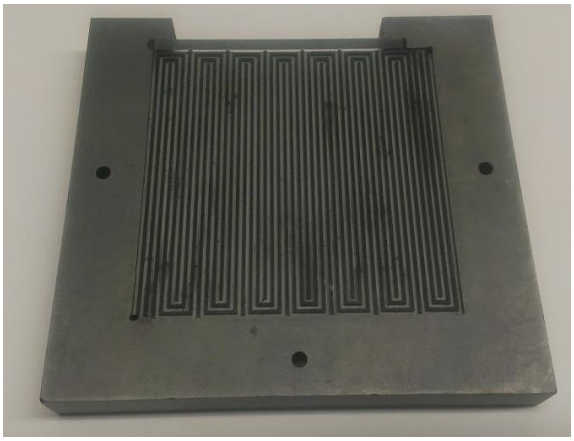

**Fig. 2.** Fuel Cell Graphite Bipolar Plate

Fuel cell channels are constructed in a metallic base plate known as bipolar plate. This plate can be manufactured using multiple techniques and multiple materials. For fuel cells having active area (> 1 $cm^3$), metallic bipolar plates are made from materials like Aluminum, Stainless steel, Titanium, Nickel and Carbon composites. The standard method for forming solid metallic bipolar plate designs is machining or stamping.

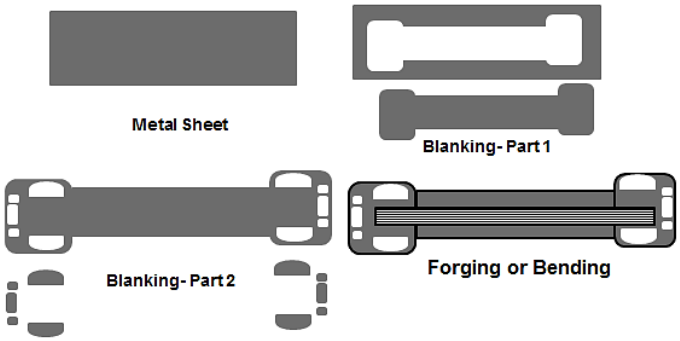


**Fig. 3.** Stamping Process for Bipolar Plates

Extensive research in cold-closed die forging, die-casting, investment casting and electroforming to manufacture metallic bipolar plates for fuel cells is being pursued. Stamping is currently the most widely used manufacturing process for manufacturing bipolar plates, which has been the

primary consideration for this work. Apart from stamping, the channel designs proposed in this study can be easily manufactured by die casting and cold-forging.

### 1.4 Water Management in PEMFC and Effect of Channel Geometry

A PEMFC usually is 40-60% efficient depending on multiple parameters. The main losses in the PEMFC system are fuel crossover loss, mass transport loss, activation loss and Ohmic loss. It can be illustrated in Figure 4 which shows a V-I curve or operational curve that illustrates cell performance and losses.

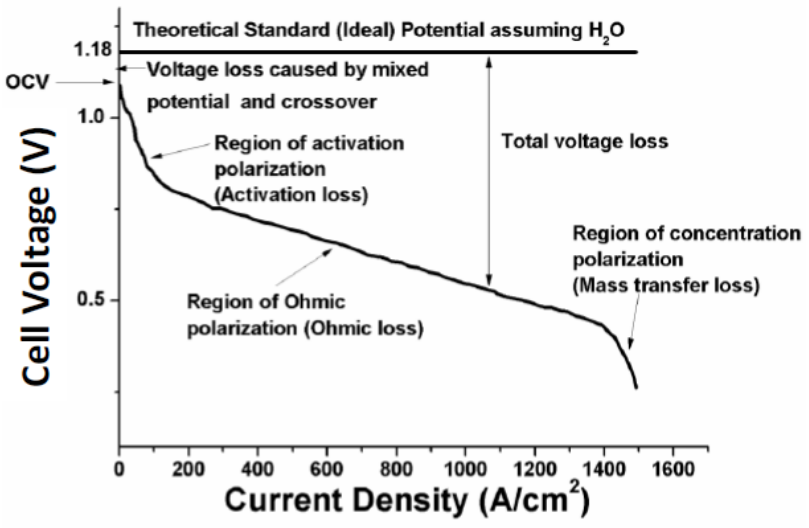


**Fig. 4.** V-I Curve of a PEMFC showing the different losses that occur during the working cycle, Adapted from [1]

The presence of water inside the fuel cell is necessary to keep the polymer electrolyte hydrated. Working of the fuel cell is by the conduction of protons through polymer membrane from the anode to the cathode. At the same time, the other cell half reaction produces electrons which travel across the circuit connected between the two electrodes. Cell power output performance

depends on the amount of electron flow in the system. The flow of electrons in the circuit is equivalent to the conduction of protons through the membrane. However, proton conduction is dependent on the water activity in the membrane. High amounts of water generated in the Cathode leads to the gas channel flooding. To achieve efficient removal of the liquid water from the gas channel, blowers are used to provide excess gas flow in the flow field. However the solution to water clogged channels cannot be blowing all the water away at high air speeds as it will result in drying out of the membrane. External humidification of reactant gases is then necessary to keep the membrane supplied with adequate water which increases the cost in terms of power losses and complexity of the system with added auxiliaries such as the external humidification system and its control system. With alternative systems, the membrane will be able to absorb the water produced by the electrochemical reaction and external humidification can be eliminated. Under normal operating conditions, water generation can be substantial enough to saturate the fuel cell and cause accumulation of liquid water in the flow channels. This causes uneven distribution of reactant gases from the flow channels to the diffusion media as water covers the GDL partially at different locations along the channel which can lead to high potential gradients can be created as areas of local reactant starvation are formed and the degradation of the catalyst material can also be accelerated.

Engineering the fuel cell for effective water removal the channels is a better approach to resolve these problems. The ability to make significant improvements over the conventional fuel cell channel design requires (1) a thorough understanding of the fundamental physics of water droplets, GDL and channel wall interactions at different PEMFC operating conditions and (2) Effect of channel geometry and channel surface modifications on the water removal from the gas channel. This is the major motivation of this work.

# 2. Literature Review and Motivation

## 2.1. Effect of Channel Geometry and Flow Field Dimensions and Geometry on Fuel Cell Performance

The Proton Exchange Membrane fuel cell consists of a flow-field which is basically a set of microchannels having dimensions of the order of ~400 to 700 micron. This flow field is responsible for carrying the reactant gases from the inlet manifold to the catalyst layer and then to the electrode where the reaction actually takes place. These channels also cause water removal from the flow field. There is a porous medium known as the gas diffusion layer that transports reactant gases from the channel to the electrode which is compressed together onto the flow field. This flow field is therefore an important structural feature of a PEM fuel cell and there has been abundant research based on the same. Multiple geometries and their different orientation and its effect on reactant gas delivery, associated pressure drop has been studied in detail.

There are also certain other studies which focused on simplifying the domain of interest and bringing these studies of pressure drop, water feature interaction to the level of a single channel. These involve scaled artificial channels that represent the problem domain of a single microfluidic channel of a fuel cell flow field. There are studies based on single channel that focus on the water droplet-sidewall interaction, force balance for the droplet under shear force due to gas flow in the channel and surface tension due to the porous medium. As the problem simplification diminishes the problem domain from a flow field, it also brings out the complexities involved in these engineering scenarios. The complexities can be mainly divided into categories of electrochemical, microfluidic and material science and engineering. Theodorakakos et al. [2] were one of the very first few authors which brought this into light.

They did an experimental and parametric study based on important parameters in terms of microfluidics and fuel cells. It involved droplet diameter, air velocity and droplet entry location in accordance to their microfluidics focus and they changed the diffusive porous media and channel material quality to see the effect of different fuel cell materials. It was observed and established by the numerical model and experimental results that droplets are removed at slower velocities when in contact with the channel sidewall, porous base surface and top surface, as compared to droplets that are just in contact with the porous medium base surface. It also stated that, if the water droplet is placed in a channel that has a sidewall having different and lesser contact angle than the porous material it is in contact with, indicates imbalance of adhesion forces between the two faces and the resultant action is liquid motion towards overall smaller adhesion force in the direction of the flow, implying faster droplet removal. This suggested motion of droplet from the sidewall to the GDL as the sidewall is hydrophilic in nature and the porous medium or the GDL is hydrophobic, however this is not an advisable condition in a fuel cell and hence having plain hydrophilic sidewalls has its own disadvantages.

Theodorakakos et al. [2] have also mentioned in their work that when in contact with the sidewall in a PEMFC channel, the droplet has a more cylindrical shape (film) than a spherical shape. This was a result of their numerical simulations which were carried out by the Volume of Fluid (VOF) method for a given size of droplet and air flow velocity. The Navier-Stokes' equation based model thus implies that film or cylindrical water features are thus produced in a cell channel if there is an imbalance of adhesion forces. The simulations showed that the adhesion force on the porous medium is larger than forces acting on the water at the top surface. This may lead to a complete detachment of droplet from the GDL, which proves to be the ideal

scenario for a fuel cell as it improves gas transport and reduces two-phase pressure drop. The cases of droplet presence that were investigated in this work are shown in Figure 5.

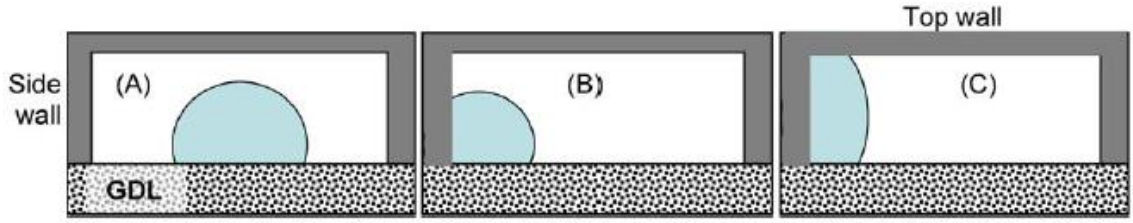


**Fig. 5.** Cases of Water Droplet Injection in a PEMFC Channel: A) Droplet in contact with GDL base (slow removal) B) Droplet touching GDL and sidewall (faster removal) C) Droplet touching GDL, sidewall and Top Wall (Fastest removal) [2]

Previous work by Lu et al. [3] and Zhu et al. [4] indicated PEFC performance to improve if sinusoidal, triangular or trapezoidal channels are used instead of rectangular channels. This was quantified and proved further by Rath and Kandlikar [5] and Gopalan and Kandlikar [6] that trapezoidal channels work better compared to triangular channels considering their feasibility in terms of experimental fuel cells. Rath and Kandlikar [5] used Concuss- Finn [7] condition to prove that for two surfaces making an angle of $52^{o}$ and lower would lead to pinning and thus then corner filling. The modified Concuss- Finn condition is shown in Figure 6. The region marked by 'R' shows the area in which if, the static and dynamic advancing/receding contact angles lie, it fills the interface created by the two walls making the angle. Thus there is a solution for points falling in 'R'. The other four regions marked by $D_1^+$, $D_1^-$, $D_2^+$ and $D_2^-$ do not have a solution. [5]

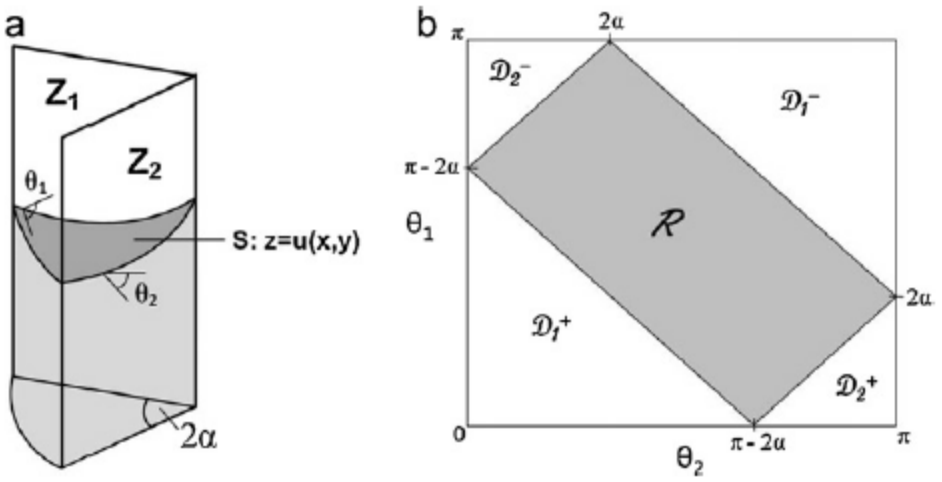


**Fig. 6.** Concuss-Finn Condition (a) Image of Concuss-Finn Wedge Container Modeled and (b) Plot of Concuss–Finn Condition for Wedge Container Reproduced from [5]

Gopalan and Kandlikar [8] extended that work with studies of effect of air flow in the channel and proved the same results. It was found that the sinusoidal channel had a lower pressure drop factor than the rectangular and trapezoidal channels for all water velocities studied [9]. There are certain limitations in manufacturing sinusoidal channels whereas trapezoidal channels are easier to manufacture. Gopalan et al. [6] conducted multiple experiments with different trapezoidal channel angles for best performance in terms of two-phase pressure drop and corner filling or non-filling characteristics by water droplets. It was established that $50^{o}$ channel angle represents the transition angle between corner filling and non-filling behavior for a given set of fuel cell air flow and water flow conditions. Thus it was recommended to use $50^{o}$ trapezoidal channel for good performance over the entire range of flow rates. This has been acknowledged and established by the Department of Energy and General Motors. [10]

Multiple benefits of trapezoidal channels and its proven behavior by manufacturing with common fuel cell materials, if fuel cell performance is to be further improved in terms of water

drainage, engineering techniques such as surface modifications and roughness manipulations need to be considered. Trapezoidal channel geometry was modified further by implementing a capillary channel on top of the triangular shape by Metz and co-workers [11]. The triangular channel lifts the water from the GDL and it is pulled up to the secondary channel due to the capillary effect. A flow-field having the hybrid geometry of triangle and a capillary was proposed, manufactured and tested by Metz et al. [11]. Figure 7 shows the schematic of the proposed channel design geometry, it also shows contact angles being measured and other dimensions of the geometry- width, depth and height.

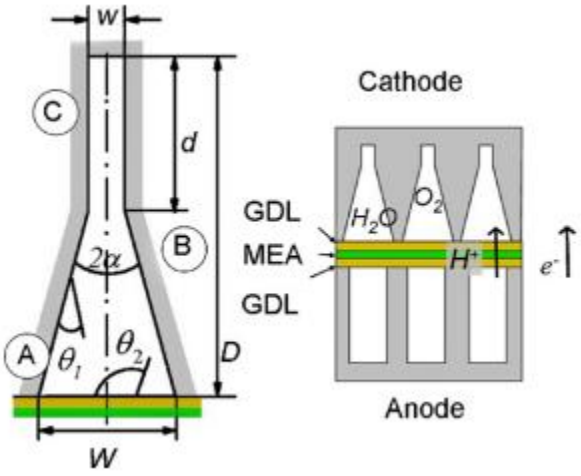


**Fig. 7.** Schematic of Channel Design and Integration in Fuel Cell Flow Field- Passive Channel- Triangular and Capillary Channel [11]

The second part of the Figure 7 shows integration of channel designs in a PEMFC flow field including the porous medium and MEA. It also illustrates the direction of fuel cell particles.

## 2.2. Microchannel Modifications for Better Water Removal Characteristics

Surface coatings which promote certain type of wetting behavior are also attractive in improving water removal behavior. Sommers et al. [12] developed a correlation between the critical velocities of air required for a droplet to move on a micro-grooved patterned surface designed to enhance its drainage on a condenser surface. They observed that for plain grooved sample, the velocities were higher than the baseline sample without grooves. However, when they coated the grooves with PDMS, which provides a hydrophobic surface, the critical removal velocities were reducedby an average of 15% for small droplet volumes (<10 μL). The results suggested that surfaces having micro grooves and coating possess an ability to prevent the droplet to move along the stream and eventually get pinned, but improved drainage along the channels. This contribution is valuable in general as well, considering application of micro-grooved surfaces to water management in fuel cells and other heat transfer devices for condensate management. Chen et al. [13] asserted the fact that surface roughness amplifies the water repellency of hydrophobic surfaces. Their numerical and theoretical work led to the conclusion that multiple equilibrium shapes that a droplet can possess on a grooved substrate and repeatability of this shape can be obtained by deciding the number of pillars on which the drop resides. Baret et al. [14] have discussed previous literature which dealt with grooves having triangular geometries. Due to dynamic instability which causes isolated drops instead of elongated droplets or films in such grooves. They could thus be never drained by capillary forces from these grooves. Hence, rectangular grooves were suggested for capillary based water removal and drainage.

Rahman et al. [15] have discussed the effect of droplet shape on water drainage from a grooved surface and effect of geometrical parameters like groove depth, pillar width and a

factor known as solid fraction ($W_P/W_P+D_G$) Where $W_P$ is pillar width and $D_G$ is groove depth. They indicate that in order to remove water easily from a grooved surface, the grooved surface should be designed such that groove width to pillar width ratio is > 0.2 (Reciprocal of Scaling Factor developed by Bhushan et al. [16]) And at the same time pillar width shouldn't be large such that solid fraction is too large, as solid fraction increases both contact angle hysteresis and sliding angle. Groove parameters discussed in [15] are shown in Figure 8.

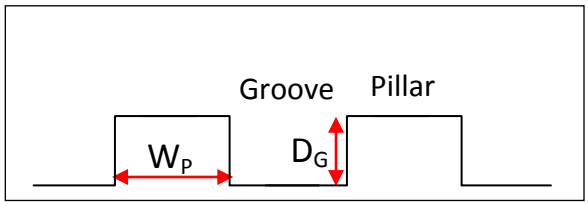


**Fig. 8.** Grooved Substrate- Parameters Studied in [15]

Rahman et al. [15] also recommend a Cassie [17] wetting regime for better water shedding and hence recommend a groove dimension design as per that for better water drainage. In another work by Gopalan and Kandlikar [18], different micro-groove patterned surfaces below 100 μm were discussed and their wetting behaviors and transitional wetting regime were analyzed in detail. From their analysis, they predicted that certain micro-grooved surface enhancements can improve water droplet removal process in a gas channel in applications such as a PEM fuel cell. This work was targeted at quantifying the dependence of water behavior on various parameters related to grooves. The land width had no effect on the wetting behavior but the channel width and depth contributed to deciding the wetting behavior and the transition from Cassie wetting to Wenzel [19] wetting surfaces. It also identified that some surfaces lied in the transition region and could not be clearly identified as any one of the two. The grooved pattern that was chosen to be used in the PEMFC microfluidic channel application was suggested to have the Wenzel

regime as it would help in absorption of water from the base porous media and carried to the top wall or forced to cling more to the sidewall and eject instead of being pinned to the GDL. Figure 9 shows the Wenzel and Cassie-Baxter wetting characteristics on a grooved surface.

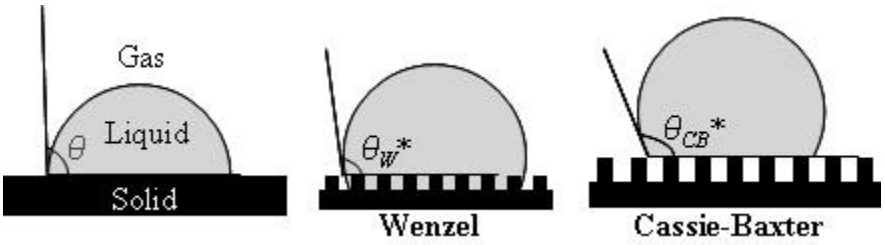


**Fig. 9.** Wetting Regimes on Grooved Substrates- Wenzel ad Cassie-Baxter adopted from [19]

The PEMFC channels face the issue of accumulation of water droplets at the edges and at the corner (sidewall-base) interface. Having established an understanding of how grooved surface morphology can affect the surface wetting, modifying channel surfaces using micro-grooves to achieve desired roughness and wetting properties was proposed. The primary aim was handling the problem of corner water accumulation when water enters the channel at a location very close to the sidewall or there is water emergence under the land [20] region through the Gas Diffusion Layer. The scaling factor method developed as a part of this work was used to predict the wetting phenomenon on a grooved surface for a PEMFC application.

Further investigation of the grooved substrates for directional wettability includes a study by Wang et al. [21] which had detailed discussions about the individual and combined wetting due to micro-grooves bearing Cassie and Wenzel roughness. It suggested that the wetting regimes observed under static conditions may not hold true during drop motion and that is when it tends to possess both wetting regimes simultaneously. Another important finding of this study was about the characteristics of droplets in Wenzel wetting regime. It was established in case of

metallic grooved surfaces that drops in Wenzel wetting state are more elongated than Cassie-Baxter wetting state. In this work, this finding of Wang et al. is highly significant, its relevance and correlation to the surfaces designed and tested in this work will be evident in the following sections. An important observation by Cheah et al. [22] is about hydrophilic sidewalls in a PEMFC channel was that the upstream contact lines never get detached and thus form films. This observation was for plain rectangular channels having hydrophilic surface wetting behavior. In their experiments, water was injected in the channel using syringe pumps in sessile or pendant droplet manner. The location of droplet entry was at the channel center. If the behavior by droplets converted to films is repeated or not needs to be validated and hence is carried out in the later part of this study. A second approach to testing the under the land and corner injection of water and its effect on flow characteristics is thus designed, tested and presented in later sections.

Hu et al. [23] established a force balance model for a droplet under air-flow shear on a micro-grooved surface, when exhibiting Wenzel mode of wetting. They found a linear relation between capillary force '$F_C$' and driving force exerted by shear flow (air flow) '$F_D$' is linear. This relationship was when the micro-grooved surface was kept horizontal and water droplets were allowed to flow over it in parallel and longitudinal direction with respect to air flow.

Previous results from Kumbur et al. [24] indicate that surface adhesion or surface tension force due to GDL in a PEMFC depended on the droplet aspect ratio (h/c) where 'h' was droplet height and 'c' was the chord length of the droplet in contact with the GDL. The relations from their force balance model and their graphical results proposed that surface tension force was proportional to 'c' and drag force was proportional to '$h^2$'.

## 2.3. Assumptions made in past PEMFC Channel Studies

Water entry in the PEMFC channel is governed by two main mechanisms: a. Dynamic Interconnected Pore network in the Gas Diffusion Layer [24] and b. Channeling by capillary action in the GDL [25]. There are passageways present within the fuel cell porous diffusion media [26]. Due to a differential in the capillary pressure between the catalyst layer and gas flow channel, water is forced to be drawn from the porous diffusion media. As hydrophobic porous media (GDL) pores are filled by the liquid water coming from the reaction on the catalyst, the liquid-phase pressure increases, eventually driving the liquid water from higher to lower pressure regions.

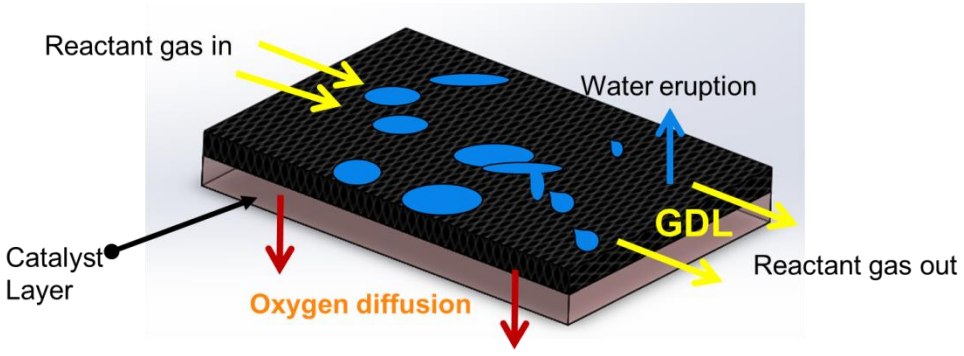


**Fig. 10.** GDL Mass Transport

This creates a saturation gradient across the diffusion media. In an actual operational PEM fuel cell, the higher saturation generally occurs in the catalyst layer after the chemical reaction produces liquid water, and it decreases in the flow channel, implying that capillary transport takes place from high- to low-saturation regions in the GDL.

This is the only governing mechanism that has been identified by researchers for water emergence in the cell flow channel. Further efforts for modeling the pore network and capillary action led to the understanding that water features can emerge along the entire channel length and width. However there will be a preferential pore network produced once the phenomenon keeps repeating and this can lead to water emergence at the given locations for a long time. [25] Figure 10 shows the GDL mass transport process, gas flow and diffusion directions in a PEMFC channel.

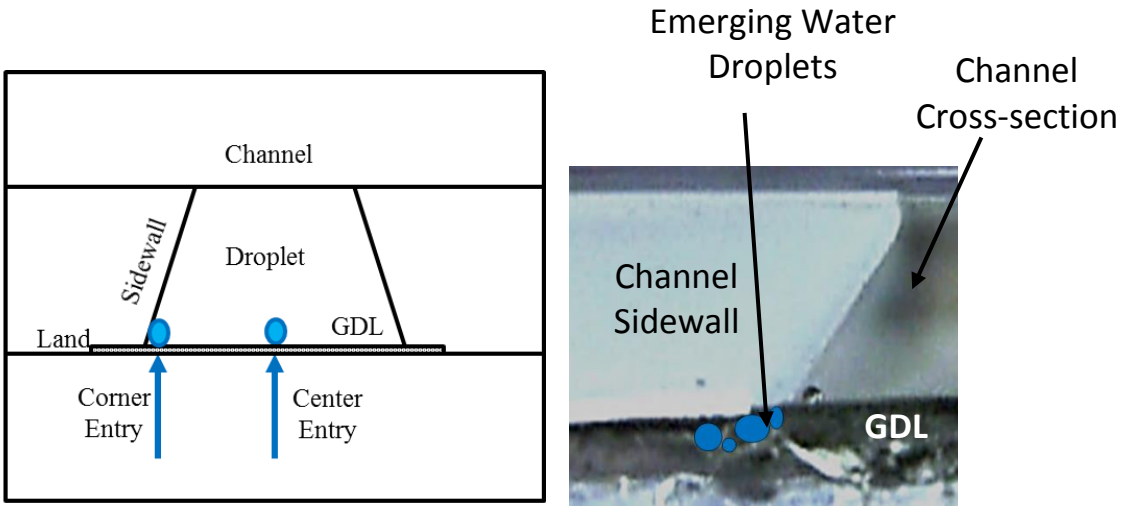


**Fig. 11.** Channel Geometry and Water Droplet Entry Locations

However, it is not guaranteed that it will be at the channel center. Other fluid and physical conditions do not promote this behavior either. There are studies that investigated the effects of water generation on the fuel cell performance in the different parts of a fuel cell channel and manifold.[20] Thus, the droplet sidewall interactions when water enters at the channel corner and under the land are essential for investigation. Preliminary efforts were done by Gopalan et al. [6] in 2012. Figure 11 shows the locations that are under consideration for droplet entry for a trapezoidal channel. It represents a single microfluidic channel in a PEM Fuel Cell flow field. It

was observed by Gopalan et al. [6] that when water enters the channel from a corner (about 0.5mm away from the sidewall), it does not follow the corner filling non-filling criteria established using the Concuss-Finn condition for water entry at the channel center.

The main assumptions made in previous literature that neglect certain flow conditions in a PEMFC channels and hence need attention are listed below:

1. Water entry in the channel at the center along the flow axis for all operating conditions in a PEMFC.
2. Effects of water eruption in the channel on the filling and non-filling characteristics at the channel exit and droplet-sidewall interactions.
3. Effect of corner and land water eruption on two-phase pressure drop and flow characteristics.
4. Effect of water generation along the entire channel length and its effects on GDL coverage and two-phase pressure drop in a trapezoidal PEMFC gas flow channel
5. Effect of channel sidewall surface modifications on flow and drainage characteristics.

## 3. Objectives

As observed from literature and work done so far, it has been recognized that modifications to the channel wall will improve water management performance of a PEMFC gas channel. The grooved surface changes the hydrophilicity of the PEMFC channel walls. This would prove crucial to the issues identified in water droplet pinning at channel exit near the edge into the channel manifold. Plain hydrophobic and plain hydrophilic surfaces have their own disadvantages for different channel shapes and sizes for a PEMFC. A review of the existing literature, in regard to the channel modifications, has been conducted and presented in the previous section. From the review, it can be seen that significant work has been done to improve the water removal characteristics. For better PEMFC performance, a minimal area of the GDL is to be covered with liquid water. This has led to the following objectives for current work.

1. Design channels with surface modifications in the form of micro-grooves which help in draining the water droplets out of the channel when water enters the channel near the sidewall or under the land region in a PEMFC channel reduce pinning of droplets near channel exit.
2. Experimental validation and analysis of artificially induced drainage behavior of micro-grooves on sidewalls of PEMFC gas channels.
3. Once water starts accumulating in the channel, channel surface modifications producing artificial pinning sites upstream the channel that prevent water from spreading on channel base surface and water features are contained to channel walls.
4. Development of an active water management strategy to reduce water blockage in PEMFC gas flow channels.

## 4. Approach

Experiments that were carried out in this work focused primarily on the phenomenon of emergence of water droplet at a point very close to the channel sidewall. In all previous works as mentioned above, it was assumed to be entering at the channel center. However, water entry in the PEMFC channel is governed by two main mechanisms: a. Dynamic Interconnected Pore network in the Gas Diffusion Layer and b. Channeling by capillary action in the GDL [24, 25]. There are passageways present within the fuel cell porous diffusion media [26].

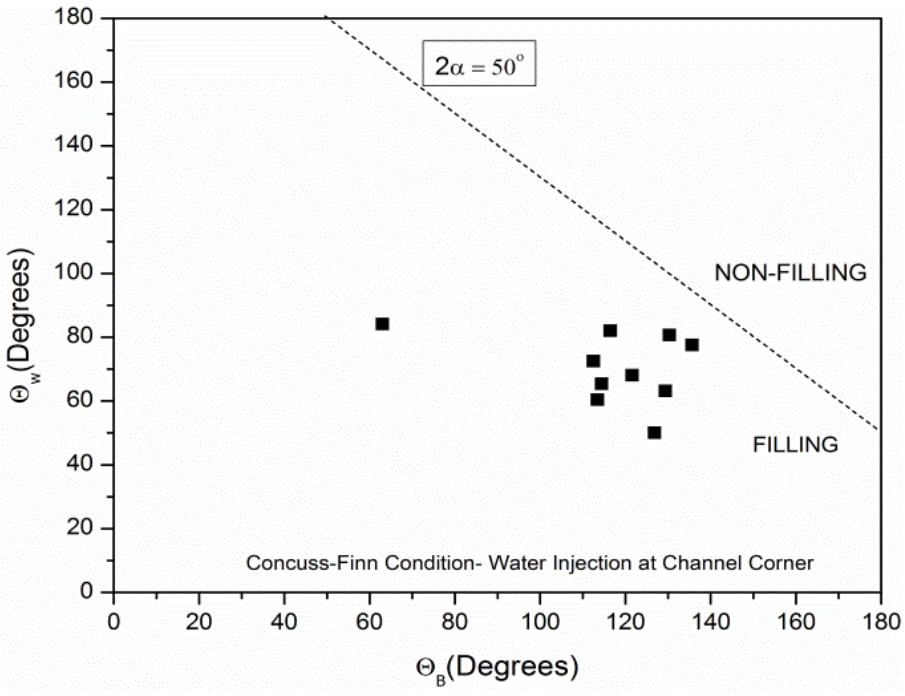


**Fig. 12.** Concuss-Finn Plot, Water Injection at Channel Corner- Filling and Non-Filling data points

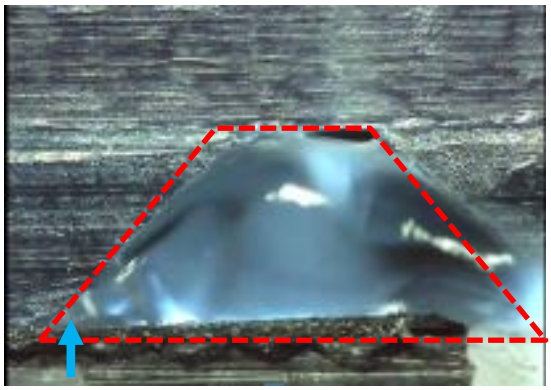

**Fig. 13.** Droplet Filling when Water is Injected at Channel Corner

It was observed by Gopalan et al. that when water enters the channel from a corner (about 0.5mm away from the sidewall), it does not follow the corner filling non-filling criteria established using the Concuss-Finn condition for water entry at the channel center. It is evident from the plot shown in Figure 12. Tests were carried out with water injection at 0.5-0.7 mm away from the sidewall in a trapezoidal channel to obtain the data points in Figure 12. The Figure 13 adjacent to it shows how a droplet entering from the corner completely fills the channel. This behavior of the fuel cell trapezoidal channels having angle $50^{o}$ indicates that certain design changes need to be made to the channel that will promote better water drainage for this condition. Prior literature suggested use of surface enhancements such as chemical coatings and microchannels or micro-groove patterned surfaces which assist and ease the liquid drainage process. The surfaces under consideration here have micro-grooves of dimensions 150 μm x 200 μm on the sidewall near the channel exit. It is first characterized using the contact angle measurements. The groove-droplet behavior when subject to water droplet entry is then documented in the experiments with detailed visual observations about the capillary rise behavior.

## 4.1. Design of Setup

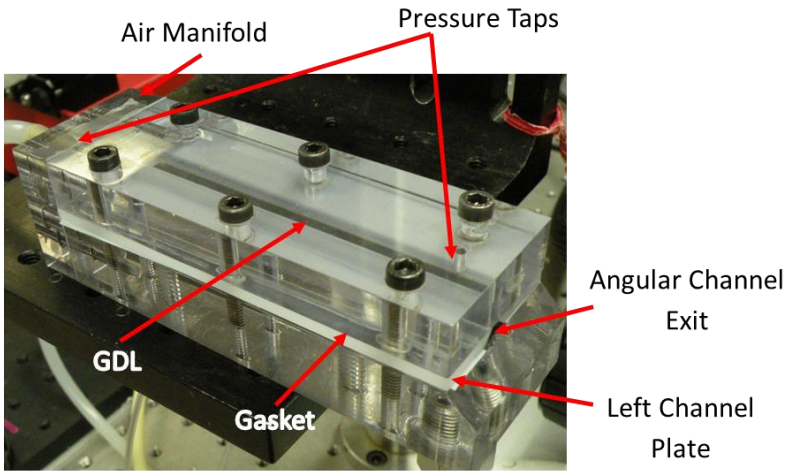


**Fig. 14.** Ex-Situ Experimental Section Assembly Parts

The setup developed for and used in this work is shown in Figure 14. It consists of four different plates made from Lexan that form the channel walls and an air manifold at the back as shown. The channel plates are 101.3 mm long and can be bolted together for forming the channel. The channel cross section is trapezoidal with an angle of $50^{o}$. The dimensions of the cross-sections of the trapezoidal channels are 3 mm height x 8 mm width. The shorter width of the channel at the top is about 4 mm. The air manifold is a square of 19.05 mm x 19.05 mm size. The channel walls in this setup are plain acrylic having contact angle of $52^{0}$ which is hydrophilic. Channel walls have traditionally been hydrophilic and channel base or the diffusion medium is hydrophobic. It is impregnated with PTFE to increase its hydrophobicity. This conventional channel had rectangular geometry in a PEMFC. However research has showed that $50^{0}$ trapezoidal channel performs the best in terms of two-phase flow characteristics and

pressure drop. Thus the same has been used as a basic channel design with additional surface modifications and coatings for the new proposed channel designs in this study.

This test setup has a base plate which defines the water entry location along the length and the width of the channel. For the second Configuration of work done in this study, effect of channel designs on water features more upstream in the channel away from channel exit were to be investigated. A new test setup was thus designed and manufactured. It was identical to the setup in Configuration 1 except the location of water injection in the channel along the length. The water injection hole of the equal diameter as configuration 1 was drilled at a distance of 76.2 mm away from the channel exit. This is 25.4 mm away from the air entry hole. This facilitates enough length for the water features to develop along the length of the channel from the point of eruption. Effect of channel surface modifications on these water features developed along the entire length of the channel can thus be studied. Figure 15 below illustrates the two setups manufactured with the distinction of water injection hole location in each configuration. Figure 15 a) shows C1 when water is injected near channel exit and Figure 15 b) shows C2 where water injection hole is upstream. The setup's components have been labeled in the figure. The bottom plate is the only component that has been changed for C2 from C1.

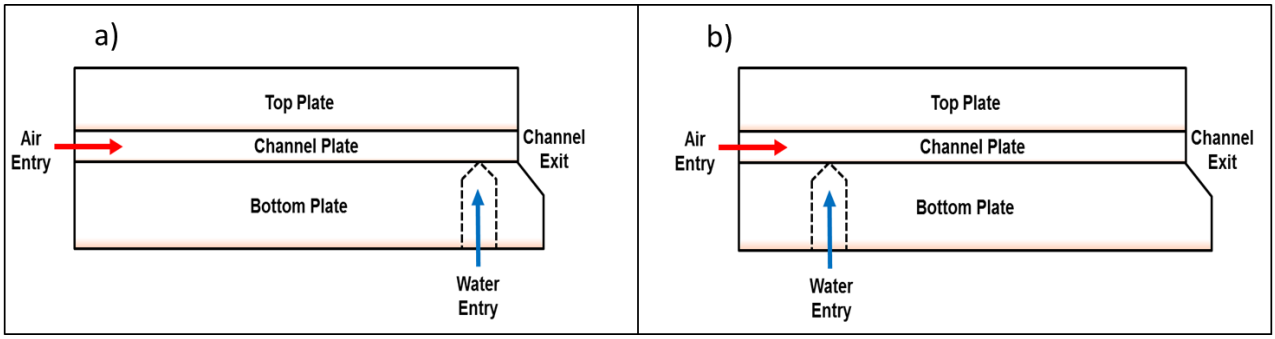


**Fig. 15.** Experimental Setups for a) Configuration 1 and b) Configuration 2

### 4.2. Grooved Channel Walls- Proof of Concept

In the following experiment, one on one comparison of plain trapezoidal channel and plain trapezoidal channel with grooves on the sidewall is presented. This served as the basic experimental proof that water is drained at a more quickly due to the presence of structured roughness on the channel sidewall. Configuration C1 was used to study the effect of grooves in this experiment. Images and description below illustrate the sequence of droplet-sidewall interaction at constant same air and water flow velocities. Time required for the droplet from eruption to ejection is measured and compared in Table 1. :

**Table 1: Experiments for the Proof of Concept**

| Sr. No. | Air Velocity (m/s) | Water Flow Rate (ml/min) | Sidewall Type | Time to Reach Top Wall (sec) | Time to Exit the Channel (sec) |
|---|---|---|---|---|---|
| 1 | 1.31 | 1.05 | Without Grooves | 73 | 64 |
| 2 | 1.31 | 1.05 | Micro-Grooved | 9 | 28 |

Droplet emerges under the land and touches the sidewall irrespective of the air flow rates or water flow rates (Stage 1). The channel-droplet interaction has been illustrated in Figure 16. These are the results from a single-run of experiments. However multiple experiments showing results that closely matched data shown here.

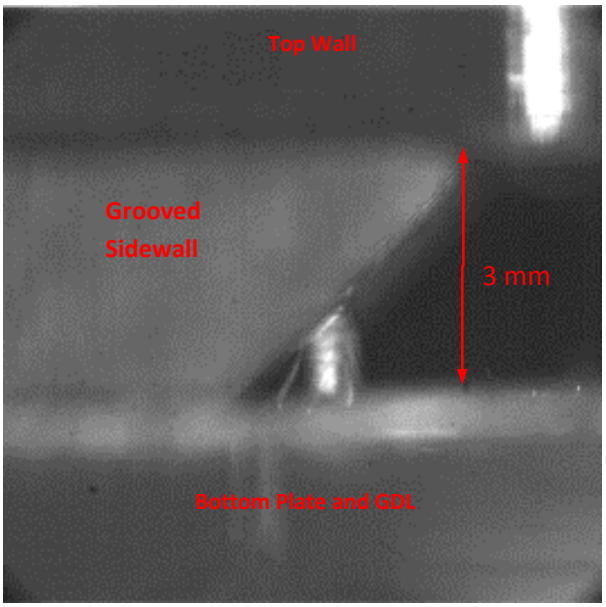


**Fig. 16.** Droplet-Grooved Sidewall Interaction- Stage 1

In both grooved sidewall and one without grooves, droplet keeps rising towards the top wall. (Figure 17). The droplet is shown rising along the sidewall in Stage 2 of the process as shown.

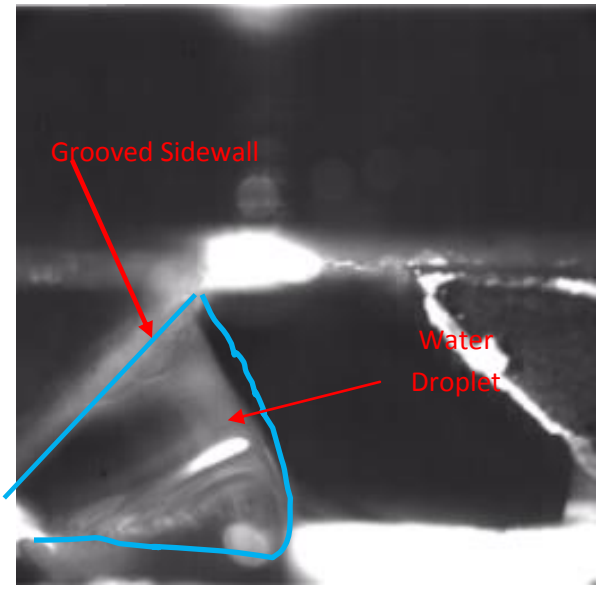


**Fig. 17.** Droplet-Grooved Sidewall Interaction- Stage 2

The droplet keeps growing and touches the sidewall very quickly and then it eventually jumps to the other wall which assists in exiting the droplet of water as illustrated by this sequence of images. (Figure 18) This has been described as Stage 3 of this water drainage process.

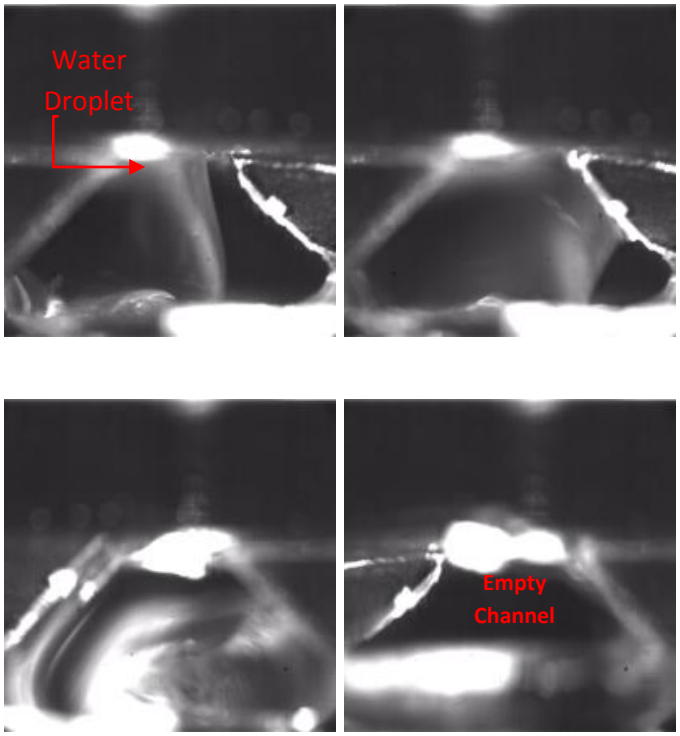


**Fig. 18.** Droplet-Grooved Sidewall Interaction- Stage 3

Figure 19 shows plain trapezoidal channel cross-section and the effect of air flow and time required for the droplet to eject.

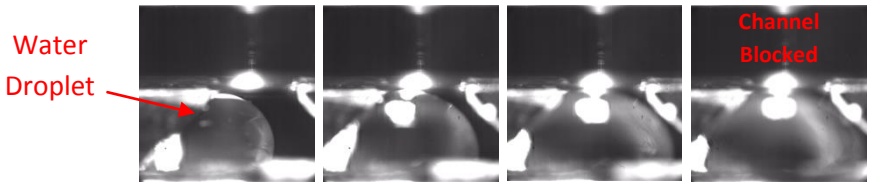


**Fig. 19.** Droplet-Plain (Non-Grooved) Sidewall Interaction

In Table 1, the time taken for droplet eruption to ejection for the two channel designs is drastically different. Another notable observation is that in case of grooves, the droplet is more stable and undergoes fewer fluctuations as it grows on the GDL surface. The microgrooves help in pinning the droplet to the sidewall and thus help reduce fluctuations. This pinning effect also avoids spreading of the water being generated. It can be thus concluded that microgrooves on the sidewall not only helped in quick removal from the GDL and avoid spreading of water droplet as it appears from under the land region in a PEMFC channel, but also a quicker removal from the channels with the aid of the top wall and the opposite sidewall.

### 4.3 Grooved Channel Design- Characterization

Further characterizing of the grooved channel surface is carried out using high speed visualization of water droplets emerging from the land region and the grooves on the sidewall. The grooves are visualized using a high-speed camera as shown in Figure 20.

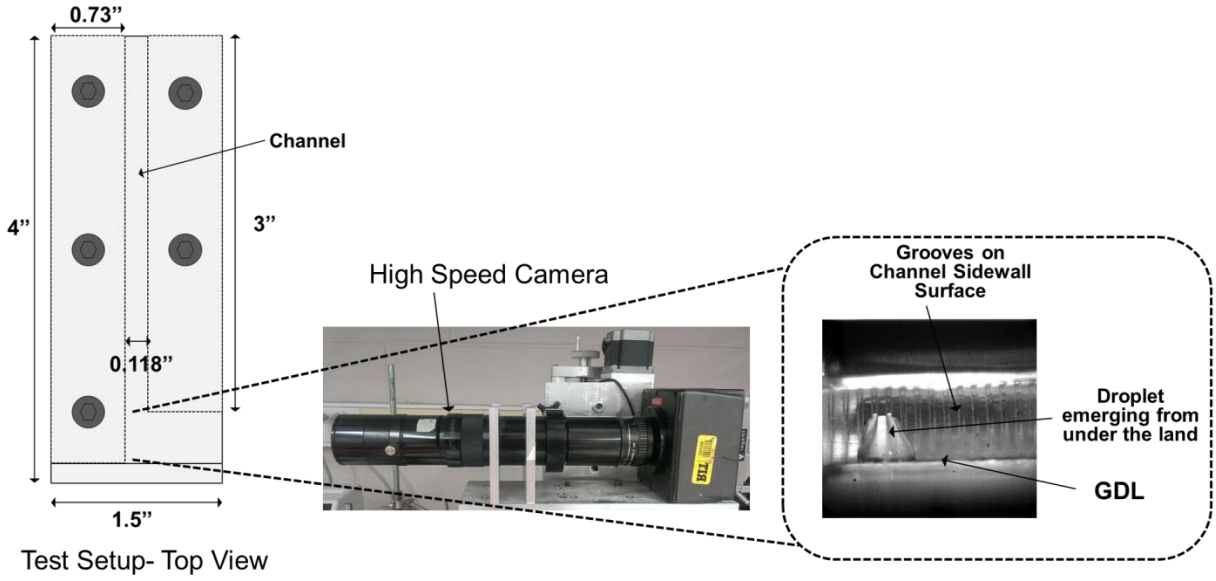


**Fig. 20.** Experimental Setup Arrangement- Grooves Visualization

The channel is not completely formed as frontal visualization of grooves is to be carried out as shown. The test is carried out in the absence of air flow. Photron Fastcam was used for this experiment. It is different than the other experiments in this study. This camera has a smaller focal distance and hence helps in visualizing the smaller region of grooves in more detail at speeds up to 100,000 fps. The images captured using these experimental arrangements are described in detail.

In the sequence shown below (Figure 21-23), water behavior when it emerges from under the land region is such that a droplet appears first and then GDL allows the water to enter the channel through multiple locations through its preferential pores. Here, a peculiar behavior was characterized where in majority of the experiments, two droplets are seen emerging and rising on the channels which combine and form a film later. Images of droplet-sidewall interaction sequence are shown in Figure 21, 22 and 23:

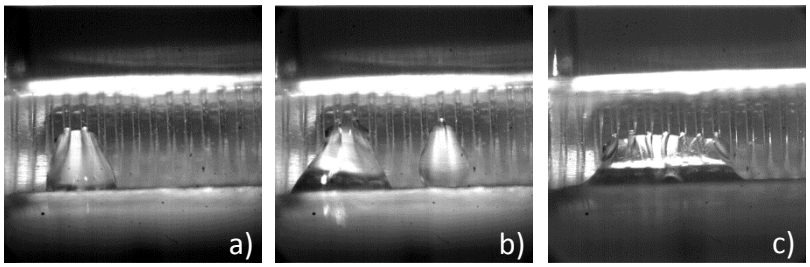


**Fig. 21.** a) 0 min: Droplet #1 Appears, Enters the Grooves, b) 10 min: Droplet #2 Appears, Enters Grooves, c) 26 min: Droplets Coalesce and Enter 7 Grooves in Total.

Figure 21 shows the early phases when the droplets grow and rise along the grooves due to the capillary effect. It has been divided in three stages described in the figure caption. It describes the process of droplet eruption and growth in contact with the grooves and the corresponding time taken for the same. The purpose of the grooves is to facilitate and force the water to the top

wall. That would help in increasing the drainage of water from the channel ends. Water usually would appear under the land and near the corner or sidewall near channel exit as per the experimental conditions set here. Water emergence and growth more upstream also is supposed to be ejected from the channel exits to the manifold and blow away. This process is easier if the water is in contact with the hydrophobic GDL (base), hydrophilic sidewalls and channel top wall which lead to water removal. Figure 22 and 23 show the consecutive stages of the droplet-groove interaction. The later stages as shown in Figure 22, 23 a), b) and c) show how a film may be generated eventually. This close observation helped in later visualization and result interpretation.

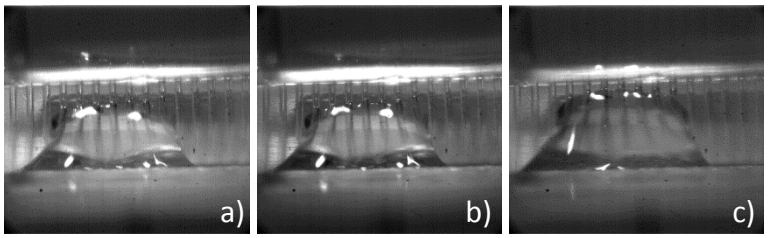


**Fig. 22.** a) 52 min: Slow Rise in Droplet Level over the Grooves and 26 Minutes after coalescing of the two Droplets, Significant Rise in Capillary Effect for Some Time. b) 81 min: The rise in the Grooves due to Capillary Effect is seen to Reach the Top Wall and the End of the Groove

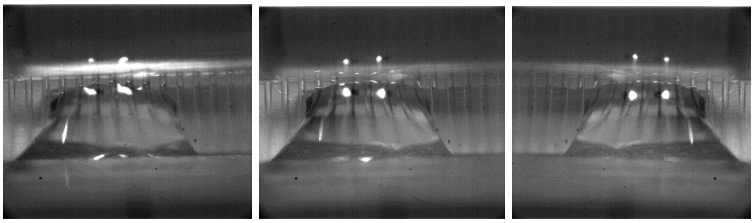

**Fig. 23.** The Droplet Reaches Top Wall and There is No More increase in its Overall Rise at the End of 99 Minutes, Where the Test was Concluded.

The left channel plate in the setup in Figure 14 has been modified for achieving better water drainage characteristics. Grooves have been incorporated along the entire height of the sidewall as shown in Figure 24 below. More detailed drawings of the test setup assembly and channel plates are in given Appendix I. The first setup was introduced by Gopalan [10] which had grooves for a length 25.4 mm (Channel length ~ 101.3 mm) from the channel entrance or edge in the upstream direction. This setup was analyzed in detail for the droplet-grooves behavior, the capillary rise action and used to form a channel with larger dimensions and provide results for experimental proof of concept and illustration of the enhanced water drainage properties imposed due to the channel design.

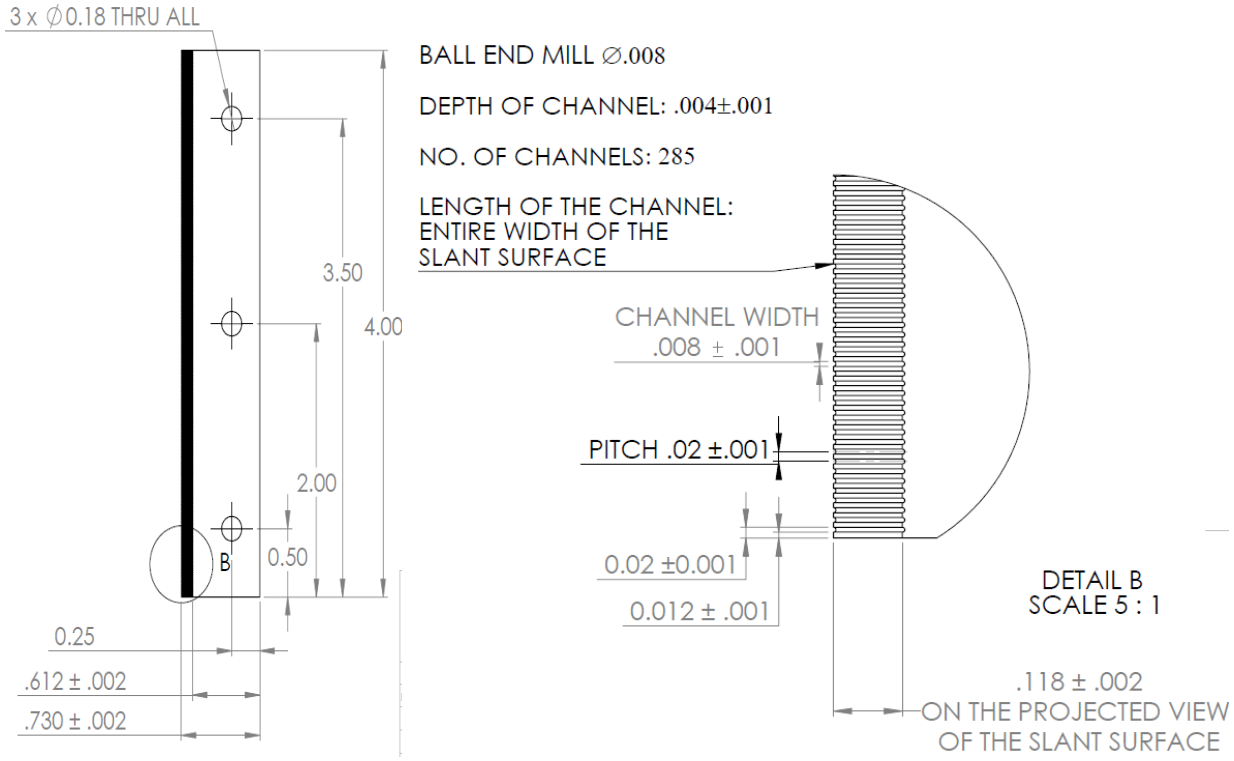


**Fig. 24.** Channel Sidewall with Grooved Surface- Groove Details

A baseline MRC-105 Gas Diffusion Layer was used for the tests. A PTFE gasket was placed between the base and sidewall plates to ensure absence of leakage of water and air during a test.

### 4.4. Data Acquisition and Reduction

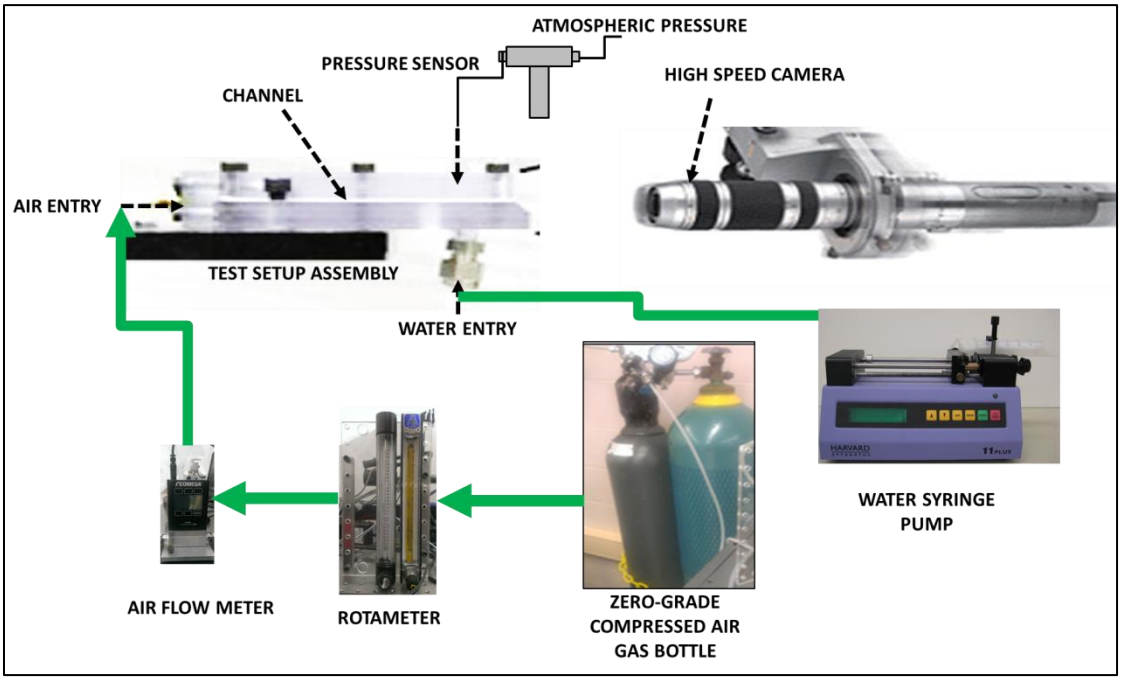


**Fig. 25.** Experimental Test Setup with Auxiliary Control Systems

Figure 25 shows the experimental setup along with the other control systems used for testing. It consists of an Air flow meter (Omega), Rotameter, Honeywell Pressure Sensor (Range 0-1 Psi) which has its one end in the channel, measuring pressure drop across the water droplet in a channel and the other end is subject to atmosphere (atmospheric pressure) as the reference temperature. A Harvard 11 Plus series syringe pump is used to inject liquid water in the channel. Zero-grade air is used and is supplied using the piping to the channel inlet manifold, through the rotameter and the air flow meter. Figures 26 show the LabView interface that was used for

acquiring data using NI DAQs. The block diagram shows the loop for measuring pressure drop and the calibration for the pressure sensor being used.

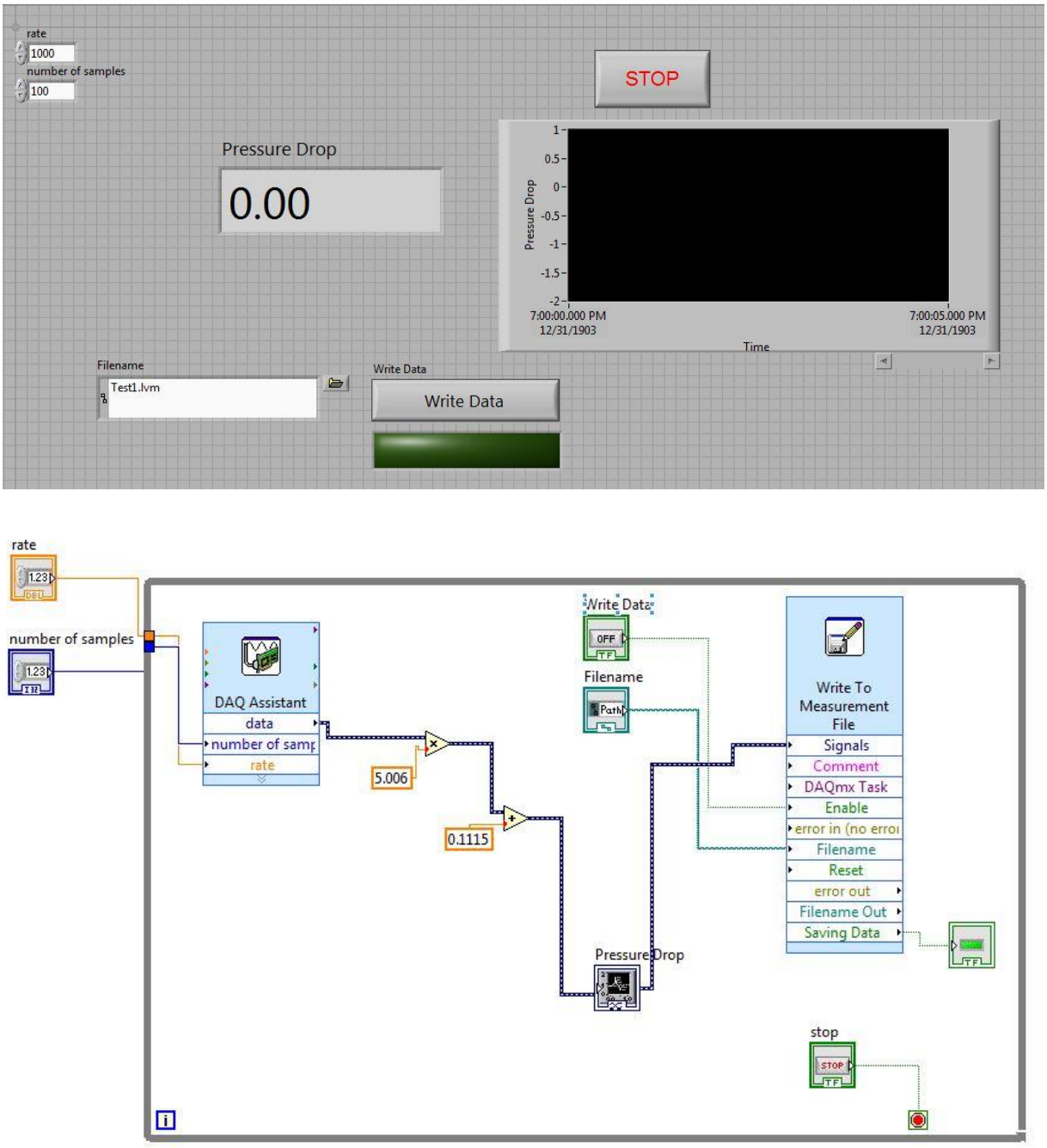


**Fig. 26.** LabView Interface and Block Diagram of the VI used for Data Acquisition

### 4.5. Experimental Procedure

Leak test was conducted after each assembly of setup with measurement of flow rates both at inlet and outlet to mitigate leakage. Gas leak testing fluid was used to find and eliminate leakages. The setup was conditioned for 15 minutes prior to testing using a higher air flow rate. Two slugs are allowed to form and pass before every test to ensure the flow is regulated and the flow patterns are repeatable. Water flow rates of 0.05 ml/min and 0.5 ml/min were used. Air flow velocities were chosen as per the standard fuel cell operating conditions. The Reynolds Number is varied from 39-390 out of which results up to Re=237 are presented. Table 2 below shows the air flow velocities used, the corresponding Reynolds Number for given channel dimensions.

**Table 2: Operating Flow Conditions used for Testing**

| Sr. No. | Current Density ($A/cm^2$) | Superficial Velocity (m/s) | Reynolds Number | Stoich (Cathode) |
|---|---|---|---|---|
| 1 | 0.1 | 0.18 | 40 | 2 |
| 2 | 0.2 | 0.36 | 79 | 2 |
| 3 | 0.3 | 0.54 | 119 | 2 |
| 4 | 0.4 | 0.72 | 158 | 2 |
| 5 | 0.5 | 0.90 | 198 | 2 |
| 6 | 0.6 | 1.09 | 237 | 2 |

The various channel designs that have been proposed and have been tested are listed below:

**Configuration C1**

**(**Water injection near channel exit (~12 mm away from channel exit))

Figure 15 a)

C1.1. Plain sidewall

C1.2. Grooved Sidewall (One channel wall grooved, other non-grooved)

a. Without Teflon

b. With Teflon (On groove land tops only)

C1.3. Grooved Sidewall (Both channel walls have grooves)

**Configuration C2**

(Water injection Upstream (~ 76 mm away from channel exit, inside the channel))

Figure 15 b)

C2.1. Plain sidewall

C2.2. Grooved Sidewall (One channel wall grooved, other non-grooved)

a. Without Teflon

C2.3. Grooved Sidewall (Both channel walls have grooves)

a. Without Teflon

For the channel designs proposed above in C1, two approaches have been investigated in this work. Local information as a droplet emerges to study filling characteristics, local pressure drop and it's variation across a single droplet and interactions with the opposite wall have been investigated in Configuration 1 by using the setup shown in Figure 15 a). In the other approach flow patterns developed upstream, middle section, and downstream locations of the channel are investigated and has been listed above as Configuration 2. The effect of new channel designs on the water features produced along the entire length of the channel has been looked at in detail. In case of local droplet-sidewall or the first approach, side view measurement of the channel using a high speed camera is done and local pressure drop across the droplet is measured and time based $\Delta P$ signatures are recorded for all air flow rates.

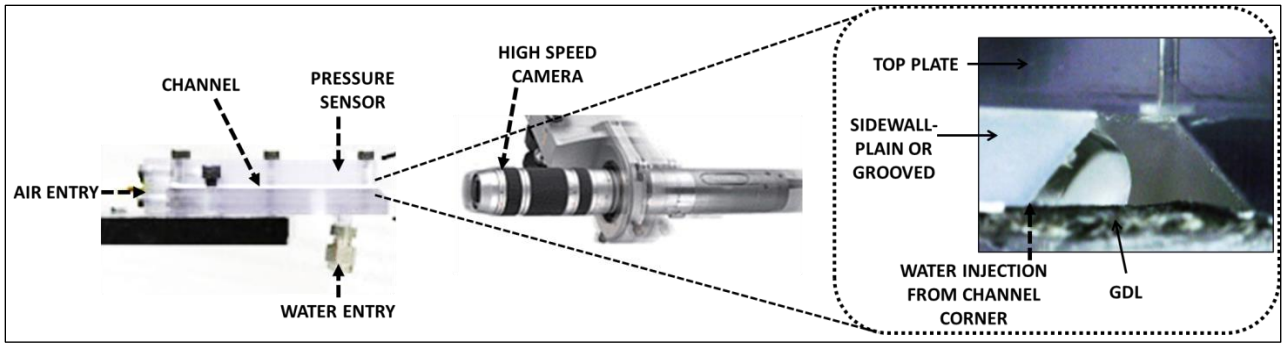


**Fig. 27.** Experimental Setup for Visualizing Droplet-Sidewall Interaction (Configuration C1)

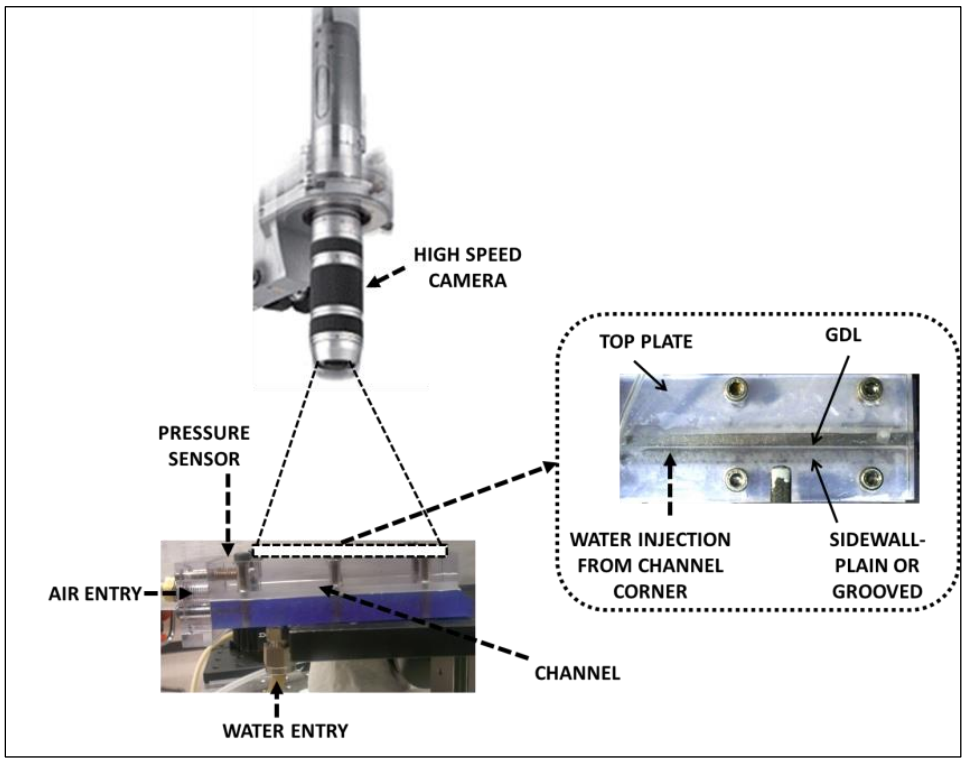


**Fig. 28.** Experimental Setup for Visualizing Droplet-Sidewall Interaction (Configuration C2)

Figure 27 shows the schematic for the setup with the high speed camera and how the visuals are set up. Droplet-sidewall interaction can thus be closely observed and studied. Pressure drop is measured locally as shown and the visual data can be correlated to the same. For the other approach, pressure drop will be measured upstream and top view measurements for slug and film flow movements will be recorded using the same high speed camera as shown in Figure 28.

Slug/film flow lengths will be measured with respect to the channel. The camera used in these experiments is Keyence VHX- Digital Microscope which has a 5X to 50X zoom. 30X zoom and a frame rate of 28 fps was used for recording images and videos. An external light source was used to illuminate the area of focus. Zero-grade pressurized air was used from a gas bottle. It was supplied through a Omega Rotameter-Air Flow Meter loop. The rotameter knob is used to control the air flow and the digital air flow meter gives direct continuous reading of the air flow rate being used.

## 5. Results and Discussion

In this section, the trapezoidal PEMFC channel was tested in an ex-situ setting where water was injected at flow rates that correspond to certain current densities (0.3- 3 A/cm$^2$,18.4 cm$^2$ Active Area) in a fuel cell and air is supplied at the corresponding velocities to the channel. The designs that have been tested are listed in section 4.5. All tests have been carried out at a constant room temperature of 25$^0$C. In the first part of the results sections, results for Configuration 1 have been discussed when water is injected in the channel near corner exit. Section 5.1 describes the results for the plain trapezoidal channel for all operating conditions when water enters at a channel corner. In section 5.2, surfaces of the channels that have been designed for overcoming the problems identified in water management at channel ends are characterized in detail. Section 5.3 discusses the channel-sidewall interaction for the grooved sidewall and it distinguishes the behavior of the droplet's movements along the sidewall and the base GDL surface. This is further validated using pressure drop measurements and one on one comparison with plain trapezoidal channel is presented in section 5.4. Section 5.5 discusses the manufacturing methods for manufacturing fuel cell channels and hence the process of adoption of the channel designs accordingly. The next section describes the experiments carried out using the second configuration of the setup (C2).

For each channel design, results for visualization were obtained along with continuous pressure drop measurements. The visualizations were in the form of high-speed videos and they were time-stamped to correlate with the pressure drop behavior. Previous research [6] has identified droplet-sidewall interaction for different channel configurations and made certain conclusions based on their observations. The geometry specified in these studies which showed best results as discussed in prior sections (2.1) is adopted to further investigate the water removal

characteristics. Surface modifications in the form of grooves and chemical coat in the form of Teflon coating is employed and tested on $50^o$ trapezoidal channels. The first tests were performed with the water entering the corner of the channel cross-section and plain sidewalls with no surface modifications or coatings. As explained previously, water entering close to the corner of the trapezoidal channel is the focus of this work.

### 5.1 Pressure Drop Validations and Visual Results Correlations for Plain Sidewall Channels (Water injection near channel exit (12.7 mm away from channel exit, C1))

Trapezoidal channels with an angle of $50^o$ are investigated with water droplets introduced at the corner or close to the sidewall. For low flow rates from 0.1 to 0.5 m/s, the channels eject water without any blockage as slugs are formed and exit the channel as shown on the pressure drop curve (Figure 30). However, as air flow rate increases, the droplet's entry location starts to affect its removal characteristics. As the slugs are formed, they start getting stuck near the channel end and the pressure drop signature fluctuates as shown in Figure 29.

Figure 29 shows the images of droplet-sidewall interactions and pressure drop curve correlated on the plot itself. The droplet image sequences have been categorized and put together in five phases as per the behavior and corresponding pressure drop fluctuations. In Figure 29, Phase 1 shows a droplet entering the channel at the corner near the sidewall. Phase 2 shows its subsequent growth along the GDL and eventual contact with the top wall and the corner with the opposite sidewall at the top. Pressure drop steadily rises as this happens. Water droplet completely blocks the channel area and the pressure drop peak is seen as pointed on the plot. The first slug thus formed exits the channel. As water is continuously injected in the channel, water rises again to form the condition as shown in Phase 4. Water keeps ejecting the channel in small drops as this happens. Three peaks are seen as the phenomenon repeats itself in Phase 5. This is

primarily caused by the channel's failure to eject the slug. Preliminary observations indicate that this happens mainly after first slug exits the channel. Hence it can be said that the residual water on the GDL and the wall opposite to water injection corner causes the water to stick to the exit as it is forced out by the air flow.

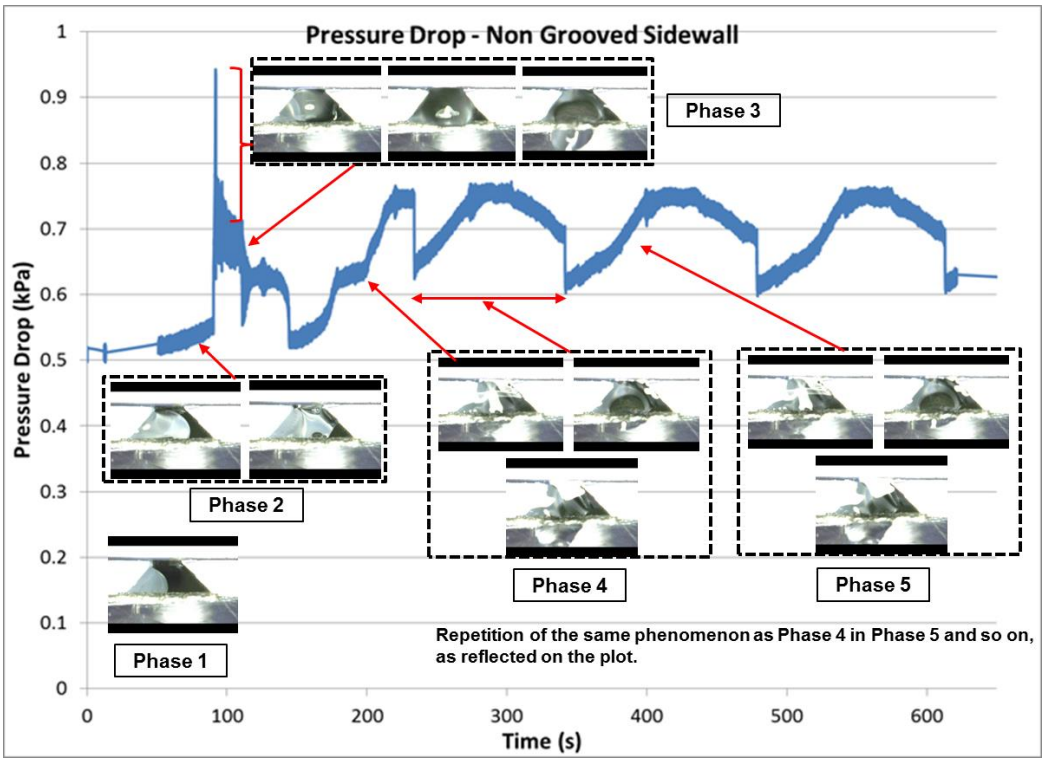


**Fig. 29.** Droplet-sidewall Interaction, Plain Trapezoidal Channel, 0.5 m/s (C1.1 a)

For low air velocities between 0.1 to 0.5 m/s slugs are formed and ejected from the channel easily with a peak in pressure drop (0.9-0.95 kPa). The plots for the same are shown below. Figure 30 shows two velocities- 0.18 m/s and 0.36 m/s. It can be seen that the pressure drop peaks are higher for the higher air flow rate but the phenomenon is the same. The pressure peaks correspond to slug formation and ejection process along with intermediate fluctuations corresponding to residual water features in the channel.

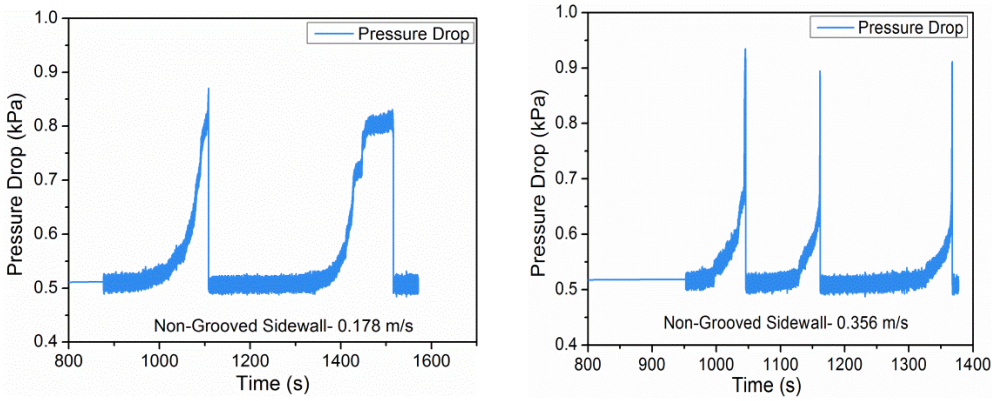


**Fig. 30.** Non-Grooved (Plain) Channel Sidewalls- Pressure Drop for Low Air Velocities (C1.1. a)

Therefore, it is clear that the problem of channel blockage at the channel exit is dominant for higher air flow velocities, where the emerging water droplet does not get enough time to attach and carry the films and slugs already present in the channel. This leads to accumulation of water near the channel exits and thus the droplet getting stuck. For two higher air velocities of 0.7 and 0.8 m/s, pressure drop plot is shown in Figure 31. The droplet-sidewall interaction is very similar to what was observed in the case of 0.5 m/s in Figure 29.

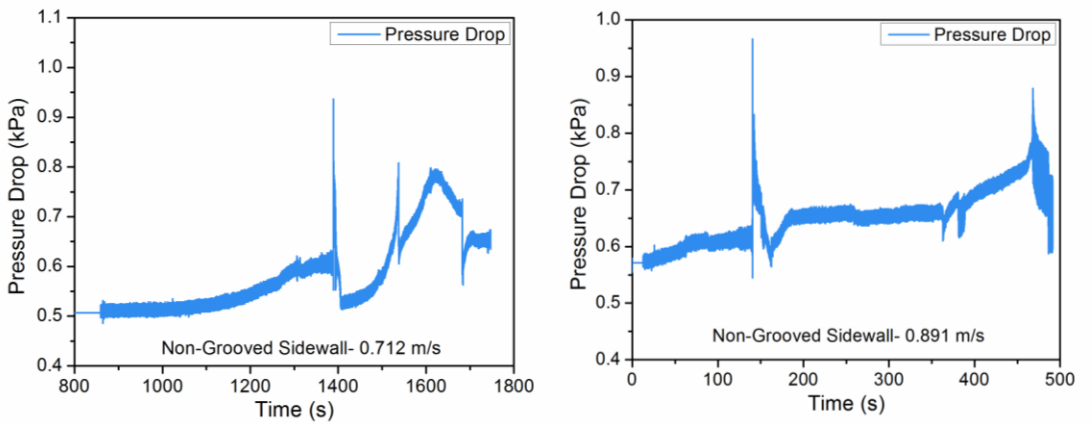


**Fig. 31.** Non-Grooved (Plain) Channel Sidewalls- Pressure Drop for High Air Velocities (C1.1 a)

It can be seen from the plots shown in Figure 30 that the first slug exits the channel corresponding to the peak in the pressure drop, but as time progresses, the droplet gets stuck near the channel exit as shown in Figure 31 for 0.7 m/s at about 1500 seconds. At 0.89 m/s, the velocity is considerably high and hence after the first slug exits, it takes more time for the other slug to be formed, which eventually gets stuck as shown about 450 seconds into the test. Figure 32 shows the behavior of the droplet near channel exit after the first slug is ejected for both air flow rates.

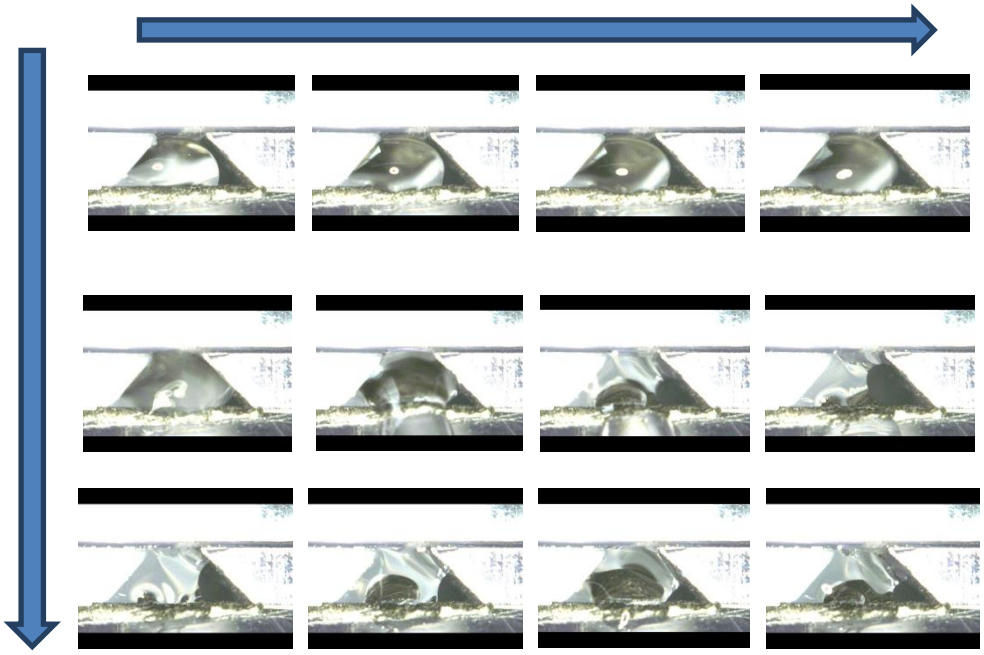

**Fig. 32.** First Slug Formation and Removal for Higher Air Velocities(≥ 0.5 m/s), 0 to 8 min

Figure 32 shows the formation of the first slug and the residual water feature after the first slug is ejected. It is clear from the images that a film is formed along the sidewall and it grows in size because the water keeps entering the channel from the same corner. This is the root cause of the water accumulation problem faced. In the last image of Figure 32, it is observed that the water starts accumulating and closing the channel area. In the sequence shown in Figure 33, it can be

seen how the water feature now keeps blocking the channel, and the process sequence in Figure 32 is not repeated.

**Fig. 33.** Droplet Sticking Phenomenon for High Air Velocities (≥ 0.5 m/s), 8-10 min

Understanding the problems associated with higher air flow velocities and droplet sticking close to the channel exit, a research problem in the case of fuel cell microfluidic channels has been identified. When looking at a channel cross-section, water is assumed to be produced in the channel at the center along the flow axis in many ex-situ studies. This assumption is primarily valid and extensively used for experimental purposes. However in a real PEMFC, the water entry is not constrained to entering the channel at the center and usually is facilitated in the channel with a Gas Diffusion Layer (GDL). Water flow or water inlet in the PEMFC channel is thus primarily driven by a dynamic interconnected pore network in the GDL and channeling of water streams through it. Although these mechanisms suggest some consistency in the water emergence, it does not or cannot predict that water will be produced at the channel center at all times. Hence, more investigations were made using water inlet at the corner or the edges of the channel which resulted in contradicting all the previous observations and conclusions thus made for the water features and their behavior for all relevant PEMFC operating conditions, leading to severe pressure drop losses due to gas flow blockage and water covering the channel diffusion media (GDL). The solution to avoid these scenarios in a fuel cell channel can be either in the

form of different operating conditions or higher air flow rates, which has its own disadvantages like added complexity to the system and increased cost.

As mentioned previously, alternatives to existing channel design- shape, geometry, surface modifications and coatings can help in changing the microfluidic drainage and retention characteristics by inducing certain wetting behaviors, difference between surface tension forces and contact angle behavior. All these factors are correlated or are inter-dependent. As mentioned previously, research has showed that grooved substrates help in changing the wetting behavior of a surface. Beyond the necessity of changing the channel wall wettability to excessively hydrophilic or hydrophobic, which can be done by applying chemical coatings such as PDMS or Teflon, the microfluidic behavior in this case needs a surface with custom or hybrid wetting characteristics. A completely hydrophobic surface will tend to push the water on the channel base surface or the GDL, blocking the chemically active region which is not suitable for PEMFC conditions. Increased hydrophilicity is one of the solutions that has been suggested by many researchers and implemented in many designs. However, for the water inlet conditions (location, position) described above, these channel walls tend to fail and cause blockage and coverage issues. As the problem identified here deals mainly with channel blockage due to accumulated water features, fully and partially, which will be aggravated as the water will tend to stick to the sidewalls (for hydrophilic plain sidewalls) leading to increased fluctuations before droplet ejection. Therefore an alternative channel surface modification in the form of grooves was designed and tested in this study. It has been characterized, compared and tested results of which are summarized in sections that follow.

The filling and Non-filling characteristics along with the individual behaviors is identified for plain non-grooved channel sidewalls (C1.1 a, Section 5.1) in Table 3 on the following page. The contact angles for this sidewall are measured and discussed in the next section. These channel walls are hydrophilic and have contact angle ~50$^{o}$.

**Table 3: Summary of Droplet-Sidewall Interaction Results- Plain Sidewalls (C1.1. a)**

| Non-grooved Sidewall (Plain Trapezoidal Channels) | | | | | | |
|---|---|---|---|---|---|---|
| **Sr. No** | **Superficial Velocity (m/s)** | **Reynolds Number** | **Stoich** | **Injection Corner** | **Opposite Corner** | **Slug Motion** |
| 1 | 0.18 | 40 | 2 | Filled | Filled | Slug removed, both corners filled |
| 2 | 0.36 | 79 | 2 | Filled | Filled | Slug removed, both corners filled |
| 3 | 0.54 | 119 | 2 | Filled | Not filled | Slug partially removed, opposite corner not filled, stuck at the channel exit |
| 4 | 0.72 | 158 | 2 | Filled | Not Filled | First slug removed, partial film left on GDL. Next slug occupies more cross section of channel compared to the first. Opposite corner not filled for all slugs |
| 5 | 0.90 | 198 | 2 | Filled | Not Filled | Slug partially removed, opposite corner not filled, stuck at the channel exit |
| 6 | 1.09 | 237 | 2 | Filled | Not Filled | Slug partially removed, opposite corner not filled, stuck at the channel exit |

### 5.2 Contact Angles for All Channel Surfaces Tested

The contact angles were measured using VCA Optima Contact angle measurement device. The sessile droplet method was used to measure and characterize the contact angles. Initially the grooves were designed to be hydrophilic in nature. Traditionally, the GDL has been impregnated with PTFE to make it hydrophobic and channel walls should ideally be hydrophilic. Hence, the grooves were designed and manufactured using a Scaling Factor [16] of 1.5 (S > 0.2) for promoting water drainage behavior. This Scaling Factor represents Wenzel [19] mode of wetting, meaning water filling the grooves. This was the proposed design so as to facilitate absorbing the water and helping it rise to the top wall of the channel to enhance and quicken the water removal process.

**Table 4: Contact Angles of All Channel Surfaces Tested**

| Sr. No. | Type of Channel | CA from VCA Optima ($^o$) | Average CA ($^o$) |
|---|---|---|---|
| 1 | **Grooved Sidewall** Hydrophilic | 48<br>47.7<br>44.4 | 45.5 |
| 2 | **Non-grooved Sidewall** Hydrophilic | 49.2<br>54.4<br>51.3 | 51.8 |
| 3 | **Grooved Sidewall** Hydrophobic (Groove Tops) | 114.5<br>108.5<br>97.2 | 103.8 |

Contact angle of all three surfaces tested in this study are listed in Table 4. Plain sidewall, Sidewall with grooves and sidewall with grooves- tops coated with hydrophobic Teflon solution. It can be seen that the grooves exhibit more hydrophilic behavior than the plain walls.

When the grooved channel is implemented in a PEMFC channel, it will be in contact with droplets emerging from the GDL. Hence only static contact angle measurement data is not sufficient to understand the droplet's behavior on this surface.

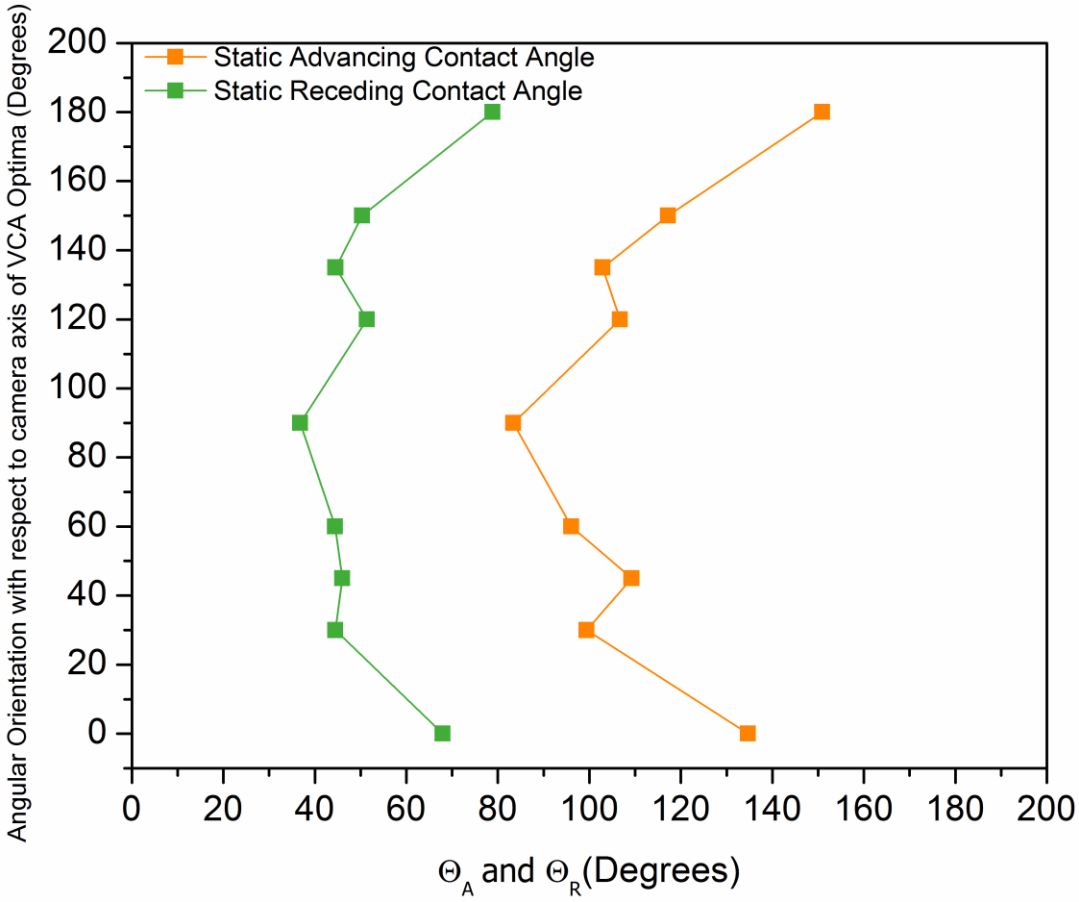


**Fig. 34.** Effect of Orientation on Static Advancing and Receding Contact Angles ($\theta_A$, $\theta_R$)

Thus, contact angle was measured along the entire periphery of the droplet. Static advancing and receding contact angles were measured using the VCA Optima. Their variation is sinusoidal and restricted within a range. This plot illustrates the contact angle behavior of the structured surface.

The results of the same are shown in Figure 34. Figure 35 shows how the droplet placed on a grooved substrate exhibits different contact angles along the periphery. The camera axis shows the axis of the camera lens of the VCA Optima Contact Angle Measurement System. All angles are with respect to this axis as reference $0^{o}$ on the plot in Figure 34.

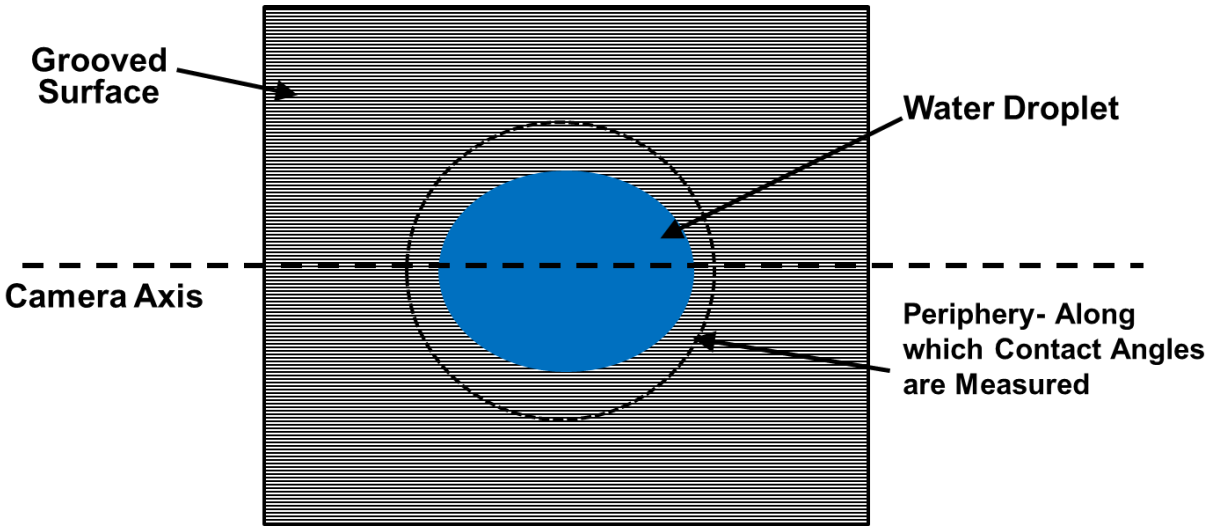


**Fig. 35.** Grooved Surface- Contact Angles Around the Droplet Periphery

### 5.3 Droplet Sidewall Interaction (Grooved Sidewall-GDL, C1.2 a)

The grooved surface on the channel sidewall is characterized in detail using high speed visualization in section 4.3, the sequences below (Figure 37) illustrate the droplet-grooved sidewall interaction and how it is different than the plain sidewall with some peculiar characterstics identified. The test setup used for the following results was obtained from the same test setup assembly with slightly different channel component arrangement. It is shown in Figure 36. The water appears at a distance of 1.5 mm from the channel sidewall. This is a very important condition considering the water appearance in fuel cell channels due to condensation of gases or cell reaction is not location specific. Most prior studies looking at droplet interaction

in the cell channel, force balance studies and slug/film flow generation and transition and modeling have neglected this factor for experimental convenience, and have droplets being generated at the channel center. Droplet generation at the channel corner has multiple issues and fails to satisfy some of the previous theoretically established facts such as the Concuss-Finn condition for filling and non-filling a channel corner [5–7].

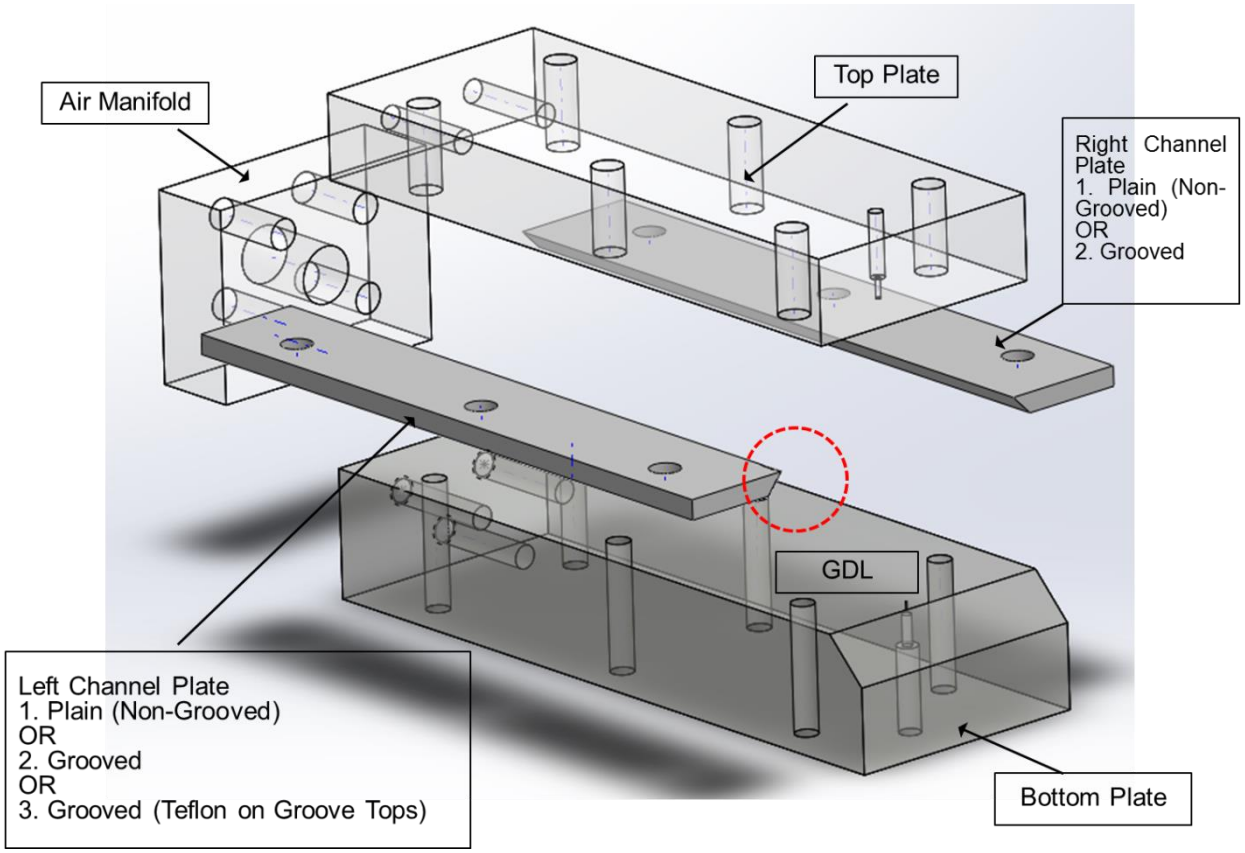


**Fig. 36.** Exploded View of the Experimental Setup Assembly Designed for Studying Effect of Grooved Sidewall

Figure 36 shows the exploded view of the test section assembly with the components labelled. The left channel plate and the right channel plate with its replacements for different tests carried out in this study are listed in the Figure 36. The components are bolted together from the holes along the entire height and desired level of compression is achieved. The

interactions are observed for the region shown by the red dotted circle in the setup of Figure 36 and the base plate on which GDL is present. Water enters the channel from the corner as shown in the Figure 13. The droplet appears on the GDL, touches the sidewall after it grows enough in size. It grows along the sidewall and on the GDL as water is being injected in the channel. The sequence is illustrated in Figure 37.

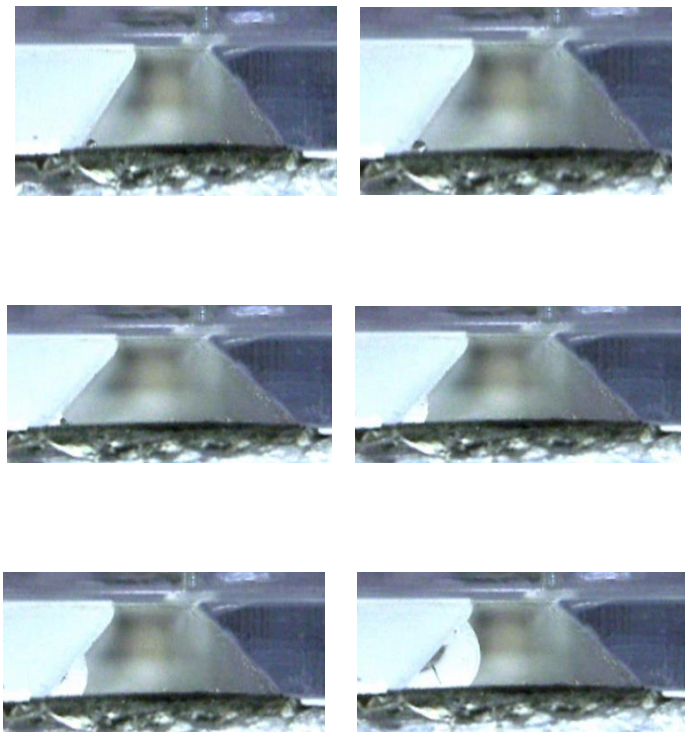

**Fig. 37.** First 7 Minutes after Droplet Emergence in the Channel

Figure 37 shows how the droplet appears in the corner and comes in contact with the sidewall soon after it grows and keeps growing in size. As it can be seen, it is sucked to the sidewall as the surface on the channel sidewall is extremely hydrophilic. The GDL-droplet contact line is retracting towards the sidewall every few seconds and the droplet-sidewall contact line keeps moving back and forth.

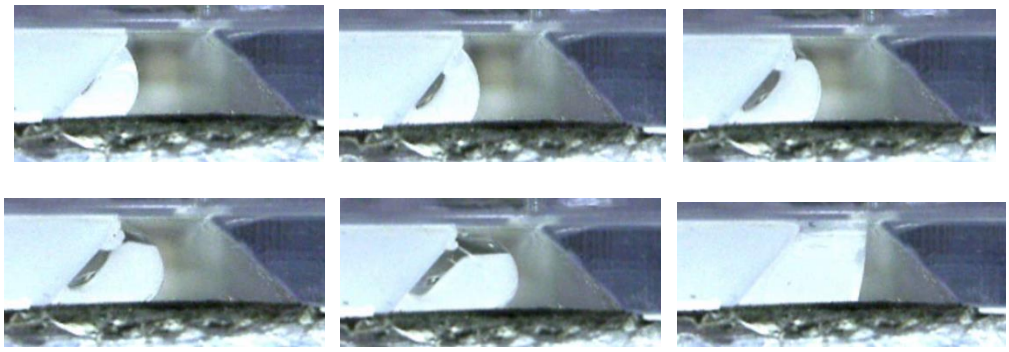

**Fig. 38.** Minutes 7-17 after Droplet Emergence in the Channel

The video clearly shows how the droplet is attached to the top wall eventually in the Figure 38. The air flow in the channel in this case is 0.178 m/s. It can be seen towards the end of the second sequence of images, how the droplet touches the top wall and tends to be away from the GDL. However, as water flow is kept running, it eventually fills the channel soon after it touches the opposite sidewall. A slug is formed, which moves and exits from the channel.

Results for the filling and non-filling channel corners are summarized in the Table 5 for the grooved sidewall (channel having one grooved sidewall and one plain sidewall) on the following page. Detailed observations of channels in the corner have also been discussed for all air flow rates.

**Table 5: Summary of Droplet-Sidewall Interaction Results- One Grooved Sidewall (C1.2 a)**

| Grooves on Entire Sidewall (One Grooved Sidewall) | | | | | | |
|---|---|---|---|---|---|---|
| **Sr. No** | **Superficial Velocity (m/s)** | **Reynolds Number** | **Stoich** | **Entry Corner** | **Opposite Corner** | **Flow Characteristics** |
| 1 | 0.18 | 40 | 2 | Filled | Not Filled | Slug removed, film formed adhering primarily to top wall |
| 2 | 0.36 | 79 | 2 | Filled | Not Filled | Slug removed, film formed adhering primarily to top wall |
| 3 | 0.54 | 119 | 2 | Filled | Not Filled | First slug removed, film formed adhering to top wall. Second slug onwards, droplets stays stuck at the channel exit, opposite corner still not filled, very less area covered |
| 4 | 0.72 | 158 | 2 | Filled | Not Filled | Water feature (Film-like slug) removed soon after touching sidewall. This motion repeats for first 30 minutes, as water keeps growing along the channel length adhering to the grooves. More cross section available for air to move and exit the channel |
| 5 | 0.90 | 198 | 2 | Filled | Not Filled | Water feature (Film-like slug) removed soon after touching sidewall. This motion repeats for first 30 minutes, as water keeps growing along the channel length adhering to the grooves. More cross section available for air to move and exit the channel |
| 6 | 1.09 | 237 | 2 | Filled | Not Filled | Water feature (Film-like slug) removed soon after touching sidewall. This motion repeats for first 30 minutes, as water keeps growing along the channel length adhering to the grooves. More cross section available for air to move and exit the channel |

### 5.4 Effect of Grooved Channel Sidewall Design on Water Accumulation (C1.2 a, C2.2 a)

Three channel design arrangements will be discussed and results for the same are presented in this study. They have been explained in the experiemental section, where it has been described as C1.1 to C1.3. Results for all three of those configurations are presented for one case here. Where C1.1 (a) denotes both plain sidewalls (non-grooved), C1.2 (a) refers to one grooved sidewall and other plain sidewall and C1.3 (a) refers to both grooved sidewalls in a channel configuration. For both C1 and C2, subsections (a) refer to absence of Teflon coating and (b) refers to application of hydrophobic Teflon coating.

The distinction between the two droplet-sidewall behaviors however is for the moderate air flow velocities between 0.5 to 0.7 m/s. It is important to identify a range of air flow rates that are important as per the fuel cell perspective, which are used in the operating range. The flow rates that were used have been mentioned in Table 1 above. When tests were conducted for all channel designs, certain flow rates were identified that exhibit peculiar behavior for each channel design.

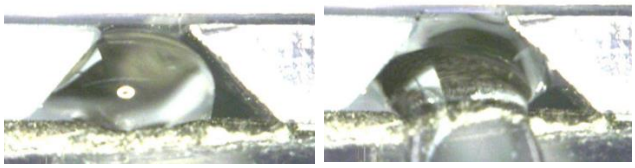

a) Non-Grooved or Plain Channel Sidewalls- 0.54 m/s (C1.1 a)

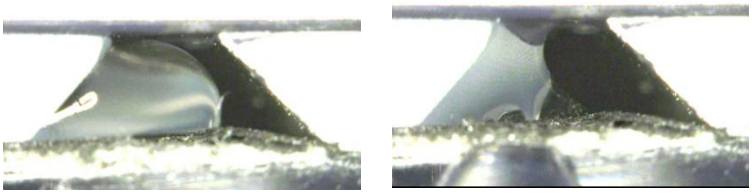

b) One Channel Sidewall Grooved, Oone Plain- 0.54 m/s (C1.2 a)

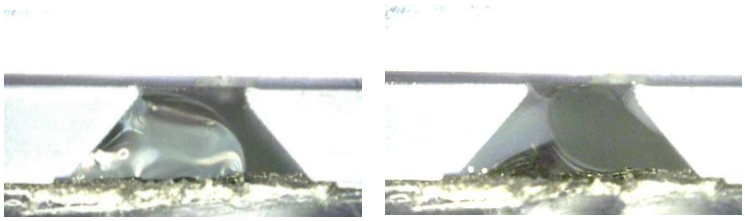

c) Both Channel Sidewalls Grooved- 0.54 m/s (C1.3 a)

**Fig. 39.** Image Sequences before and just after Slug Ejection- a) Plain Channel (C1.1 a) b) One Grooved sidewall (C1.2 a) c) Both Grooved Sidewalls (C1.3 a)

At the air velocity of 0.54 m/s, which is moderate and corresponds to a current density of 0.3 $A/cm^2$ for the given channel dimensions. The behavior of water features for all three channel designs that were proposed as a part of this study have been illustrated in Figure 39 and how each channel design affects the water behavior during and after the slug ejection. Figure 35 shows pressure drop plots for the plain and one grooved sidewall channel designs for the same air velocity. The duration of pressure drop measurements is about 600 to 700 seconds which vary with channel design and entire droplet formation to ejection process is illustrated. Figure 40 a) shows the pressure drop curve for a plain channel sidewall with a trapezoidal geometry having an angle of $50^o$. The droplet sidewall ineraction for the non-grooved or plain channel sidewall with correlation between images of droplet-sidewall interaction and pressure drop signature has been described in Figure 29 in Section 5.1. The same curve has been shown in Figure 40 a). Figure 40 b) shows the visualization of the grooved sidewall-droplet interaction in phases and the corresponding response by the pressure sensor displaying local pressure drop. Phase 1 to Phase 3 show formation of droplet to slug, slug's ejection and then the second slug getting pinned and blocking the channel cross-section in Phase 4.

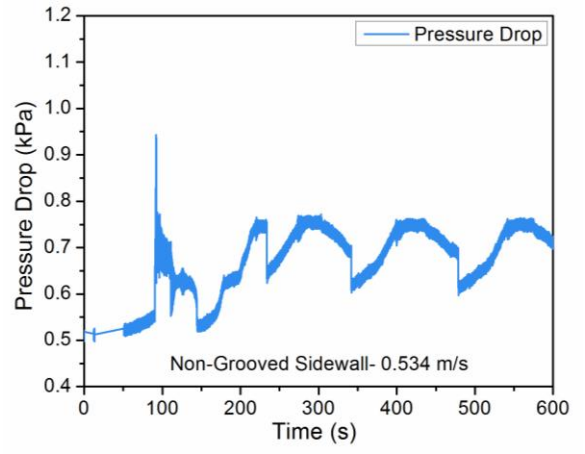


a)

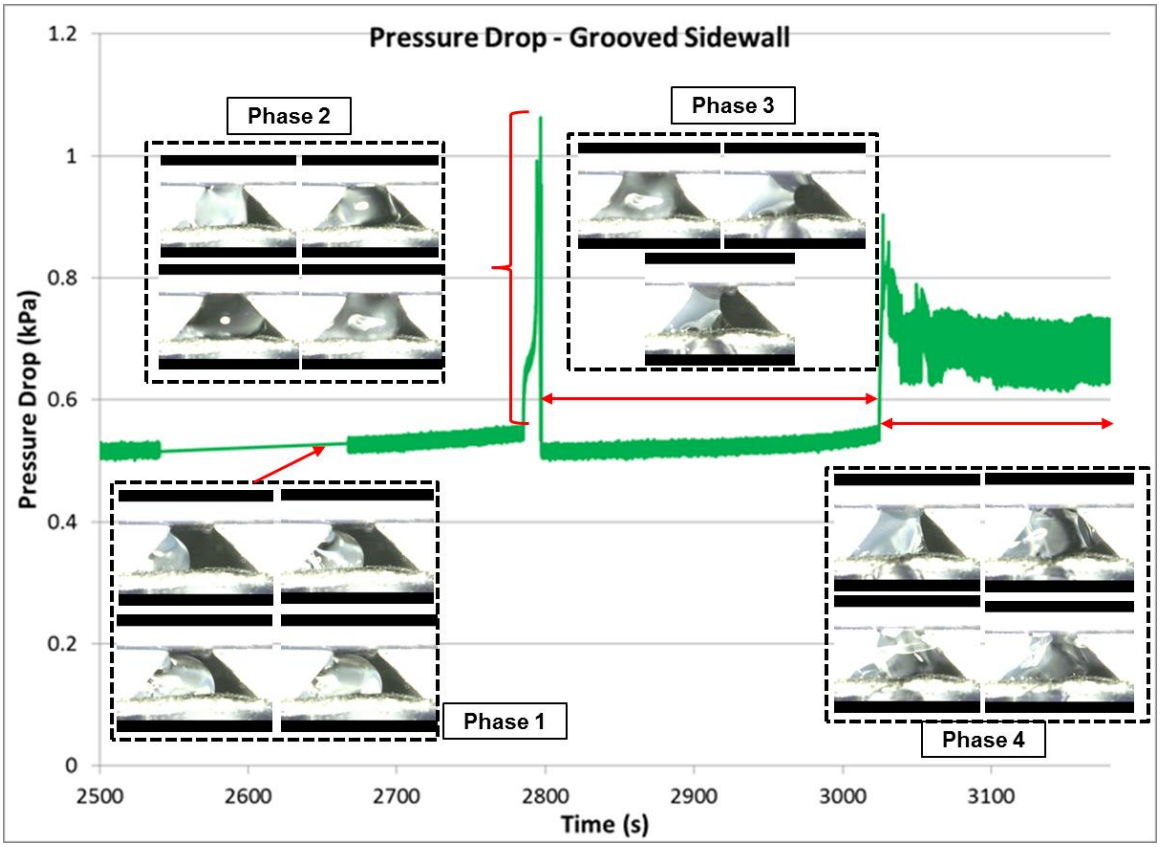


b)

**Fig. 40.** Pressure Drop Signatures for: a) Plain Channels (C1.1 a), b) One Grooved Sidewall Channel- Visualization Phases Correlation (C1.2 a)

The pressure drop curve in Figure 40 a) shows that around 150 seconds later, the first slug is ejected, but as it is shown in earlier image sequence in Figure 37, the slug water content is

ejected, although the water does not completely clear the channel cross section and keeps filling. Small amounts of water keep ejecting from the slug sitting at the channel exit in the form of droplets. This causes the constant change in the pressure drop signal. This also indicates that the slug is occupying not only the channel cross section near the channel exit but also the GDL area is covered in the same region. This behavior means less active area available for the chemical reaction to take place. In order to avoid this blockage and improve water drainage characterstics, channels with micro-grooves on the sidewall are designed and tested. The image sequence from Figure 39 b) shows that the grooved channel is able to eject the water slug and also clear out most of the water from the cross-section. However if the pressure drop signature is observed in Figure 40 b) for the same channel, it is evident that after the first slug exits the channel, the droplet gets stuck at the channel exit with a very high rate of fluctuations. Figure 41 shows growth of second slug and its accumualtion and blockage of channel. This is Phase3 and 4 combined as per Figrure 40 b).

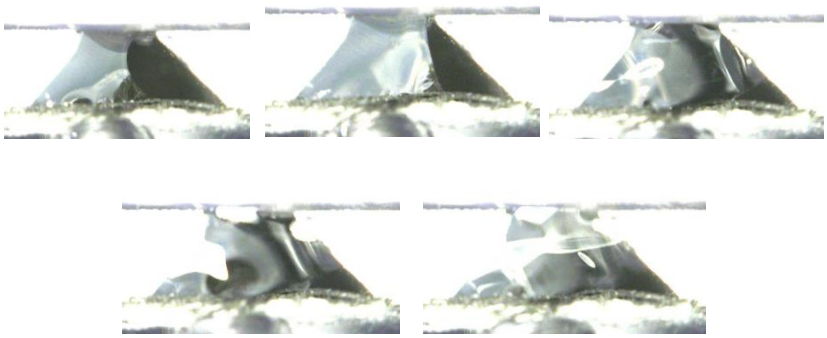

**Fig. 41.** Droplet Accumulation and Blockage after Slug 1 Exits the Channel- One Grooved Sidewall (C1.2 a)

Before manufacturing considerations for these channels are taken into account, it was important that the channel design concept with grooves on one sidewall and the other being

plain (non-grooved) be implemented succesfully with elimination of prior microfluidic water management issue for the certain fuel cell operating condition posed here. Hence coating of the groove-tops with hydrophobic solution of Teflon has been identified as a probable solution and tested. The visualisation results and the pressure drop plot comparison for the same time frame of about 700 seconds is illustrated in Figure 42 and 43.

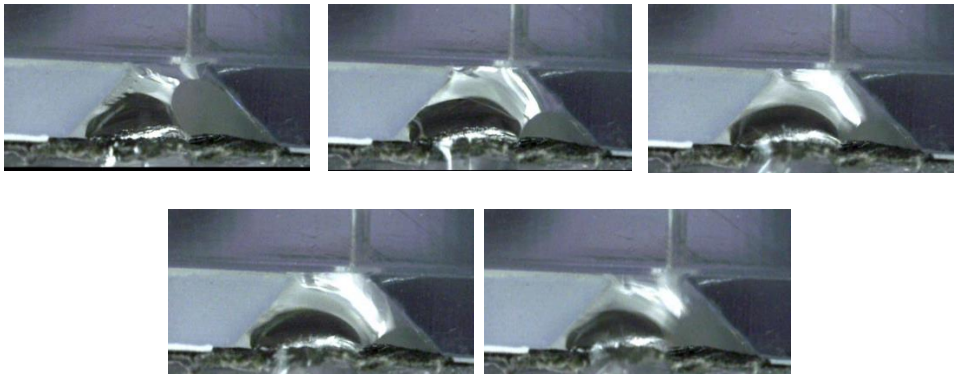

**Fig. 42.** Droplet Accumulation and Blockage after Slug 1 Exits the Channel- One Grooved Sidewall (C1.2 b), Effect of Teflon Coating

It is clear from the images that the problem is not completely solved as the water feature does not completely clear the channel. However, slug is able to completely exit the channel and thus resistance to flow of air through the channel is eliminated. It can be seen from the pressure drop signature in Figure 43.

Comparing Figure 43 with Figure 40 b), it can be concluded that the pressure drop characterstics have improved due to the chemical treatment of the groove tops with hydrophobic Teflon. The hydrophobicity of the groove top surfaces combined with Wenzel wetting behavior of grooves which is hydrophilic, imparts the hybrid wetting regime to the grooved surface.

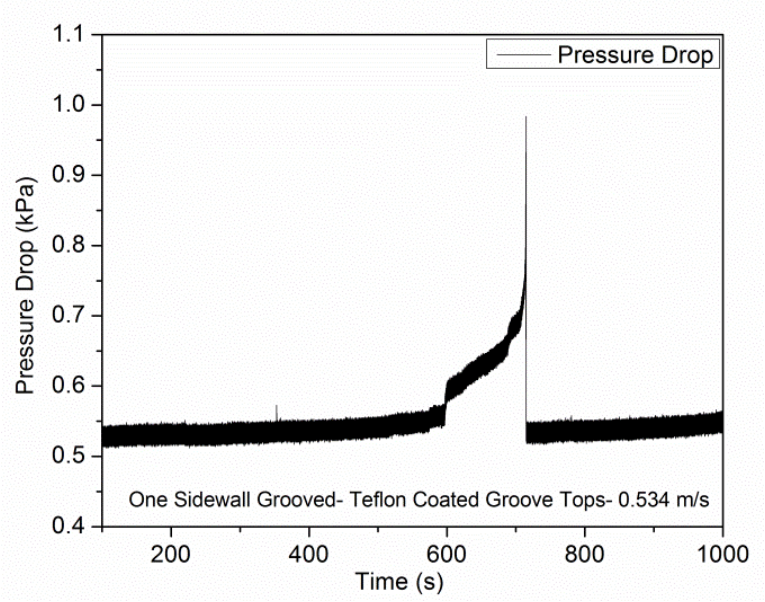


**Fig. 43.** Pressure Drop Signature- One Grooved Sidewall- Teflon Coating on Groove Tops (C1.2 b)

### 5.5 Manufacturing Considerations and Grooved Channels

Fuel cell channels are incorporated as embedded in a metallic base plate and known as bipolar plate. This plate can be manufactured using multiple techniques and multiple materials. For fuel cells having active area (> 1 $cm^3$), metallic bipolar plates are made from materials like Aluminum, Stainless steel, Titanium, Nickel and Carbon composites [27]. The standard method for forming solid metallic bipolar plate designs is machining or stamping. A lot of research is being put in cold-closed die forging, die-casting, investment casting and electroforming to manufacture metallic bipolar plates for fuel cells. Stamping is the current most widely used manufacturing process, which has been the primary consideration for this work. Apart from stamping, the channel designs proposed in this study also can be easiliy manufactured by die casting and cold-forging. Considering that stamping process needs to accommodate modified process sequence to manufacture the surface modifications or grooves

on channel walls, the forming stage of the stamping process would be less complicated with grooves on both sidewalls of the channels. The forming dies would be easier to design, manufacture and to execute the process.

The third channel design (C1.3, C2.3) thus tested and presented here is a channel having micro-grooves on both sidewalls. As it can be seen from the results shown for grooves on both sidewalls shown in Figure 40 (c), water generation and ejection characteristics are very similar to the channel having grooves on one sidewall except the fact that the ejection process for this channel is faster and leaves less residual water along the grooves and the channel. The pressure drop signature for the same in Figure 45 reflects this with continuous subsequent peaks in pressure drop as slugs are formed and ejected. It can be seen that compared to first two cases (C1.1, C1.2), overall peak pressure drops are higher for this case, primarily because of the fact that slugs or film- like slugs are formed for all air speeds which lead to channel blockage.

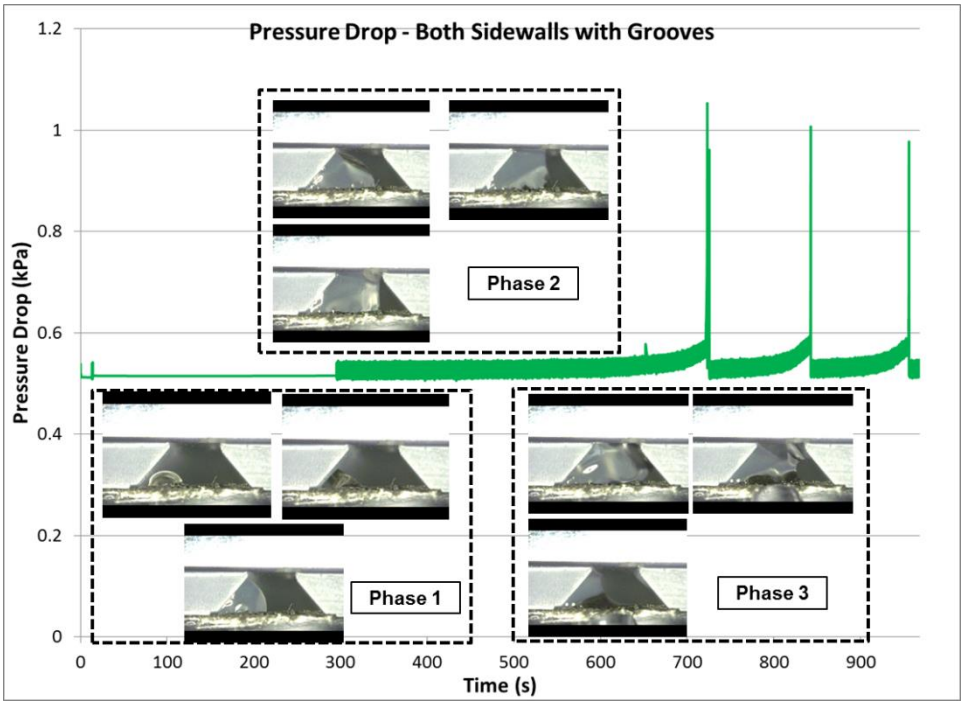


**Figure 44.** Droplet-Sidewall Interaction (Both Grooved Sidewalls, C1.3, 0.5 m/s)

Figure 44 shows the droplet sidewall interaction when both sidewalls have grooves that make it slightly more hydrophilic than the plain hydrophilic walls. The interaction is divided in three phases with the first phase showing droplet's emergence from the corner of the channel near the sidewall. The second phase shows the growth of the droplet along the top wall and finally as it slowly covers the entire cross section. It can be seen that the opposite corner is not filled in Phase 3's first picture. It is indicating that the slug is more of a film-like slug and hence is not blocking the flow completely. At the end of phase 3, it can be seen that this phenomenon repeats itself even after the first slug exits the channel evident from the pressure drop curve in Figure 45. The same is illustrated in Figure 39 c) with direct comparison to one grooved sidewall and plain or non-grooved sidewall.

The scenario where channel is blocked and droplet fluctuation is not caused leads to an overall high pressure drop. But this causes constant removal or ejection of slugs which is the ideal or expected situation. The second channel wall having grooves helps enhancing the water drainage behavior as it triggers faster removal. It increases the hydrophilicity of the channel overall, causing the water to be associated more with the channel walls compared to the base making the energy transfer from the base-sidewall interface to sidewall-sidewall interface. The slug ejection process became repeatable for the third channel design as illustrated by three consecutive pressure drop peaks in Figure 45. The important consideration for this design is now that how it performs after the first slug is ejected. As it can be seen in Figure 45, there are continuous peaks in pressure drop indicating non-accumulation and quick removal of water slugs as they are formed.

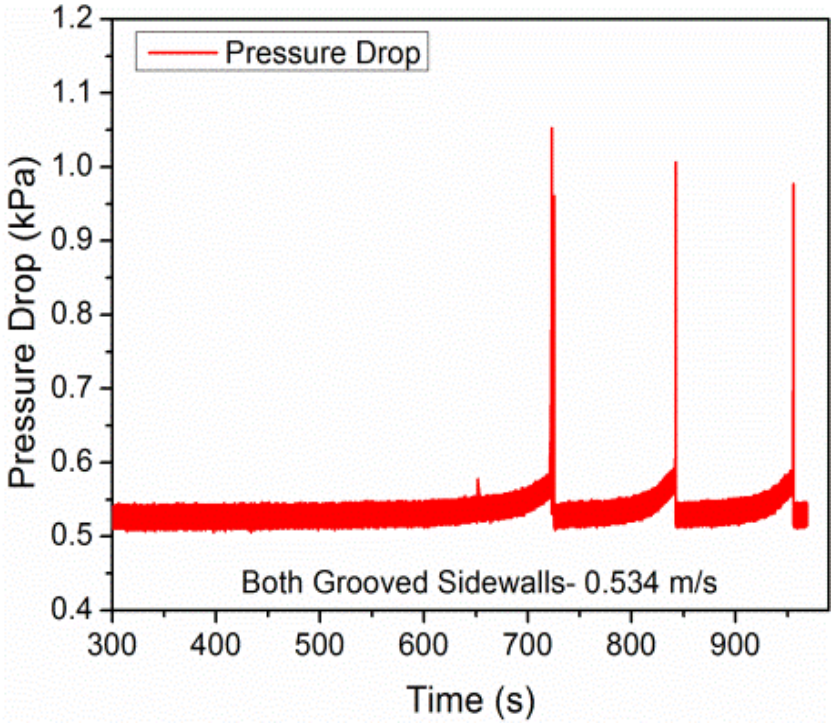


**Fig. 45.** Pressure Drop Signature- Both Grooved Sidewalls (C1.3 a)

The second grooved wall aids in the removal of water features as air flow velocities increase and only water residuals are absorbed by the grooves not forming significantly large slugs or films that would cause accumulation and lead to blockage. The visuals shown in Figure 39 c) are thus repeated slug after slug and thus the new channel design proposed here overcomes the channel end water accumulation and blockage problems. This design with two grooved sidewalls is thus proposed to be adopted in order to eliminate channel end pinning and water accumulation. Therefore, this is the channel that will be compared with the conventional trapezoidal channel in the sections that follow for the second setup configuration C2. As the issues faced by channels that have one grooved sidewall have been overcome in this channel design and it is also a more practical solution as explained above with manufacturing considerations into account.

## 5.6 Pressure Drop Validations and Visual Results Correlations for All Channel Designs (Water Injection Upstream (~76.2 mm away from channel exit, inside the channel, C2))

The channel designs that have been proposed and tested in the earlier sections of this work need further validation in terms of real fuel cell operating conditions when water features are generated all along the length of the channel.

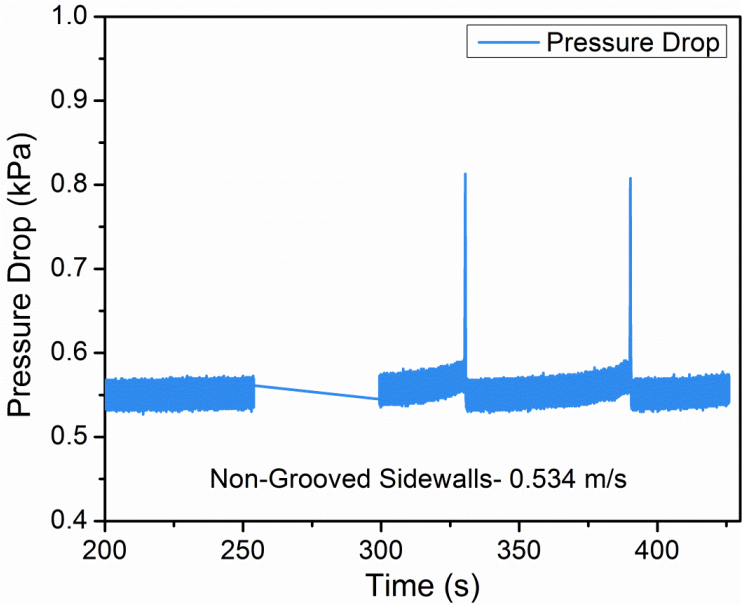


**Fig. 46.** Pressure Drop Signatures- Water Entry Upstream C2- Plain Sidewall Channel (C2.1 a)

In an actual fuel cell channel and flow field, water is produced along the entire length of the channel and not just near the exit. The issue of water accumulation and blockage is identified and studied near the exit as it also signifies other issues such as droplet pinning. However, over the years, fuel cell channels have been studied for flow patterns along the entire length of the channel at different air and water flow velocities.

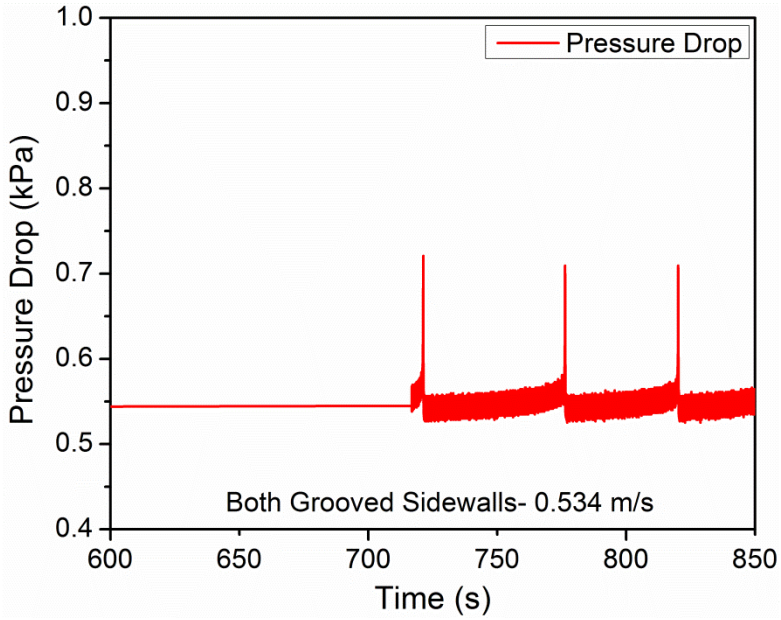


**Fig. 47.** Pressure Drop Signatures- Water Entry Upstream C2- Both Grooved Sidewalls (C2.2 a)

These studies [28] were carried out in-situ where techniques such as neutron radiography [32] imaging was used to identify flow patterns in the GDL, channel flow field and catalyst layer. There have been many ex situ studies [30][33] as well which have looked at film and slug flow along the entire channel length.In this work, the primary aim is to characterize the flow parameters along the entire channel length and simultaneously study the effect of water entering the channel at the corner or under the land. As the previous sections have shown the use of grooved sidewalls help improving drainage characteristics and thus avoid water accumulation, the effect of water features upstream the channel with these channel designs is studied and presented here.

The flow rates that were used for these experiments were kept the same as in the case of experiments in Configuration 1. Figure 46 and 47 show the images of pressure drop plots of

the two channel designs- plain non-grooved channels and channels with grooves on both sidewalls at the same air velocity of 0.5 m/s, when the water is being injected near the air entry hole. This air velocity is particularly important as it was identified to have issues in the previous sections and hence water flow characteristics upstream the channel at this and higher velocities will be studied. The visualization for these experiments was done using the same high speed camera (Keyence VHX-Digital Microscope). The results show distinct difference in behaviors with the droplet entry, formation of slug and ejection process for the two channel designs. For the plain or non-grooved sidewalls, the injected droplet converts to a film which after coming in contact with the opposite sidewall, gets converted in a slug. This slug travels at a very high velocity for a small distance and then stays at the same location for some time. The form of the slug is now more of a film and slug together with its tail along the channel sidewall surface. This sequence and shapes of water features are illustrated in Figure 48. Similar studies were carried out by Cheah et al. [22] and their results showed films being formed in channels coated with Teflon as against slugs in plain (non-Teflon) channels. In their work, rectangular acrylic channels were investigated, with and without Teflon coating. [22]

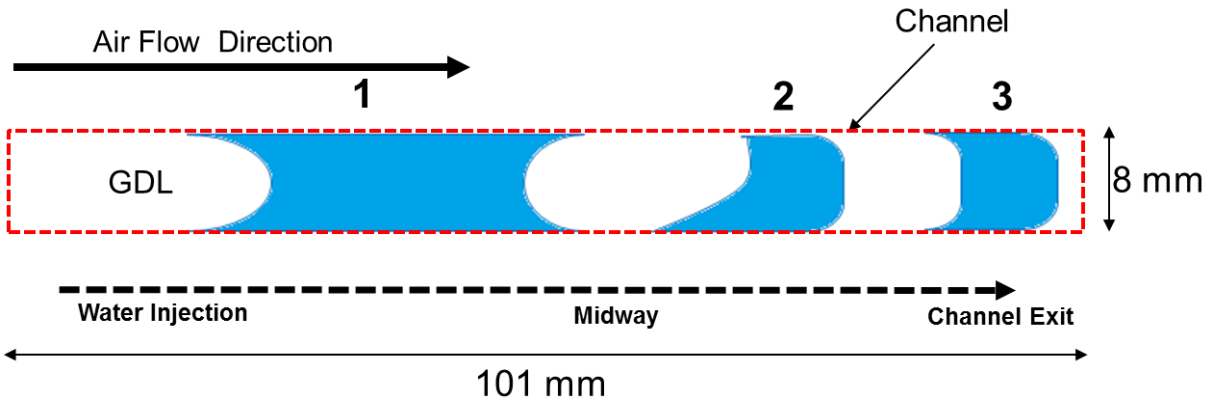


**Fig. 48.** Water Feature Size and Shape Transition- Upstream to Ejection (C2.1 a)

This is a very specific behavior to water entering the channel at a corner. The transition from slug formation to travel and finally ejection is illustrated in the Figure 48. The slug formed breaks down after traveling a small distance and converts to a smaller slug which has a tail-like water feature on the sidewall. This feature later converts to a smaller slug which exits the channel very quickly. Cheah et al. [22] have recorded similar observations before for water entering the channel upstream in a rectangular channel. However experimental results here denote the case of water entering the channel from the corner near the sidewall and hence exhibits unique flow patterns as shown which have been identified. Cheah et al. [22] noted that residual water on channel faces forces slugs to be formed. However, it was found in this study that slugs are formed even in completely dry hydrophilic channels.

For the new channel design that has been proposed in prior sections (4.3, 5.5) with grooves on both sidewalls, the droplet formed in the channel near the point of injection forms a film that travels along the channel wall grooves. The film formed keeps growing along the grooved sidewall and ultimately grows into another film near the channel end and the two films being in contact with each other with tails along the grooves. Figure 50 illustrates this.

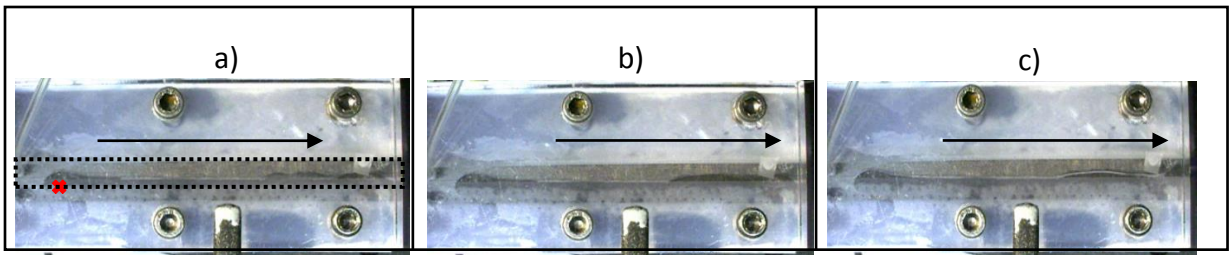


**Fig. 49.** Both Grooved Sidewalls (C2.3a) - Top View Image Sequence (L-R)

In Figure 49 a), the Red Cross symbol denotes the location of droplet injection in the channel and the arrow denotes the flow of air stream. The black dotted line denotes the channel area

under consideration. In Figure 49 a), the droplet has converted into a film near the point of entry and a small trace of the same film which has travelled along the grooves is seen near channel exit. In Figure 49 b) it can be seen that the film at the point of water injection remained of the same size and the film near channel exit grew in size and length. The same film ultimately touches the top wall as seen in Figure 49 c) it is ejected from the channel by a small slug like feature at the channel end. It is shown in a blown-up illustration in Figure 50.

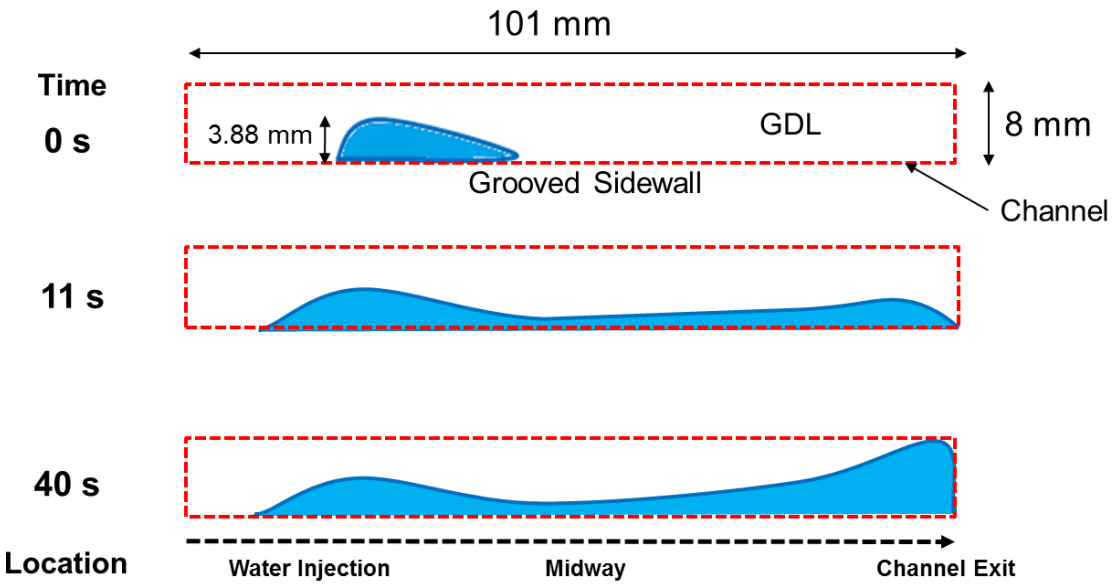


**Fig. 50.** Water Feature Size and Shape Transition- Upstream to Ejection (Both Grooved Sidewalls)

In Figure 50, the red box shows the channel area with sidewalls, GDL base along with the water features produced and its comparative dimension (size) with the channel. It also shows the time taken for the transitions to happen from 0-40 seconds. At zero seconds, droplet is shown growing in a film along the grooved sidewall. This film grows in length in the direction of air flow as time progresses. This growth is quick as water is continuously being injected in the channel. After about 30 seconds of water accumulation, the film at the end of the channel

grows in width till the opposite wall as shown and gets ejected and goes back to its state at 11-15 seconds as shown. The conversion of water feature from 15 to 40 s is highly repeatable and has a much regulated pressure drop signature as shown in Figure 47 compared to that for the plain sidewall channel in Figure 46. The grooved sidewall channel thus causes more peaks in pressure drop as the process of water drainage is faster. Films that quickly travel on grooved surface tops are responsible for the quick water removal. This behavior is found for air velocities $\geq 0.5$ m/s.

Results for all flow rates and the flow characteristics inside the channel have been summarized in Table 6 below for the second approach as per configuration C2. It compares the behavior of water once injected in the channel, its interaction with the sidewall and ejection and flow characteristics.

**Table 6: Summary of Droplet-Sidewall Interaction Results- Water Injection Upstream (C2.1, C2.2, C2.3 a)**

| Sr. No | Superficial Velocity (m/s) | Non Grooved Sidewall | One Grooved Sidewall (No Teflon) | Both Grooved Sidewalls |
|---|---|---|---|---|
| 1 | 0.178 | Water not restricted to one single slug, multiple films formed along the sidewall. Films much upstream the channel which tend to spread along the GDL closer to the opposite wall | Droplets grow into elongated films close to the grooved sidewall. The grooves keep retracting water back to the sidewall so that water stays in the form of a film avoiding channel blockage due to a slug. This film, keeps moving downstream which ultimately gets converted to a slug at a point very close to the channel exit and is ejected instantly. Another good observation from the top view visualization of grooves is how it does not let water to spread on the GDL and form a continuous water film along the grooves. | This implementation of the design is tested to prove the concept of grooved channels. Considering the practical aspect of the channel design and fabrication- these channels will be stamped in the bipolar plate and hence the design with only one grooved sidewall won't suffice. These tests underline and confirm the behavior of water features in the channels. The first slug ejects in a manner very similar to that of a channel having a one grooved sidewall. The behavior of water films formed after the first slug in the channel is very similar, but in this case much longer films are formed near the channel exit which grow wide enough and are ejected. The distinct observation about this channel design is the minimal or none residual water after slug ejection compared to previous designs. |
| 2 | 0.356 | Droplet grows into film, slowly forms a slug. The slug moves along the channel, first in steps of small distances. Again breaking into smaller films, due to the presence of small droplets on the sidewalls. The slug is formed again which resides for some time and then is ejected. | The phenomenon observed for the first air flow velocity is repeated in this case as well. The movement of the film is however a little quicker. More water is in contact with the top wall compared to lower air flow speeds. | The phenomenon observed for the first air flow velocity is repeated in this case as well. The movement of the film is however a little quicker. More water is in contact with the top wall compared to lower air flow speeds. |

| Sr. No | Superficial Velocity (m/s) | Non Grooved Sidewall | One Grooved Sidewall (No Teflon) | Both Grooved Sidewalls |
|---|---|---|---|---|
| 3 | 0.534 | Droplet grows into a long film which forms a slug near water entry location. The slug moves halfway towards the exit, and then again comes in contact with water droplets on both sidewalls, which leads to stalling of the slug, residing for some more time and then ejected from the channel | The phenomenon observed for the first air flow velocity is repeated in this case as well. The movement of the film is however a little quicker. More water is in contact with the top wall compared to lower air flow speeds. The channel's grooved sidewall has a thin layer of water along the entire channel length now after the first slug exits the channel. This leads to formation of one long thin film along the channel sidewall with grooves as water is being injected and the film near the channel exit grows wider and eventually ejects the water leading to a film that is very thin and touching the top wall, leaving most of the GDL uncovered. This explains the retraction of water after a slug exits the channel, seen or reported in the side-view visuals. | For this air velocity, water keeps ejecting as small films from the channel end, and as it comes in contact with the opposite grooved sidewall, it tends to break the film into smaller films and usually instead of two, three films are seen after first slug exits the channel. |
| 4 | 0.712 | Droplet forms a film at water entry location which is blown away to a further point in the channel and the process is repeated and the film near the exit is ejected ultimately. | The phenomenon in the previous air flow velocities is repeated, however the films are longer. The pattern in which the films are produced is highly repeatable and can be accorded to the high flow rates and the grooved sidewall's nature and the presence of water thin film along it. | The behavior for the first slug and the later film related behavior in the channel is repeated for this air flow as well. However, this flow rate is very high and hence causes quicker removal of the films of small widths and lengths toward the channel exit. The overall growth of the film along the sidewall is uniform but breaks down |

| | | | | |
|---|---|---|---|---|
| | | | | once it comes in contact with the opposite sidewall with grooves. |
| **Sr. No** | **Superficial Velocity (m/s)** | **Non Grooved Sidewall** | **One Grooved Sidewall (No Teflon)** | **Both Grooved Sidewalls** |
| 5 | 0.891 | High air velocities make the water droplet grow into a film that is spread along the wall. The film pushes water downstream and is pushed out soon after it grows wide enough towards the opposite sidewall. | The phenomenon in the previous air flow velocities is repeated, however the films are longer. The pattern in which the films are produced is highly repeatable and can be accorded to the high flow rates and the grooved sidewall's nature and the presence of water thin film along it. | Phenomenon is repeatable with variable film length and width. As the air velocity increases, the water near the channel ends tends to start blocking more area compared to low air speeds. This problem was identified for grooved channel tests with water entry near the exit. This phenomenon is believed to be dependent on multiple parameters including GDL wetting and water content on the opposite sidewall. As air flow rates increase, films tend to exit the channel when they are located much upstream as compared to lower air speeds. |
| 6 | 1.069 | High air velocities make the water droplet grow into a film that is spread along the wall. The film pushes water downstream and is pushed out after touching opposite sidewall. | The phenomenon in the previous air flow velocities is repeated, however the films are longer. The pattern in which the films are produced is highly repeatable and can be accorded to the high flow rates and the grooved sidewall's nature and the presence of water film along it. | Water behavior at this air speed is much similar to the prior one. The films being ejected tend to move downstream in the direction of air flow and as they are shifted, after each slug, the location of formation of next film to slug moves more downstream. |

It has been suggested in prior literature how water travels along the groove top-surfaces [14, 15, 21, 23, 32]. An important observation from the top-view visualizations is how the liquid spreads along the grooves. Once the droplet has risen completely to the top wall or till the end of the groove length, it has motion in two directions, as mentioned above, it will collapse when it comes in contact with the opposite sidewall. As soon as it collapses, it will then start spreading on the grooves in a direction perpendicular to the groove length (along the channel). It depends on the air velocity in the channels if its in the direction towards channel exit or air entry (opposite to that). A lot of research has been done regarding the force balance of a liquid droplet on grooved [22] or micro-grooved substrates [31] [34]. Baret et al. [14] have proposed that for a grooved substrate, the driving force and viscous force are the only two active forces. It uses Stoke's Law to estimate the flow rate of liquid on a grooved surface. It is given by:

$$Q = \frac{W^4}{\eta} \frac{\partial P}{\partial y} . G(A) \quad \text{.....} \quad (1)$$

Where,

W is the groove width

$\frac{\partial P}{\partial y}$ is the pressure difference along the liquid filament.

G(A) is the geometry-dependent factor along the flow-field (grooves)

In this case, G(A) is a function of groove aspect ratio, velocity of droplet along the grooves at different air velocities and water pumping rates. As the groove dimension used in this work is constant, the above equation becomes:

$$Q = \frac{W^4\,(Constant)}{\eta\,(Constant)}\ \frac{\partial P}{\partial y}\ .\ G(A) \qquad \text{.....(2)}$$

$$Q\ \alpha\ [\Delta P\ .\ G(A)] \qquad \text{.....(3)}$$

Therefore, the flow rate of water on the grooves is directly proportional to the pressure drop across the feature, groove dimensional aspects and air flow velocity. The plot in Figure 51 shows the results for peak pressure drops in all channel designs for the same set of fuel cell operating conditions for Configuration C1 of droplet injection method.

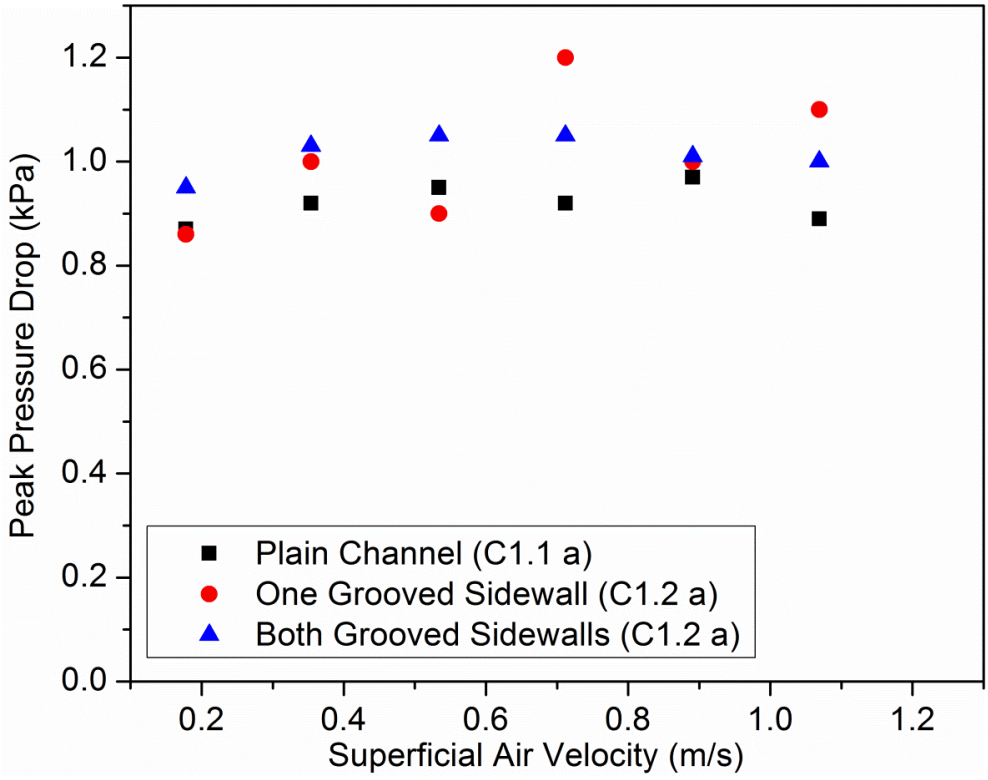


**Fig. 51.** Peak Pressure Drop- All Channel Designs and Air Flow Velocities (Water Injection Near Channel Exit, C1)

Figure 51 shows peak pressure drop values which vary with air flow velocities. It can be seen that peak pressure drops in the case of channels with both grooved sidewalls are higher than

plain sidewalls and those values are also more regulated than that of single grooved channel sidewall. For low air flow velocities below 0.5 m/s the pressure drop values are fairly close to each other and for velocities 0.5 and 1 m/s, the values differ by a significant margin. Looking at the blue triangles, it can be said that the peak pressure drop in the grooved channel will remain within a small range and it will be maximum in the moderate flow rates.

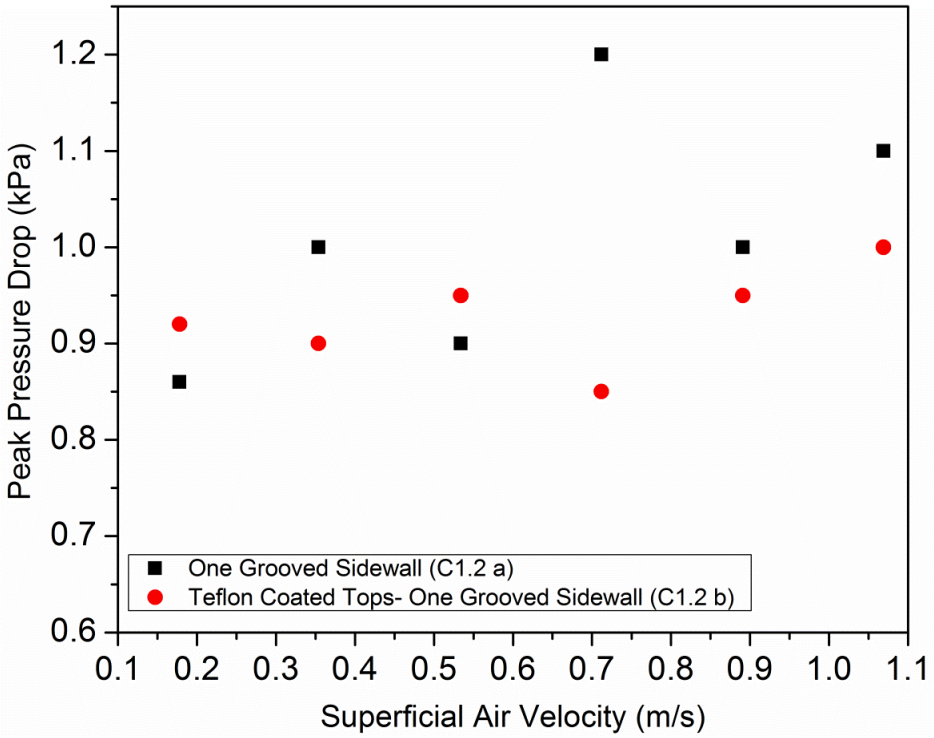


**Fig. 52.** Pressure Drop Variation for Channels with One Grooved Sidewall (Effect of Teflon Coat on Groove Tops- C1)

It can be seen how the variation of peak pressure drops is regulated due to the effect of hydrophobic Teflon coating in Figure 52. Hence it also falls within the similar range of peak pressure drops (0.85-1 kPa) as that for both grooved sidewalls (0.95-1.05 kPa) as shown in Figure 51.

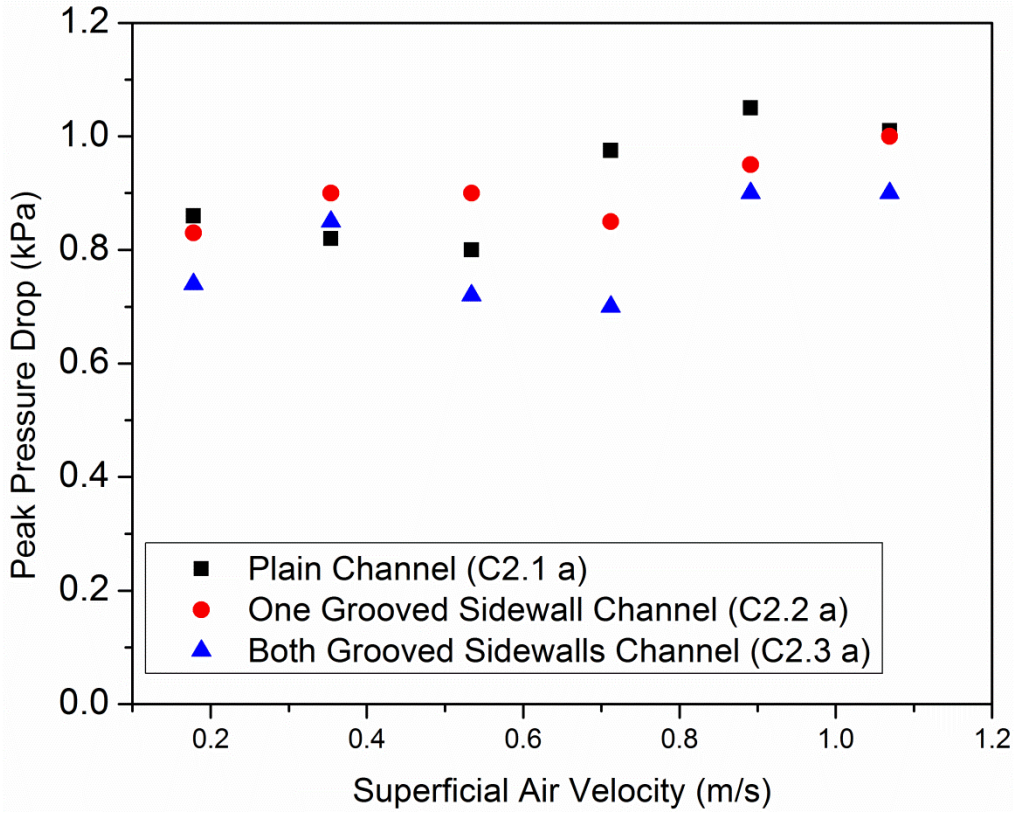


**Fig. 53.** Peak Pressure Drop- All Channel Designs and Air Flow Velocities (Water Injection Upstream, C2)

Figure 53 shows the peak pressure drops for all three channel designs (C2.1-3), for the experimental setup configuration C2. It can be seen that the peak pressure drop variation is within the same range as that of configuration C1 as shown in Figure 51. However, the both grooved sidewalls channel setup (C2.3 a) shows least peak pressure drop in all but one data points, which is in contrast to peak pressure drop results for C1 where peak pressure drops were the highest for grooved sidewalls. This indicates reduced slug blockage and easy removal of water accumulated in the form of elongated films due to the effect of grooves upstream. When Figure 51 and 53 are compared, we can observe the peak pressure drop trends. It is clear that peak pressure drop is the lowest (0.7-0.9 kPa) out of all three channel designs in the

configuration C2 (Figure 53) while it is the highest (0.95-1.105 kPa) for all but one data points in case of configuration C1 (Figure 51) for the channel design with both grooved sidewalls.

The peak pressure drop plots for C1 and C2 need to be compared and their correlation to the expression in equation (3) needs to be established. It is seen in Figure 51 that the peak pressure drop for the channel with both grooved sidewalls is higher than one grooved sidewall for all but two data points, this shows that liquid flow rate over grooves for the design proposed and tested in C1.3 (a) is higher than for the one grooved sidewall design C1.2 (a). This is valid for grooves in a channel near the channel exit. If observed in Figure 53, the peak pressure drops for both grooved sidewall are lower than for one grooved sidewall. This shows that the flow of liquid over grooves is faster near the channel exit than upstream which is evident from the visualization results. It was observed in most cases for C2.2 (a) that water film moves very slowly once formed upstream and its motion is very quick as it reaches near the channel exit, just before it is ejected. There is no other parameter that is affecting the flow velocity of liquid water such as gravity in this case. Hence these findings can be justified in the form of conclusions as stated above.

As described and mentioned by de Gennes et al. [27] in their book, for a grooved substrate, the contact angle produced by a liquid is different than actual and hence is denoted as apparent contact angle $\theta^*$.

$\text{Cos } \theta^* = 1 - \phi_s + \phi_s \text{ Cos } \theta_E$ .....(4)

$= 1 - \phi_s (1 - \cos \theta_E)$

Where $\text{Cos } \theta_E = \frac{\gamma_{SV} - \gamma_{SL}}{\gamma_{LV}}$ .....(5) Young's equation [14,28]

Where $\phi_s$: Solid fraction (ratio of total spiked area to total solid area of grooved or textured surface)

$\theta_E$: Contact angle of the surface

$\gamma$: Surface tension (SV- Between Solid and Vapor phases, SL- Solid and Liquid phases, LV- Liquid and Vapor phases)

For a droplet advancing on the grooves as it advances on each isle or pillar, let the advancing distance be 'dx'. This distance 'dx' changes for every air flow velocity, and hence energy gradient keeps changing, initiating droplet movements. The wet surface area is 'r.dx' where 'r' is surface roughness. When the droplet travels along the direction of air flow, it leaves the previously occupied area partially dry and wet. That area is given by $A= \phi_s . dx$ [27]

It has also been predicted that energy variation is given by:

$$\Delta E= (r- \phi_s). ( \gamma_{SV} - \gamma_{SL}). dx + (1- \phi_s) \gamma_{LV} . dx \quad .....(6)$$

The surface roughness 'r' is constant for the grooved sidewall in this study. The surface tension between interfaces depends on the temperature of fluids which remains constant here but will be varying in an actual fuel cell gas flow channel. This theoretical correlation proves the relationship between grooved channel wall and base surface tension differential which causes the water features to move. The energy keeps varying and thus gives a complex, hybrid wetting behavior on the grooves. This is as per the theoretical prediction of Wenzel's law and that total wetting cannot be induced by surface texture and a partial wetting regime is thus present. This energy gradient on the grooved surface needs to be negative (- $\Delta E$) so that there is constant movement of water on the textured or grooved surface. For that, after introducing Young's equation (equation 5), it becomes

$$\Delta E= (r- \phi_s). ( \gamma \cos \theta ). dx + (1- \phi_s) \gamma_{LV} . dx \quad .....(7)$$

For $\Delta E < 0$,

$$\text{Cos } \theta_E > \frac{1-\emptyset s}{r-\emptyset s} \quad \text{.....(8)}$$

Where, $\phi_s$ is solid fraction given by the ratio of total spiked area to total solid area of grooved or textured surface. [39]

$$\phi_s = \frac{Groove\ Tops\ Area}{Total\ Area\ including\ groove\ tops,depths\ and\ heights} \quad \text{..... (9)}$$

$$= \frac{No\ of\ groove\ tops\ or\ spikes\ X\ Area\ of\ Top}{[(No.of\ Grooves\ X\ Groove\ Width\ X\ Groove\ Height)+(No\ of\ Groove\ Tops\ or\ Spikes\ X\ Top\ width\ X\ Top\ length)+ (No.of\ channels\ X\ 2\ X\ Channel\ DepthX\ Channel\ height)]}$$

$$= \frac{142\ X\ (0.118\ X\ 0.012)}{[(285\ X\ 0.008\ X\ 0.118)+(142\ X\ 0.118\ X\ 0.012)+ (285\ X\ 0.004\ X\ 0.118)]}$$

$$= 0.2727 \text{ or } 27.27\% \quad \text{..... (10)}$$

On the other hand, surface roughness 'r' of a grooved pattern is given by [37]

$$r = \frac{Actual\ Solid\ Area}{Projected\ Solid\ Area} \quad \text{..... (11)}$$

$$= \frac{0.118\ X\ 4}{142\ X\ 0.118\ X\ 0.012}$$

$$= 2.34 \quad \text{..... (12)}$$

Substituting the values of equations 10 and 12 in equation 7, [37]

$$\text{Cos } 45.1 > \frac{1-0.2727}{2.34-0.2727} \quad \text{..... (13)}$$

$$0.7 > 0.3518$$

Thus the grooved surface designed in this study satisfies the condition given by equation (8) for $\Delta E < 0$. The critical angle that needs to be followed by the groove designs for this energy gradient ($\Delta E < 0$) to be negative is found out by [38–40]:

$$\text{Cos } \theta_C = \frac{1-\emptyset s}{r-\emptyset s} \quad \text{..... (14)}$$

$$\theta_C = 69.35^o$$

For the grooves implemented in this study, $\theta_E = 45.1^o$ which is less than $\theta_C$. The range of contact angles that the grooved surface thus should ideally be $45 \leq \theta \leq 69.35$. More experimentation can be done for grooved surfaces that are more hydrophilic ($30 \leq \theta \leq 45$) in nature. However, groove dimensions for the same can be very small and hence difficult to manufacture. Such superhydrophilic surfaces have been created by researchers but their implementation in PEMFC gas channels is not feasible. This proves that textured or grooved surfaces can be engineered to have a specific behavior. Here the target was to induce contact angles and wetting behavior that would cause the droplets to move quickly along a surface and also form films that are partially imbibed in the grooves and partially lie on the surface. Contact angle along the entire periphery of the grooves are found in Section 3.2. They can be integrated using an expression to find out the surface tension of water on the grooved surface. Also, as mentioned above and given by equation (4), contact angle on a rough or grooved surface is different than on a plain surface.

Using this correlation and applying to static advancing and receding contact angles to check the linearity between equation (4) above and the equation (15) below which describes cases when $\theta_C < \theta_E$ [36]:

$$\text{Cos } \theta^* = r \cos \theta \quad \text{..... (15)}$$

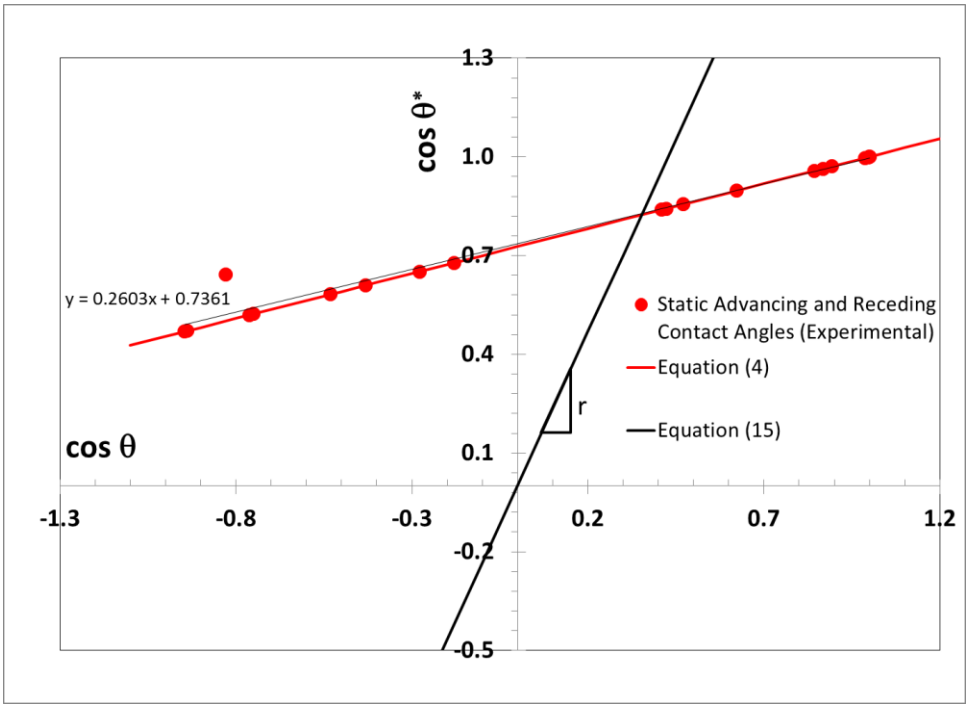


**Fig. 54.** Comparison of Theoretical Predictions with the Experimental Data Showing the Variation of Grooved Surface Contact Angle with Plain Surface Contact Angles

Figure 54 shows strong agreement of theoretical to experimental data for the static contact angles on the grooved surface and theoretical equation for the same. When the experimental data is curve-fitted, the equation thus produced gives solid fraction value of 26.03% when the theoretical value is 27.27% (equation 10). The error in the measurement is thus given by a constant C= 0.2639 when the equation (4) and equation for the curve are equated. It also displays the difference between the wettability produced by a plain and a rough surface.

This theoretical correlation proves the relationship between grooved channel wall and base surface tension differential which causes the droplet to move. The red line represents the equation for the effect of surface roughness on the contact angle when and thus in turn the wettability of the substrate. The black straight line represents the contact angle for cases when partially imbibed film regime is not expected. The energy keeps varying and thus gives a complex, hybrid wetting behavior on the grooves. They have been measured on the VCA Optima for the grooved surface along the entire periphery of the droplet that is released or withdrawn on the grooves. The grooved sidewall in this work has been designed to possess Wenzel wetting regime for a scaling factor > 0.2 [18]. Wetting transition $\theta^*$ as per Wenzel's law for a textured surface would be zero, which is contradicted by the plot in Figure 54 and $\theta^*$ remains non-zero. [39].

Figure 55 shows speeds of the slug or film-like slugs that were formed and removed from each different channel design that was studied in this work. For plain channel sidewall, slug motion speed decreases after superficial air velocity crosses the 0.5 m/s mark. It increases again after that, but the effect of increase in air superficial velocity is not highly pronounced. On the other hand, change in slug motion speeds for sidewall with grooves (one or both) is prominent. It is significantly high for air velocities higher than 0.5 m/s. The value of slug motion speed for one grooved sidewall reaches to as high as 38 mm/s as shown on the plot. The change in slug speeds for grooved sidewalls is more obvious in case of flow rates $\geq$ 0.5 m/s.

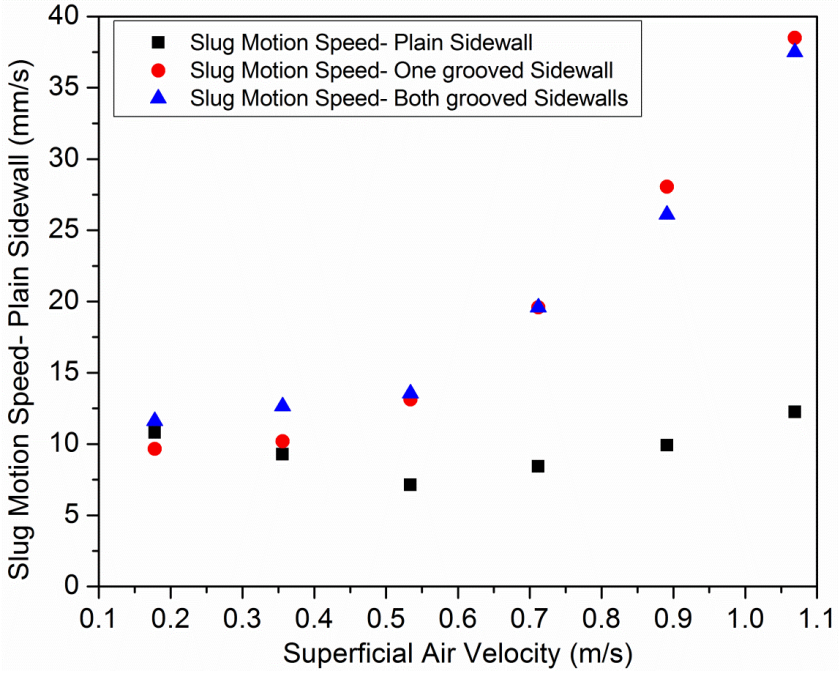


**Fig. 55.** Slug Motion Speeds as a Function of Superficial Air Velocities for Configurations C2.1a, C2.2a and C2.3a

From Figure 55 it is also clear that surface modifications in the form of grooves help in the drainage characteristics and help in removing water features quickly, avoiding blockage and thus accumulation. The peak pressure drop in case of these new channel designs is higher compared to conventional plain trapezoidal channels, however the water features that are generated or forced to be generated are removed at a rate quicker than the plain trapezoidal channel. This also validates the energy variation equation above which expresses the motion or transition of a droplet over a grooved substrate due to an energy gradient.

## 6. Conclusions

In this work surface modifications in the form of grooves on the sidewalls were introduced on PEMFC channel sidewall surfaces to cause the transition of water features in the desired direction to avoid GDL wetting and improve water removal characteristics when water enters in a PEMFC channel under the land region. Below are the important conclusions that can be drawn from the results and discussion:

- For conventional plain trapezoidal channels, water droplets block and accumulate at the channel exit for velocities greater than or equal to 0.5 m/s.
- Water droplet generation at channel corner or under the land in plain sidewall channels causes filling of the entry and opposite corners, contradicting the Concuss- Finn conditions for all air flow velocities.
- Grooved surface on gas channel sidewalls can prove useful by producing required surface energy gradient which leads to water feature transition in the desired direction at desired speeds.
- Rectangular cross-section grooves on the surface of a PEMFC trapezoidal gas channel helps in improving drainage characteristics by forcing formation of films which eventually produce film-like slugs. These flow patterns do not completely block the channel and hence can be removed from the channel with relative ease and reduced two-phase pressure drop.
- Channel with one grooved sidewall improves removal characteristics for low air velocities, but at higher velocities, the pinning effect of the grooves becomes prominent with slugs having film-like tails on the grooved surface. The increased 'hybrid hydrophilicity' due to the grooves leads to the pinning effect.

- In case of a channel with one grooved sidewall, coating the groove-tops of the grooved sidewall with hydrophobic solution of Teflon helped in overcoming the pinning of the droplet on grooved surfaces and regulated the pressure drop signature. However it led to excessive GDL coverage which is adverse for fuel cells as less area is available for the chemical reaction and more is covered with water features.
- Channels with both grooved sidewalls are a more feasible solution than one grooved sidewall with manufacturing methods of these channel plates into consideration. Channels with both sidewalls having grooves do not face issues related to pinning, as the grooves on the opposite sidewall aid in the motion of the films and film-like slugs on the groove tops in the direction of air flow by inducing a constant energy differential between the sidewall-GDL interface which is absent in case of one grooved sidewall or plain sidewall channels.
- The hybrid wetting regime induced due to the specially designed grooves in a dynamic flow condition cannot be classified just as hydrophilic or hydrophobic (contact angle results suggest hydrophilic, 45.1$^{o}$, Section 4.2). This unique wetting condition that shows both hydrophilic (Impregnation of water drops and film in the grooves) and hydrophobic (Longer films partially sitting on groove tops) nature is suitable for PEM fuel cell gas channel water management.
- Slug removal speeds are significantly increased due to the grooved surface modifications of PEMFC channel walls.
- For water injection near the channel exit (C1) and pressure drop being measured across the droplet, peak pressure drops are higher by 0.1 kPa for channels with grooved sidewalls due to the increased pinning effect, shorter slug residence times and formation

of longer films which lead to slugs that lead to higher peak pressure drops than the plain channel.

- For water injection more upstream the channel (C2) and pressure drop being measured near the air inlet hole, overall pressure drops are lower by 0.1 kPa for channels with grooved sidewalls as water tends to stay mainly in the film flow regime, whereas a plain sidewall trapezoidal channel leads to formation of slugs causing higher pressure drops.
- For water features produced upstream, the pressure drop for both grooved sidewalls is the lowest over the entire range except one data point. This shows that for water features produced upstream the channel, two-phase pressure drop is lower compared to a plain sidewall channel and hence improved two-phase flow characteristics are achieved with reduced slug blockage and quick, easy removal of accumulated water.

## 7. Future Work

In this work, effect of grooved channels in a PEMFC was studied at the ex-situ single channel level. These advanced channel designs need to be converted in the form of the entire flow-field and the effect of the same on fuel cell performance needs to be analyzed and understood. Similar work has been done in the past and effect of new channel designs on water management has been carried out. Manufacturing of these channels and flow field is a challenge in itself. It thus would be a very good idea to simulate these designs using numerical techniques. Results from this work will guide and help in setting up these numerical simulations.

The other focus of this work was the effect of water droplet generation in the channel corner or under the land. This has been evaluated using numerical techniques and also by local cell voltage measurements. However, its effect on two-phase pressure drop and flow characteristics hasn't been studied. Hence starting with rectangular channels of larger dimensions to facilitate visualization and water droplets to be injected from the channel corner, it can be quantified. The effect of the same on two-phase pressure drop can be recorded and compared to data available for droplets injected at channel center. The slug removal time and velocities can also be compared in a very similar manner.

The studies done in this work can be expanded by carrying out repeatability tests which will generate more data and peculiar droplet conditions that are repeated can be analyzed and a force balance model can be set up. Effect of PDMS coating on plain channel sidewall and groove-tops will be very interesting to note. The hybrid wetting behavior displayed by the grooves in the channel due to the dynamic wetting and contact angles needs to be quantified and thus further guide in proposing new channel designs with grooves.

# APPENDICES

## APPENDIX I

**Table A1: All Flow Rates for Testing**

| Sr. No. | Current Density A/cm$^2$ | Area cm$^2$ | Current A | Mass Flow Rate (Air) SLPM | Superficial Velocity(CA) m/s | Reynolds Number |
|---|---|---|---|---|---|---|
| 1 | 0.1 | 18.4 | 5 | 0.178 | 0.2 | 40 |
| 2 | 0.2 | 18.4 | 10 | 0.356 | 0.4 | 79 |
| 3 | 0.3 | 18.4 | 15 | 0.534 | 0.5 | 119 |
| 4 | 0.4 | 18.4 | 20 | 0.712 | 0.7 | 158 |
| 5 | 0.5 | 18.4 | 25 | 0.891 | 0.9 | 198 |
| 6 | 0.6 | 18.4 | 30 | 1.069 | 1.1 | 237 |
| 7 | 0.7 | 18.4 | 35 | 1.247 | 1.3 | 277 |
| 8 | 0.8 | 18.4 | 40 | 1.425 | 1.4 | 316 |
| 9 | 0.9 | 18.4 | 45 | 1.603 | 1.6 | 356 |
| 10 | 1 | 18.4 | 50 | 1.781 | 1.8 | 396 |

**Table A2: Actual Channel Dimensions and Calculation Parameters**

| | | |
|---|---|---|
| **Channel Area ($m^2$)** | 0.00001725 | |
| **$mm^2$** | 17.25 | |
| **f x Re** | 15.12 | |
| **Le [Channel Length] mm** | 101.6 | |
| **Plane Sidewall Setup** | channel top width | 3 |
| **Grooved Sidewall Setup** | land width | 0.07 |
| **All dimensions in mm** | channel depth | 3 |
| | channel width | 8.5 |
| | Dh | 3.785 |
| | Dh squared | 14.324 |

**APPENDIX II**

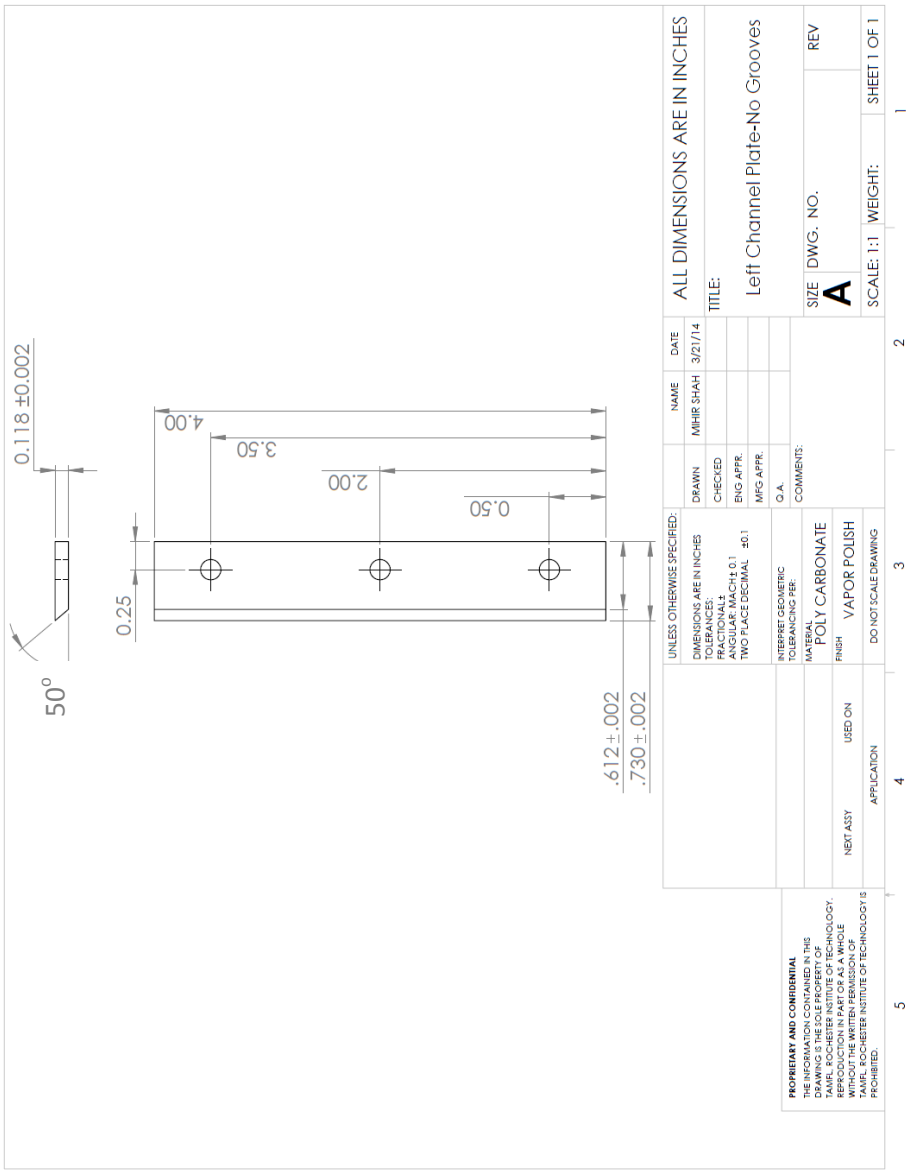


**Figure A1: Left Channel Plate- Engineering Drawing-Plain C1.1**

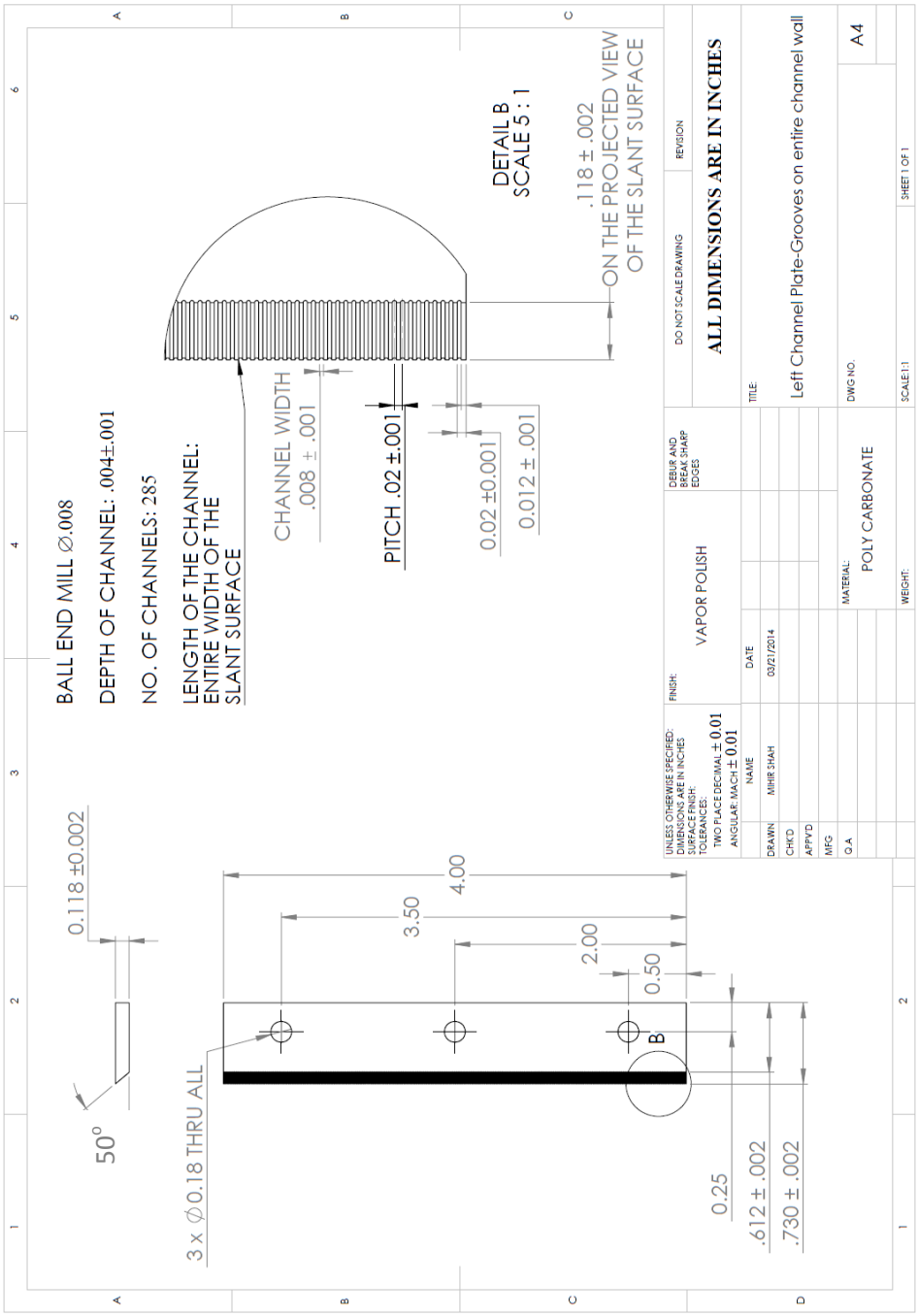


**Figure A2: Left Channel Plate- Engineering Drawing-Grooved C1.2**

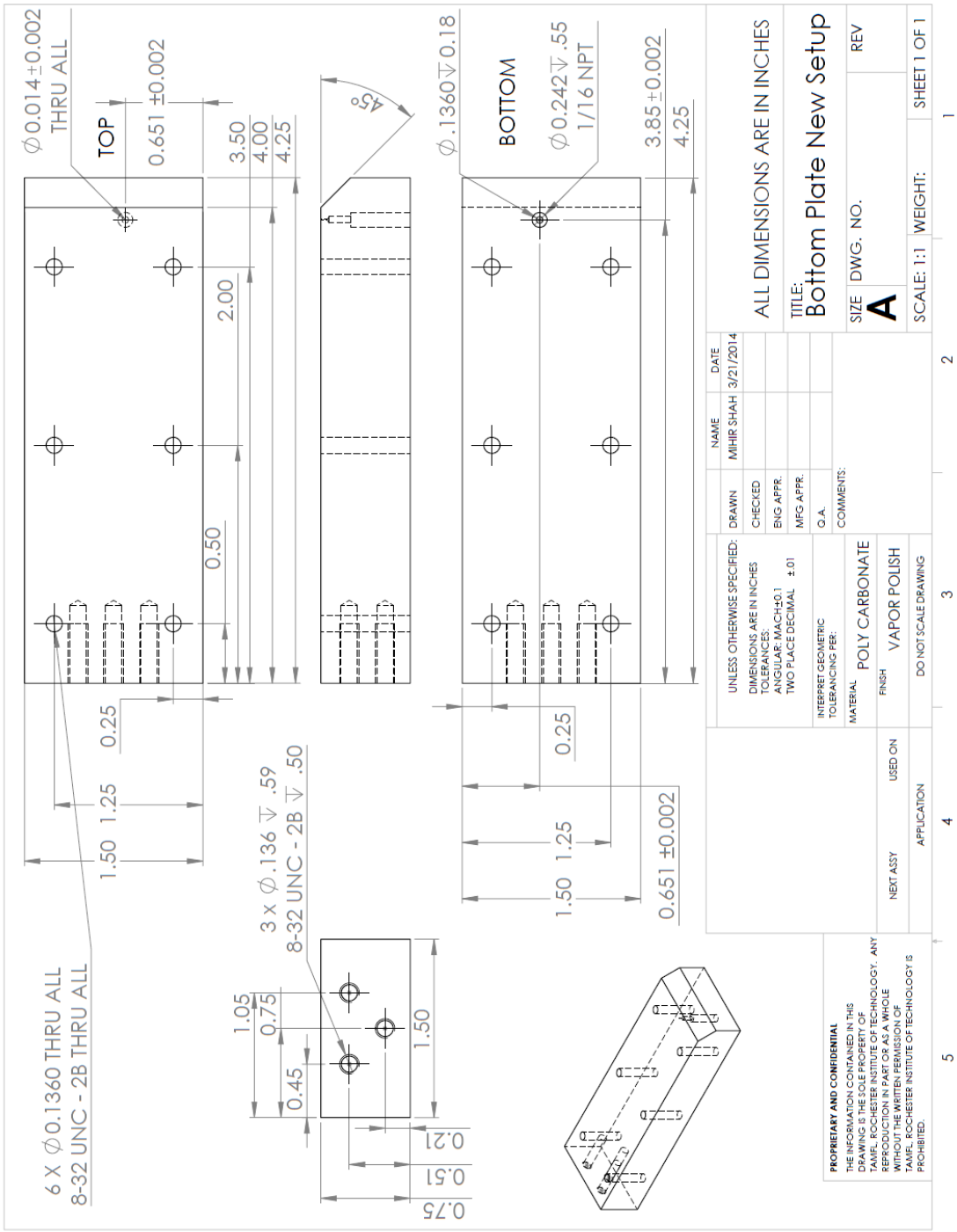


**Figure A3: Bottom Plate- Engineering Drawing- C1**

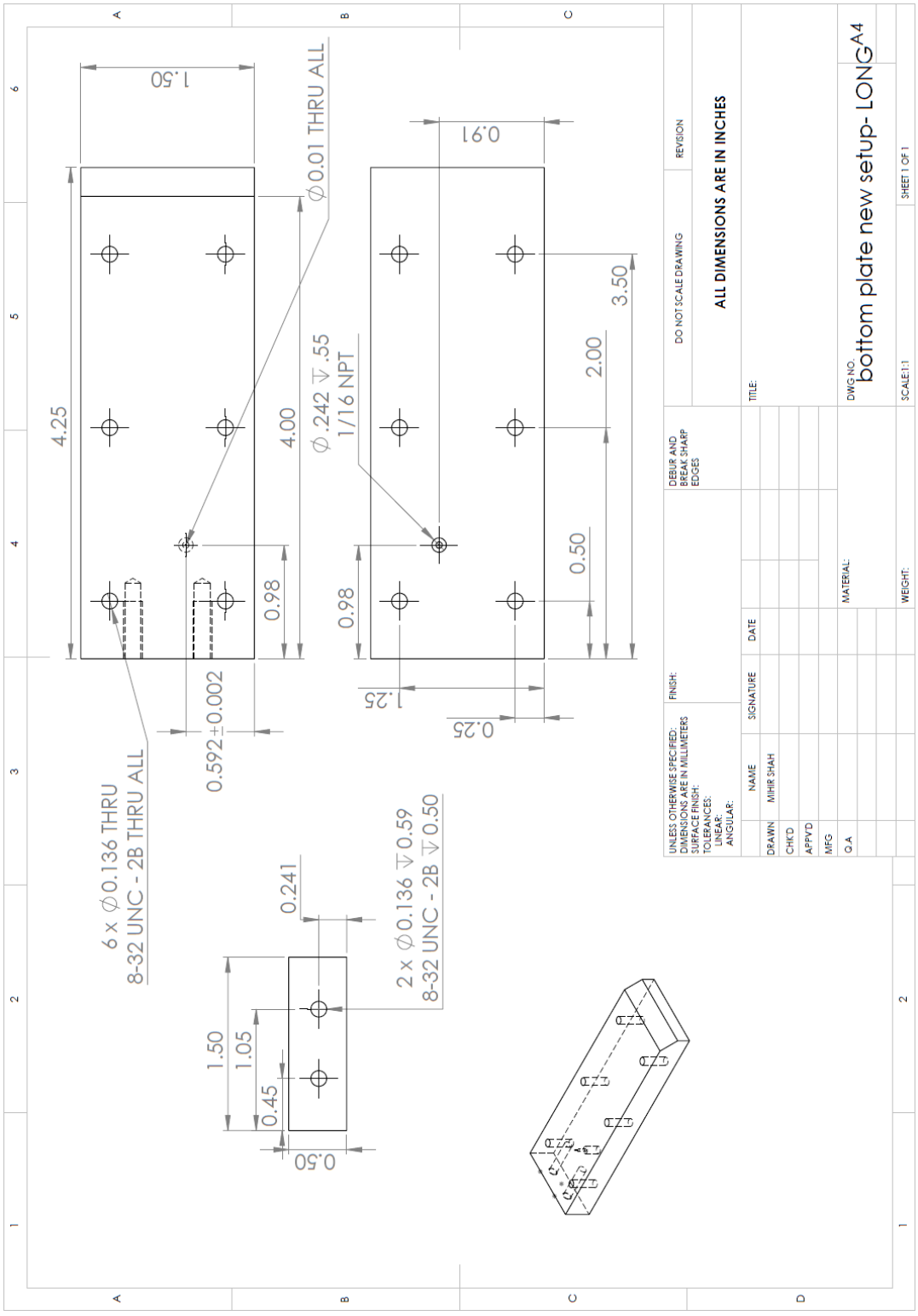


**Figure A4: Left Channel Plate- Engineering Drawing- C2**

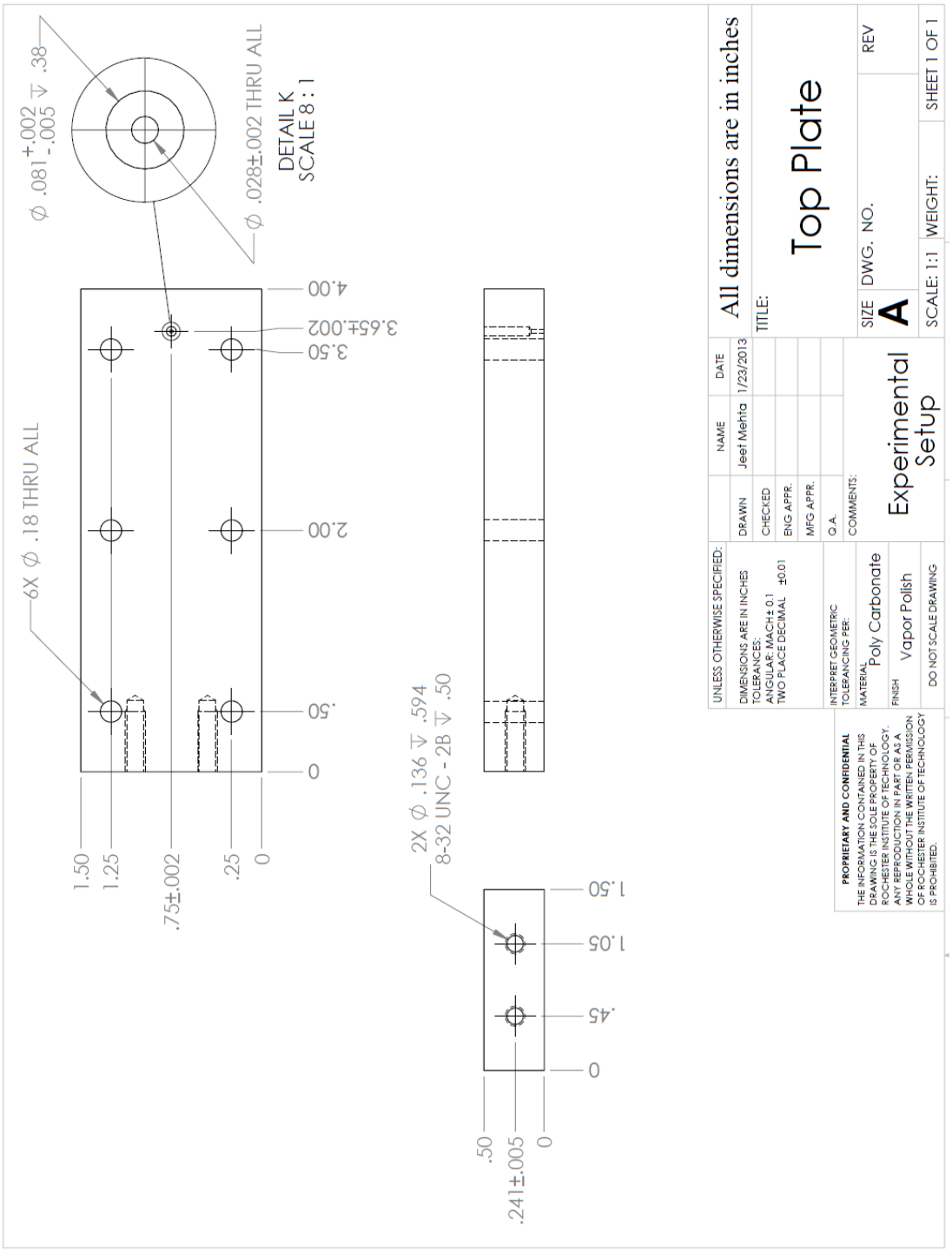


**Figure A5: Top Channel Plate- Engineering Drawing, C1 and C2**

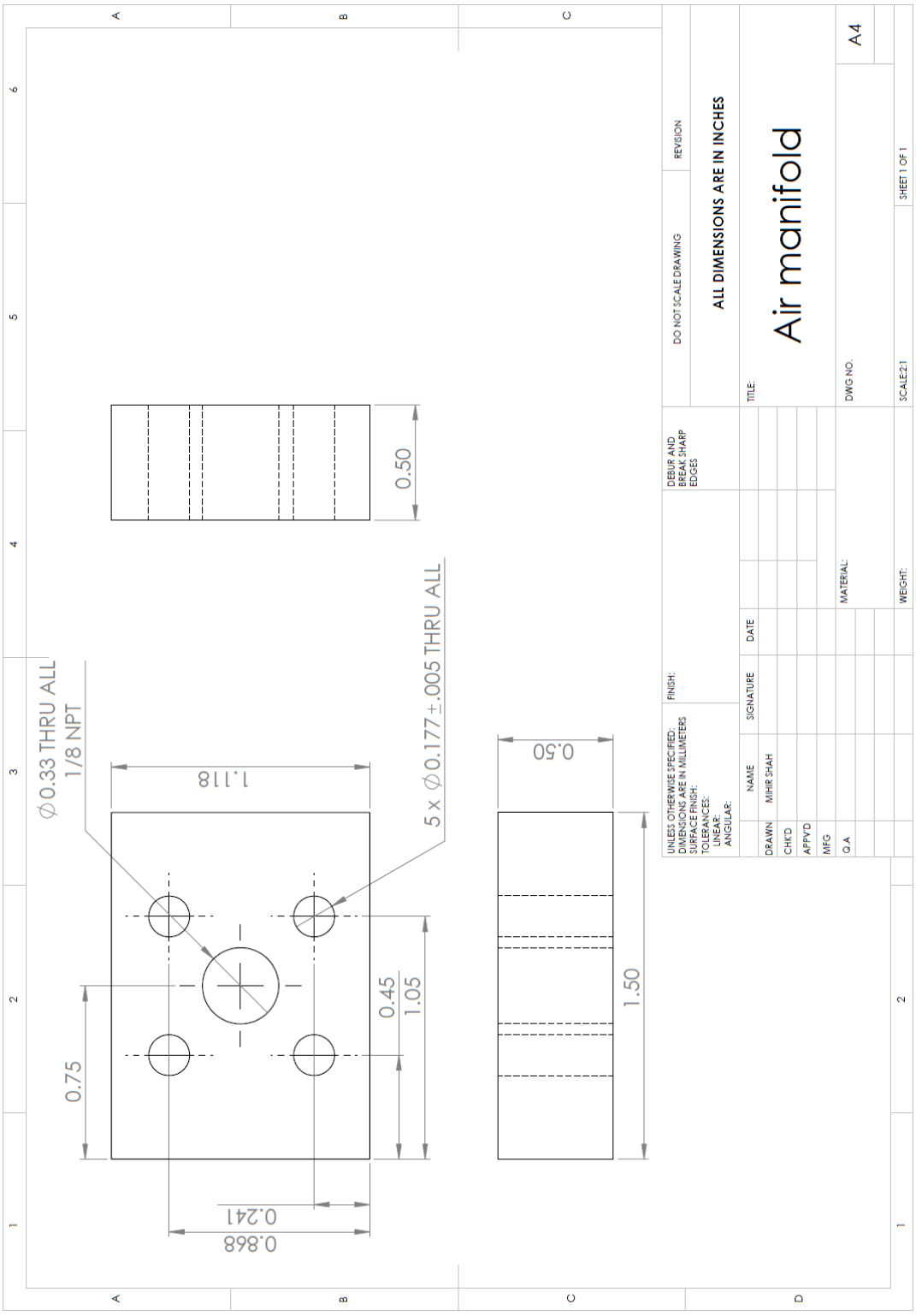


**Figure A6: Air Manifold- Engineering Drawing, C1 and C2**

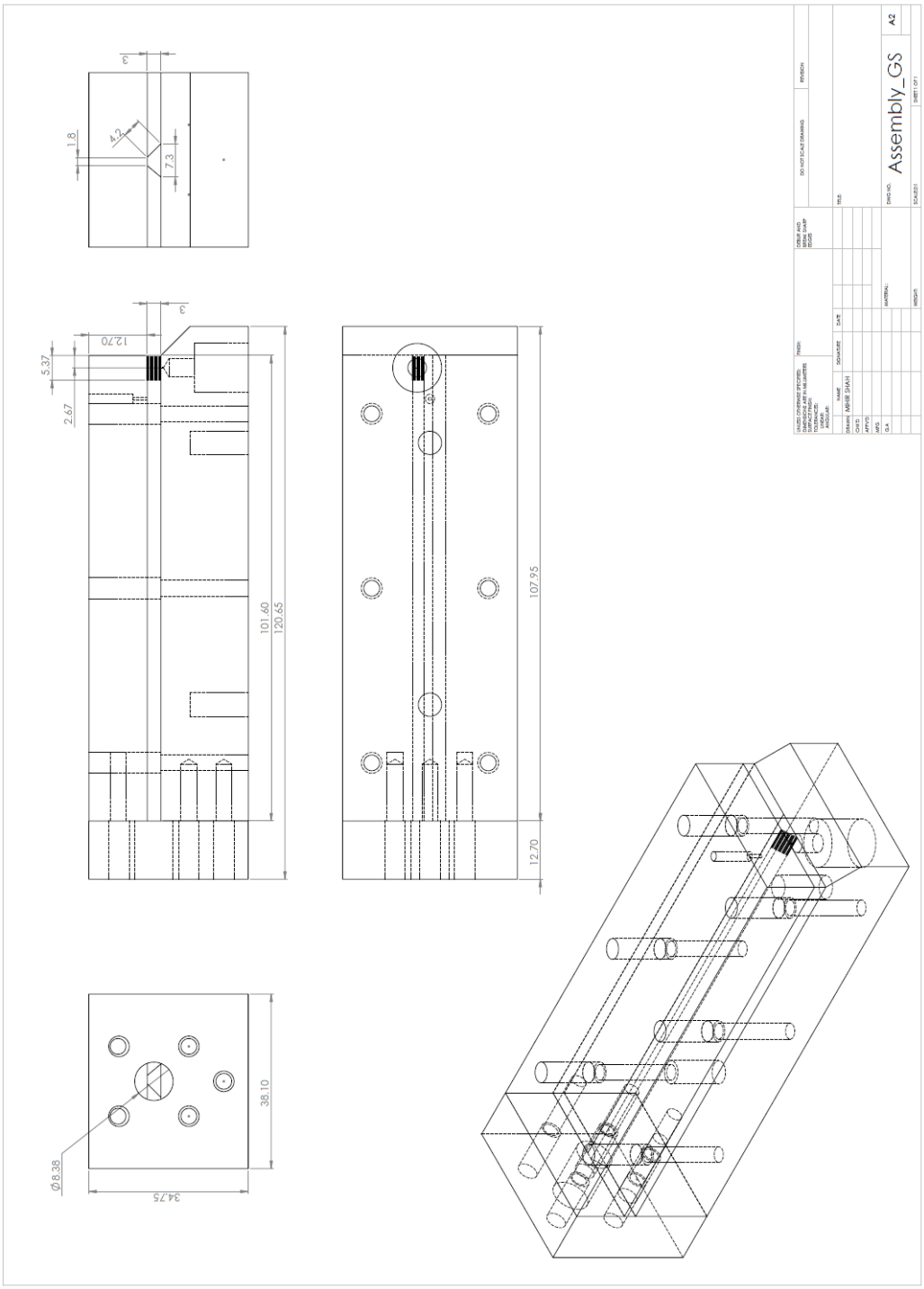


**Figure A7: Setup Assembly- Engineering Drawing, C1**

## REFERENCES


[1] Larminie, J., and Dicks, A., 2003, Fuel Cell Systems Explained, J. Wiley.

[2] Theodorakakos, A., Ous, T., Gavaises, M., Nouri, J. M., Nikolopoulos, N., and Yanagihara, H., 2006, "Dynamics of water droplets detached from porous surfaces of relevance to PEM fuel cells," Journal of Colloid and Interface Science, **300**(2), pp. 673–687.

[3] Lu, Z., Kandlikar, S. G., Rath, C., Grimm, M., Domigan, W., White, A. D., Hardbarger, M., Owejan, J. P., and Trabold, T. A., 2009, "Water management studies in PEM fuel cells, Part II: ex situ investigation of flow maldistribution, pressure drop and two-phase flow pattern in gas channels," International Journal of Hydrogen Energy, **34**(8), pp. 3445–56.

[4] Zhu Xun, Qiang Liao, P.C. Sui, Ned Djilali, 2009, "Numerical Investigation of water droplet dynamics in a low-temperature fuel cell microchannel: Effect of channel geometry," **195**, pp. 801–812.

[5] Rath, C. D., and Kandlikar, S. G., 2011, "Liquid filling in a corner with a fibrous wall—An application to two-phase flow in PEM fuel cell gas channels," Colloids and Surfaces A: Physicochemical and Engineering Aspects, **384**(1-3), pp. 653–660.

[6] Gopalan, P., and Kandlikar, S. G., 2012, "Droplet-Sidewall Dynamic Interactions in PEMFC Gas Channels," Journal of the Electrochemical Society, **159**(8), pp. F468–F475.

[7] Concus, P., and Finn, R., 1994, "Capillary surfaces in a wedge: Differing contact angles," Microgravity Science and Technology, pp. p. 152–155.

[8] Gopalan, P., and Kandlikar, S. G., 2014, "Effect of channel materials and trapezoidal corner angles on emerging droplet behavior in Proton Exchange Membrane Fuel Cell gas channels," Journal of Power Sources, **248**, pp. 230–238.

[9] Zijie Lu, Rath, C., Guangsheng Zhang, and Kandlikar, S. G., 2011, "Water management studies in PEM fuel cells, part IV: Effects of channel surface wettability, geometry and orientation on the two-phase flow in parallel gas channels," International Journal of Hydrogen Energy, **36**(16), pp. 9864–75.

[10] Gopalan, P., and Kandlikar, S. G., 2014, "Contact line characteristics of liquid–gas interfaces over grooved surfaces," Microfluid Nanofluid, pp. 1–10.

[11] Metz, T., Paust, N., Müller, C., Zengerle, R., and Koltay, P., 2008, "Passive water removal in fuel cells by capillary droplet actuation," Sensors and Actuators A: Physical, **143**(1), pp. 49–57.

[12] Sommers, A. D., Ying, J., and Eid, K. F., 2012, "Predicting the onset of condensate droplet departure from a vertical surface due to air flow—Applications to topographically-modified, micro-grooved surfaces," Experimental Thermal and Fluid Science, **40**, pp. 38–49.

[13] Chen, Y., He, B., Lee, J., and Patankar, N. A., 2005, "Anisotropy in the wetting of rough surfaces," Journal of Colloid and Interface Science, **281**(2), pp. 458–464.

[14] Baret, J.-C., Decré, M. M. J., Herminghaus, S., and Seemann, R., 2007, "Transport Dynamics in Open Microfluidic Grooves," Langmuir, **23**(9), pp. 5200–5204.

[15] Rahman, M. A., and Jacobi, A. M., 2012, "Wetting Behavior and Drainage of Water Droplets on Microgrooved Brass Surfaces," Langmuir, **28**(37), pp. 13441–13451.

[16] Nosonovsky, M., and Bhushan, B., 2007, "Hierarchical roughness optimization for biomimetic superhydrophobic surfaces," Ultramicroscopy, **107**(10–11), pp. 969–979.

[17] Cassie, A. B. D., 1948, "Contact angles," Discuss. Faraday Soc., **3**(0), pp. 11–16.

[18] Preethi Gopalan, Satish Kandlikar, 2012, "CONTACT LINE CHARACTERISTICS OF LIQUID-GAS INTERFACES," Proceedings of the 3rd European Conference on Microfluidics -

Microfluidics 2012, SHF, Heidelberg, Germany, pp. 1–9.
[19] "Extreme caution suggested: Superhydrophobic surfaces may have weak icephobic properties | The American Ceramic Society" [Online]. Available: http://ceramics.org/ceramic-tech-today/extreme-caution-suggested-superhydrophobic-surfaces-may-have-weak-icephobic-properties. [Accessed: 01-Jul-2014].
[20] Von Dahlen, S., and Schneider, I. A., 2012, "Local Flooding Phenomena in Channel and Land Areas Occurring during Dynamic Operation of a PEFC," Fuel Cells, **12**(6), pp. 1004–1008.
[21] Wang, X., Rahman, M. A., Jacobi, A. M., and Hrnjak, P. S., 2013, "Dynamic Wetting Behavior and Water Drops on Microgrooved Surfaces," Heat Transfer Engineering, **34**(13), pp. 1088–1098.
[22] Cheah, M. J., Kevrekidis, I. G., and Benziger, J. B., 2013, "Water Slug to Drop and Film Transitions in Gas-Flow Channels," Langmuir, **29**(48), pp. 15122–15136.
[23] Hu, H., Huang, S., and Chen, L., 2013, "Displacement of liquid droplets on micro-grooved surfaces with air flow," Experimental Thermal and Fluid Science, **49**, pp. 86–93.
[24] Kumbur, E. C., Sharp, K. V., and Mench, M. M., 2006, "Liquid droplet behavior and instability in a polymer electrolyte fuel cell flow channel," Journal of Power Sources, **161**(1), pp. 333–345.
[25] Bazylak, A., Sinton, D., and Djilali, N., 2008, "Dynamic water transport and droplet emergence in PEMFC gas diffusion layers," Journal of Power Sources, **176**(1), pp. 240–246.
[26] Lu, Z., Daino, M. M., Rath, C., and Kandlikar, S. G., 2010, "Water management studies in PEM fuel cells, part III: Dynamic breakthrough and intermittent drainage characteristics from GDLs with and without MPLs," International Journal of Hydrogen Energy, **35**(9), pp. 4222–4233.
[27] Mench, M. M., 2008, Fuel Cell Engines, Wiley Online Library.
[28] Yao, C. W., Garvin, T. P., Alvarado, J. L., Jacobi, A. M., Jones, B. G., and Marsh, C. P., 2012, "Droplet contact angle behavior on a hybrid surface with hydrophobic and hydrophilic properties," Applied Physics Letters, **101**(11), p. 111605.
[29] Öner, D., and McCarthy, T. J., 2000, "Ultrahydrophobic Surfaces. Effects of Topography Length Scales on Wettability," Langmuir, **16**(20), pp. 7777–7782.
[30] Spiegel, C., 2007, Designing and building fuel cells, McGraw-Hill, New York.
[31] Grimm, M., See, E. J., and Kandlikar, S. G., 2012, "Modeling gas flow in PEMFC channels: Part I – Flow pattern transitions and pressure drop in a simulated ex situ channel with uniform water injection through the GDL," International Journal of Hydrogen Energy, **37**(17), pp. 12489–12503.
[32] Trabold, T. A., Owejan, J. P., Jacobson, D. L., Arif, M., and Huffman, P. R., 2006, "In situ investigation of water transport in an operating PEM fuel cell using neutron radiography: Part 1 – Experimental method and serpentine flow field results," International Journal of Heat and Mass Transfer, **49**(25–26), pp. 4712–4720.
[33] Banerjee, R., and Kandlikar, S. G., 2014, "Liquid water quantification in the cathode side gas channels of a proton exchange membrane fuel cell through two-phase flow visualization," Journal of Power Sources, **247**, pp. 9–19.
[34] Seemann, R., Brinkmann, M., Herminghaus, S., Khare, K., Law, B. M., McBride, S., Kostourou, K., Gurevich, E., Bommer, S., Herrmann, C., and Michler, D., 2011, "Wetting morphologies and their transitions in grooved substrates," Journal of Physics: Condensed Matter, **23**(18), p. 184108.
[35] Hao, L., and Cheng, P., 2010, "An analytical model for micro-droplet steady movement

on the hydrophobic wall of a micro-channel," International Journal of Heat and Mass Transfer, **53**(5-6), pp. 1243–1246.
[36] Subedi, D. P., 2011, "Contact angle measurement for the surface characterization of solids," Himalayan Physics, **2**(2), pp. 1–4.
[37] Swain, P. S., and Lipowsky, R., 1998, "Contact Angles on Heterogeneous Surfaces: A New Look at Cassie's and Wenzel's Laws," Langmuir, **14**(23), pp. 6772–6780.
[38] Gennes, P.-G. de, 2004, Capillarity and wetting phenomena: drops, bubbles, pearls, waves, Springer, New York.
[39] Bico, J., Tordeux, C., and Quéré, D., 2001, "Rough wetting," EPL, **55**(2), p. 214.
[40] Bico, J., Marzolin, C., and Quere, D., 1999, "Pearl drops," Europhys. Lett., **47**(2), pp. 220–226.